

by the emissivity of the particles and by the fraction of ignited particles, and therefore the shape can be used to determine the particle temperature. As discussed above, the scale factor is the product of the emissivity times the ignited fraction. Table II.C-1 shows the average particle temperatures for different runs. A scale factor was not determined since it appears all the particles are ignited.

In the region where there are absorbing gases (e.g., H₂O and CO₂) the gas emission is partially blocked by the particles, and vice versa. To deconvolute the gas and particle contributions in these regions, we use the fact that the absorbances (=log(transmission)) add linearly (Beer's Law).

$$A(\text{total}) = A(\text{gas}) + A(\text{particles}) \quad (\text{II.C-1})$$

so that the fraction of the emission due to gases is

$$f_g = 1 - A(\text{particles})/A(\text{total}) \quad (\text{II.C-2})$$

The particle absorbance spectrum is assumed to be relatively structureless, so the first step is to compute the absorbance from Fig. II.C-9a as shown in Fig. II.C-10a, and fit a smooth baseline to the resulting spectrum A(total) to obtain A(particles). Fig. II.C-10b shows the fraction of absorbance due to gases, f_g. The total normalized emission is given by

$$E_T = f_g * E_g + (1-f_g) * E_p \quad (\text{II.C-3})$$

where E_g is the gas emission and E_p is the particle emission. Solving this for the gas emission (for which the emissivity is unity) we find

$$E_g = (E_T - (1-f_g) * E_p) / f_g \quad (\text{II.C-4})$$

which is shown in Fig. II.C-10c. From Fig. II.C-10b and c, we show the regions where the water and CO₂ emission occurs, and note that in the cross-hatched region the CO₂ is totally opaque, so that the emission can be seen only from an unknown depth into the flame. Thus, as indicated by the emission curves of Fig. II.C-10c, we can determine the gas temperatures for water and CO₂ by comparison with the black-body curves. At high temperatures, CO is in equilibrium with CO₂. Shown in Table II.C-1 are the gas temperatures computed in this manner, from a few wavelength regions.

Note that the gases are not all at one temperature. Since this is a line of sight measurement, the instrument is seeing a distribution of gas temperature; cold gases near the reactor walls and hot gases in the center of the combustion zone. These different temperature gases have specific regions in the infrared where their effect is maximized since different populations of rotational states are produced. Thus, water at 3150 cm⁻¹ and CO/CO₂ near 2000 cm⁻¹ is representative of the hotter zones while water at 4100 cm⁻¹ and CO₂ at 2350 cm⁻¹ represent colder regions. A more exact mathematical deconvolution of temperatures across a line of sight is given by Krakow (1966) and may be used in future measurements.

Gas temperatures were distributed over a 1500 K range and were up to around 1400 K hotter than the particles which were between 1500 K to 1600 K for all the runs. Given the noise level in the data, particle temperatures appear to be accurate to 25°C and gas temperatures (at specific wavelengths) to 50°C.

II.C.7. Submodel for Soot Radiative Properties

Under this subtask, work was done on developing a radiative model for soot as part of the soot submodel and the results were sent to BYU. The inputs will be the volume fraction of soot and the temperature. The output will be the average soot emissivity. The main difficulty will be to correct for the

Table II.C-1. Summary of Experimental Results from Application of FT-IR Diagnostics to BYU Gasifier.

Run #	Coal	O ₂ /Coal	Avg. Particle Temperature (K)	CO/CO ₂ Temperature (K)			H ₂ O Temperature (K)		
				2350 cm ⁻¹	2000 cm ⁻¹	2200 cm ⁻¹	4100 cm ⁻¹	3150 cm ⁻¹	3700 cm ⁻¹
24	Alberta	1.06	1500	1300	2800	2100	1750	2700	1900
27	Alberta	.92	1525	1350	2700	2150	1700	2700	1900
36	Utah	1.65	1550	1400	2950	2000	1800	2850	1950
37	Utah	1.17	1525	1400	2700	2050	1750	2800	1850
38	Utah	.96	1575	1400	2900	1950	1650	2600	1800
39	Utah	.50	1550	1400	2550	1900	1500	2300	1850

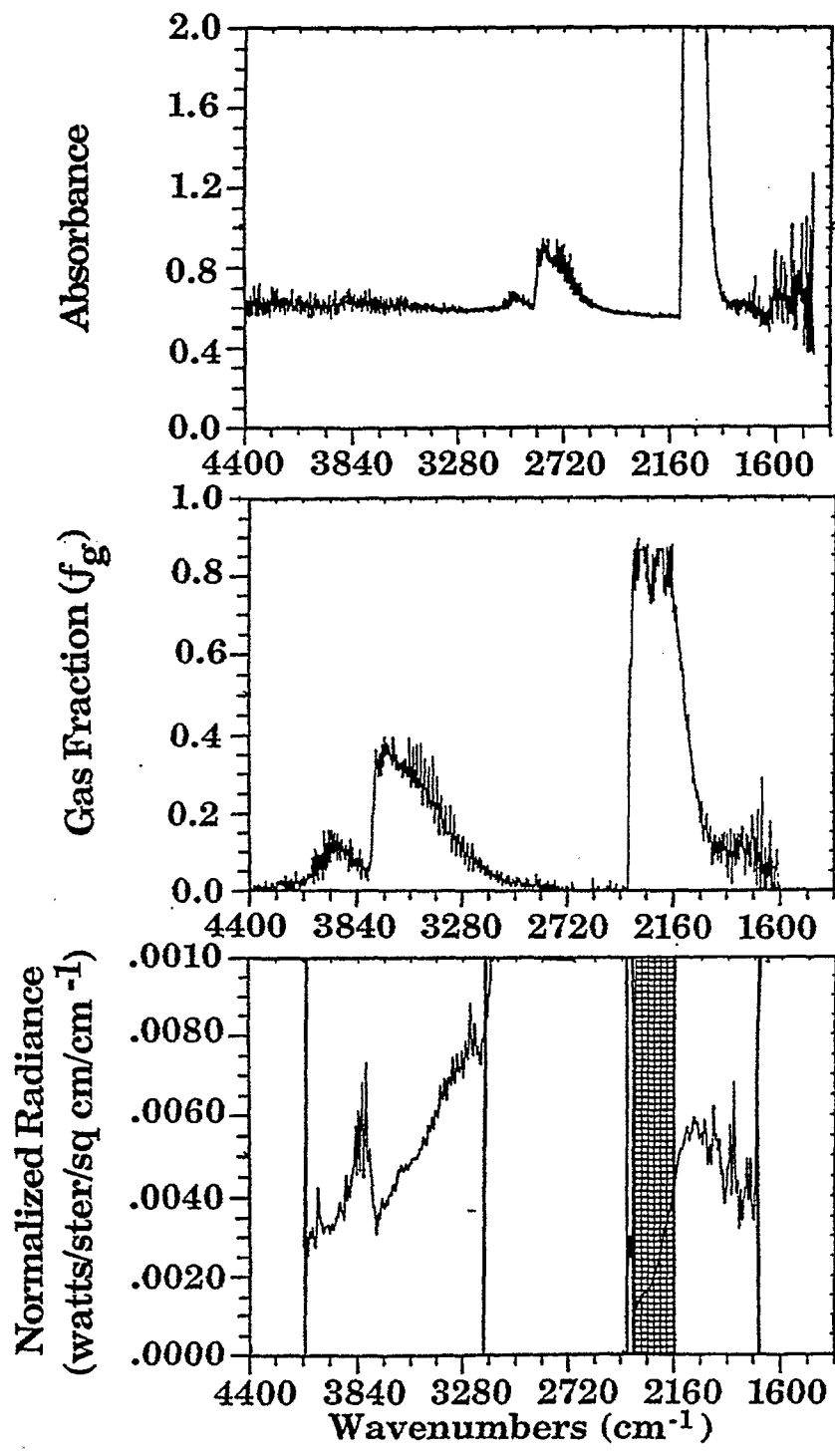


Figure ILC-10. Absorbance, Gas Fraction and Normalized Radiance for Gas Obtained from Utah Blind Canyon Bituminous Coal in the BYU Pilot Flame.

presence of CO₂ and H₂O. This work is being done jointly with BYU since the radiation model is an integral part of PCGC-2. A literature correlation is being used (Kent and Honnery) to make predictions of the average soot emissivity. Correlations from Hottel and Sarofim (1967) are being used to correct for the contributions of water and CO₂. Based on comparisons to an actual measured soot, water and CO₂ spectra, it appears that these corrections are accurate to within 5%.

A primary concern was to correct for the effect of the water and CO₂ bands. It turns out that these bands are sufficiently close to the location of the average wavelength of the soot radiation that the soot acts like a grey body.

The work on the soot radiative properties submodel was completed and these changes have already been implemented into PCGC-2. This includes a correction factor due to the overlap of the soot continuum with spectral lines for H₂O and CO₂.

In previous work, equations II.C-5a and 5b were developed to describe the soot radiative properties as a function of temperature. However, these equations did not have a correction factor due to the overlap of the soot continuum with H₂O and CO₂ lines. The equations were of extinction coefficients, as follows:

$$K_{soot\ em} = (1.9 \times 10^3 \times f_v \times T_e \text{ (m}^{-1}\text{)}) \quad (\text{II.C-5a})$$

$$K_{soot\ abs} = (1.9 \times 10^3 \times f_v \times T_b \text{ (m}^{-1}\text{)}) \quad (\text{II.C-5b})$$

where f_v is the volume fraction, and T_e , T_b are the appropriate temperatures, in Kelvin, for emission and absorption, respectively. The correction terms for the overlap of soot and vapor radiation features are described below.

Hottel and Sarofim (1967) describe a correction due to such overlap, $\Delta\epsilon$, (their Eq. 6-58) as

$$\Delta\epsilon = \sum_j \epsilon_j - [1 - \tau_j (1 - \epsilon_j)] \quad (\text{II.C-6})$$

With a three component model for flame radiation (soot, H₂O, and CO₂), and with the correction due to the overlap of CO₂ and H₂O lines already included in PCGC-2, the additional correction simplifies to two pairwise corrections, for soot-CO₂ and soot-H₂O, respectively.

In that case, Eq. II.C-6 simplifies to

$$\Delta\epsilon_{soot, CO_2} = \epsilon_{soot} \times \epsilon_{CO_2} \quad (\text{II.C-7})$$

and

$$\Delta\epsilon_{soot, H_2O} = \epsilon_{soot} \times \epsilon_{H_2O} \quad (\text{II.C-8})$$

However, Eq. II.C-6 only applies if all but one of the species is a grey-body radiator; not the case for soot. In this section, the proper calculation for the correction term is described, and it is shown that Eqs. II.C-7 and II.C-8 calculate the correction to within 4% for all temperatures and concentrations of interest.

The optical constants of soot from Habib and Vervisch (1988) were used them to calculate the soot absorption constant, k

$$k_{v,s} = \frac{36\pi \times n_v K_v v}{(n_v^2 - k_v^2 + 2)^2 + 4 n_v^2 k_v^2} \quad (\text{II.C-9})$$

and the emissivity, ϵ for eight values of f_v between 5×10^{-6} and 5×10^{-4} .

$$\epsilon_{v,s}(f) = 1 - e[-k_{v,s} \times f_v] \quad (\text{II.C-10})$$

For each f_v , "average" (as opposed to "spectral") quantities were calculated.

$$\epsilon_s(F) = \frac{\int \epsilon_{v,s}(f) R_v^b d_v}{\int R_v^b d_v} \quad (\text{II.C-11})$$

where R_v^b is the Planck function. These ϵ 's were calculated for temperatures of 1500 K, 1800 K and 2100 K.

From measured absorbance spectra of water, $A_{v,\omega}$, and seven values of water concentration, X_ω , the emissivity of water vapor was calculated.

$$\epsilon_{v,s-w} = 1 - \exp[-K_{v,s} f_v + A_{v,\omega} X_\omega] \quad (\text{II.C-12})$$

and hence average emissivity

$$\epsilon_\omega = \frac{\int \epsilon_{v,\omega} R_v^b d_v}{\int R_v^b d_v} \quad (\text{II.C-13})$$

In similar fashion ϵ_{v,CO_2} and ϵ_{CO_2} for carbon dioxide were calculated. Finally, the emissivities, $\epsilon_{s,w}$ and ϵ_{s,CO_2} , for soot-water and soot- CO_2 , respectively, were calculated.

For soot-water:

$$\epsilon_{v,s-w} = 1 - \exp[-K_{v,s} f_v + A_{v,\omega} X_\omega] \quad (\text{II.C-14})$$

$$\epsilon_{av,s-w} = \frac{\int \epsilon_{v,s-w} R_v^b d_v}{\int R_v^b d_v} \quad (\text{II.C-15})$$

$$\Delta \epsilon_{s-w} = \epsilon_{av,s-w} - \epsilon_{soot} - \epsilon_{water} \quad (\text{II.C-16})$$

The correction, and this correction was compared with the prediction of Eq. II.C-4 by taking the ratio

$$\Delta \epsilon_{s-w} / \Delta \epsilon_{soot-H_2O} = \Delta \epsilon_{s-w} / \epsilon_{CO_2} \times \epsilon_{soot} \quad (\text{II.C-17})$$

A similar calculation was done for soot- H_2O .

The ratios are plotted as "spectra" with the x-value representing different combinations of f_v , X (or ϵ_{soot} , ϵ_{CO_2}) in Figs. II.C-11 and II.C-12. For one value of X_{CO_2} , f_v is changed over its range, giving rise to the down sloping line at the left of Fig. II.C-11. Then a new value of X_{CO_2} is chosen, and the cycle of f_v repeated for this value, and so on for the seven values of X_{CO_2} . The results show that the simple correction of Eqs. II.C-7 and II.C-8 is correct to within 5%, and that is the correction which we recommend. It turns out that the water and CO_2 bands are sufficiently close to the location of the average wavelength of the soot radiation that the soot acts like a grey-body.

II.C.8. Submodels for Ignition and Soot Formation

Under this subtask, models for ignition and soot formation were developed. An outline of the proposed particle ignition submodel is shown in Fig. II.C-13. The essential ingredients of the ignition model are already in PCGC-2. What is needed is to refine the assumptions regarding the fraction of CO_2 formed at the surface, as opposed to the gas phase, and the amount of energy feedback to the particle from the oxidation reaction of CO. These are related questions. The results of changing these assumptions on the PCGC-2 predictions of the laminar coal flame experiments are discussed in Brewster et al. (1993).

An outline of the proposed soot submodel is shown in Fig. II.C-14. The current soot formation model includes a calculation of the equilibrium amount of condensed carbon. This does a good job of predicting the location of the soot maximum but not the magnitude or the burnout. What is needed is an improved kinetic model for soot formation and destruction. This will require additional work.

These issues are also discussed under Subtask 3.a.

References for Subtask 2.c.

- Best, P.E., Carangelo, R.M., Markham, J.R., and Solomon, P.R., *Combustion and Flame*, **66**, 47 (1986).
- Brewster, B.S., Smoot, L.D., and Solomon, P.R., Structure of a Near Laminar Coal Jet Diffusion Flame, Poster Session, 23rd Symposium (Int) on Combustion, The Combustion Institute, Orleans, France (1990).
- Brewster, B.S., Smoot, L.D., Solomon, P.R., and Markham, J.R., Structure of a Near-Laminar Coal Jet Flame, *Energy and Fuels*, **7** (6), 844 (1993).
- Fletcher, T.H., Time-Resolved Particle Temperature Measurements and Mass Loss Measurements of a Bituminous Coal during Devolatilization, *Combustion and Flame*, **78**, 223 (1989).
- Habib, Z.G. and Vervisch, P. *Comb. Sci. & Technol.*, **59**, 261 (1988).
- Hottel, H.C. and Sarofim, A.F. *Radiative Transfer*, McGraw Hill, NY (1967).
- Krakov, B., Spectroscopic Temperature Profile Measurements in Inhomogeneous Hot Gases, *Applied Optics*, **5**(2), 201, (1966).
- Markham, J.R., Zhang, Y.P., Carangelo, R.M., and Solomon, P.R., FT-IR Emission/Transmission Tomography of a Coal Flame, 23rd Symposium (Int) on Combustion, The Combustion Institute, Orleans, France, pp 1869-1875 (1990).
- Serio, M.A., Hamblen, D.G., Markham, J.R., Solomon, P.R., *Energy & Fuels*, **1**, 138 (1987).
- Solomon, P.R., and Hamblen, D.G., Pyrolysis, in *Chemistry of Coal Conversion*, Plenum Press, (R.H. Schlosberg, Ed.), New York, 1985, ch. 5, p. 121.

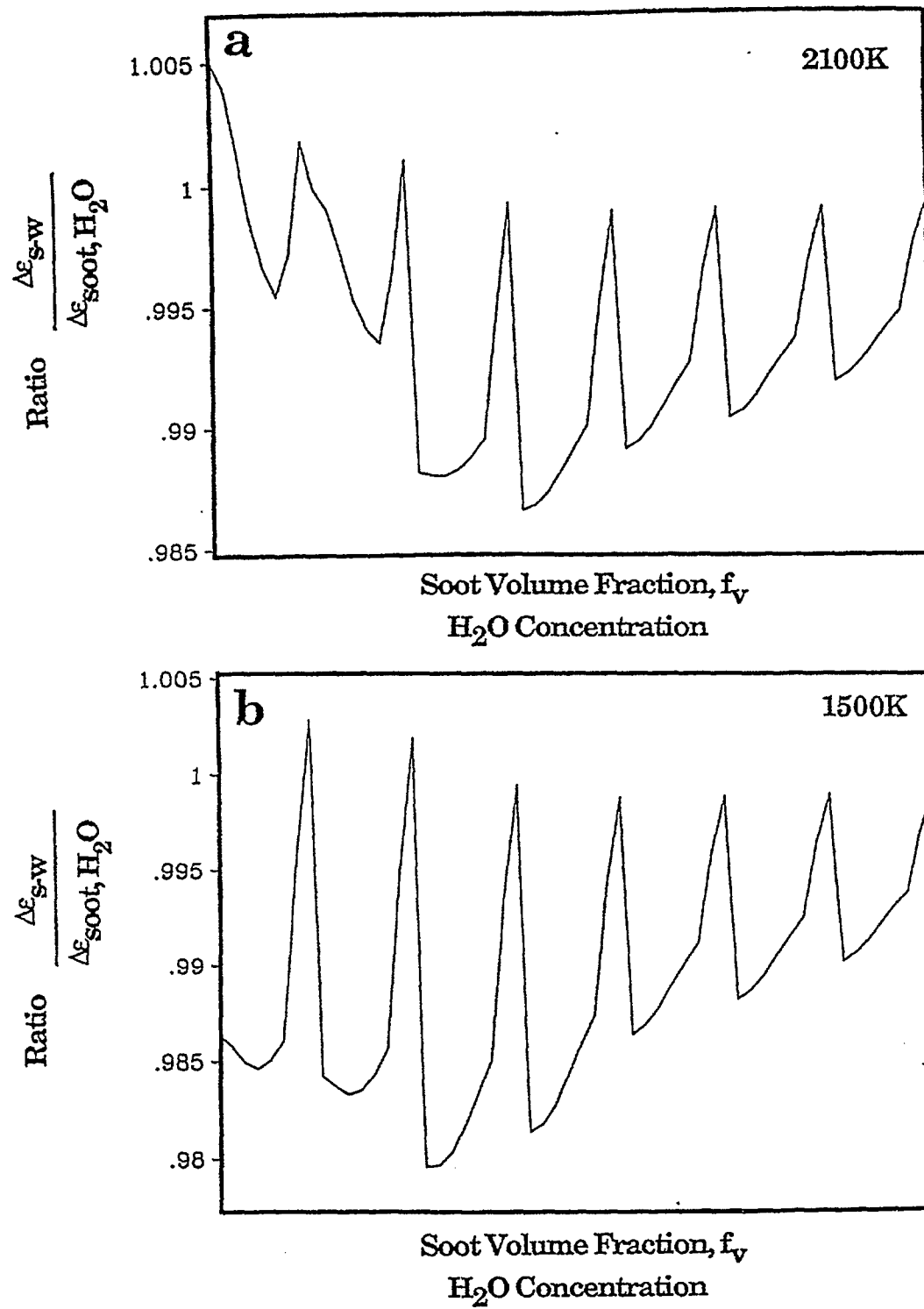


Figure II.C-11. Ratio of Correction Factors for Soot and H₂O at a) 2100K and b) 1500K.

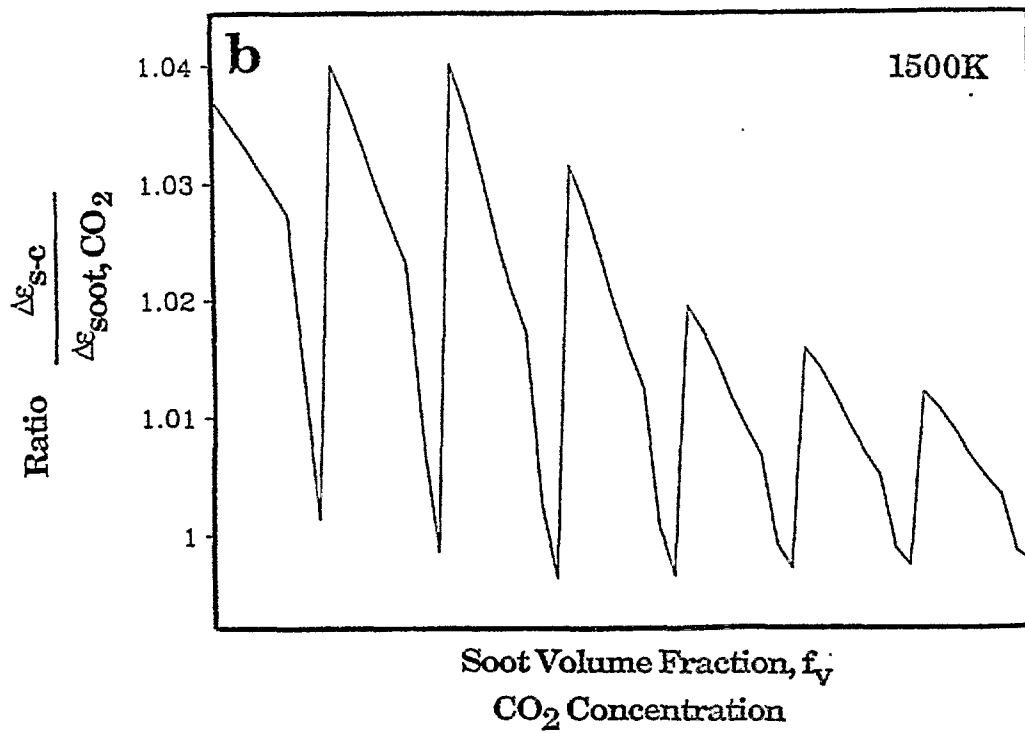
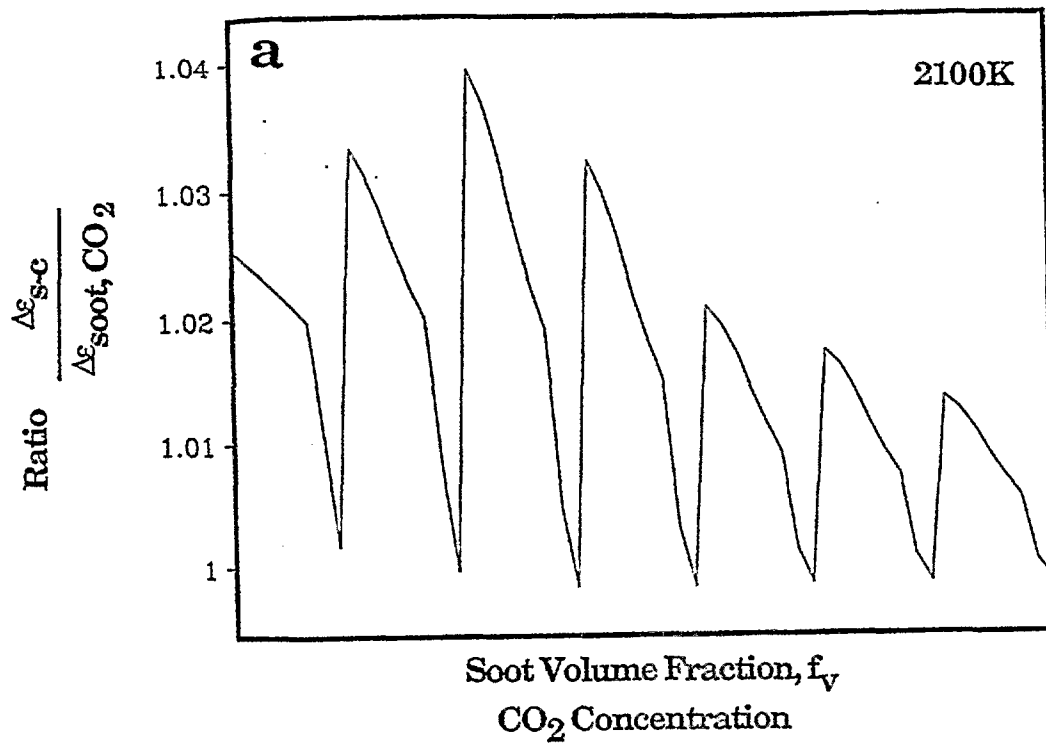
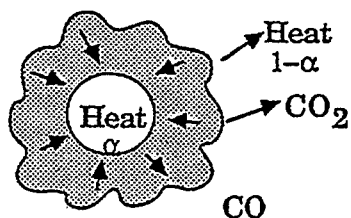


Figure II.C-12. Ratio of Correction Factors for Soot and CO₂ at a) 2100K and b) 1500K.

Input

Particle Temperature (PCGC-2)
Char Reactivity
Volatile Evolution (FG-DVC)
Emissivity
Oxygen Concentration (PCGC-2)

Ignition Model



Output

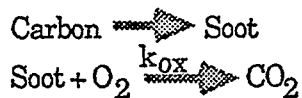
Particle Temperature
Particle Reactivity Rate

Figure II.C-13. Outline of Particle Ignition Submodel.

Input

Equilibrium Carbon (unoxidized)
Temperature

Model



Output

Soot Concentration

Figure II.C-14. Outline of Soot Formation Submodel.

- Solomon, P.R., Serio, M.A., Carangelo, R.M., and Markham, J.R., Very Rapid Coal Pyrolysis, Fuel, **65**, 182-194 (1986).
- Solomon, P.R., Carangelo, R.M., Best, P.E., Markham, J.R., and Hamblen, D.G., Fuel, **66**, 897 (1987a).
- Solomon, P.R., Chien, P.L., Carangelo, R.M., Best, P.E., and Markham, J.R., Application of FT-IR E/T Spectroscopy to Study Coal Combustion Phenomena, paper presented at the Int. Coal Combustion Symposium, Beijing, China (1987).
- Solomon, P.R., and Serio, M.A., in *Fundamentals of the Physical-Chemistry of Pulverized Coal Combustion*, Martinus Nijhoff Publishers, (J. Lahaye and G. Prado, Eds.), p. 126 (1987).
- Solomon, P.R., Chien, P.L., Carangelo, R.M., Best, P.E., and Markham, J.R., Application of FT-IR Emission/Transmission (E/T) Spectroscopy to Study Coal Combustion Phenomena, The 22nd Symposium (Int) on Combustion, The Combustion Institute, Pittsburgh, PA, p. 211 (1988).
- Solomon, P.R., Best, P.E., Markham, J.R., and Klapheke, J., The Study of Coal Flames Using FTIR Emission/Transmission Tomography, Int. Conference on Coal Science Proceedings, IEA, Tokyo, Japan, p. 329 (October 23-27, 1989).
- Solomon, P.R., Chien, P.L., Carangelo, R.M., Best, P.E., and Markham, J.R., Application of FT-IR Emission/Transmission (E/T) Spectroscopy to Study Coal Combustion Phenomena, 22nd Symposium (Int) on Combustion, The Combustion Institute, Pittsburgh, PA (1989c).
- Solomon, P.R., Serio, M.A., Hamblen, D.G., Smoot, L.D., and Brewster, B.S., Measurement and Modeling of Advanced Coal Conversion Processes, 11th Quarterly Report, Advanced Fuel Research, Hartford, CT, DOE-METC Contract No. DE-AC21-86MC23075, (1989c).
- Solomon, P.R., Serio, M.A., and Markham, J.R., Kinetics of Coal Pyrolysis, Int. Conference on Coal Science Proceedings, IEA, Tokyo, Japan, p. 575, (October 23-27, 1989).
- Solomon, P.R., Chien, P.L., Carangelo, R.M., Serio, M.A., and Markham, J.R., New Ignition Phenomenon in Coal Combustion, Combustion & Flame, **79**, 214 (1990).
- Solomon, P.R., Markham, J.R., Zhang, Y.P., and Carangelo, R.M., FT-IR Emission/Transmission Tomography of Coal Flames, ACS Div. of Fuel Chem. Preprints, **35**, (3), 746, (1990).
- Solomon, P.R., and Best, P.E., Fourier Transform Infrared Emission/Transmission Spectroscopy in Flames, in *Combustion Measurements*, (N. Chigier, Ed.), Hemisphere Publishing Corp. pp. 385-344 (1991).
- Solomon, P.R., On-Line Fourier Transform Infrared Spectroscopy in Coal Research, in *Advances in Coal Spectroscopy*, (H.L.C. Meuzelaar, Ed.), Plenum Publishing Corp. pp. 341-371 (1992).
- Solomon, P.R., Serio, M.A., and Suuberg, E.M., Coal Pyrolysis: Experiments, Kinetic Rates, and Mechanisms, Progress in Energy and Combustion Science, **18**, pp 133-220 (1992).

II.D. SUBTASK 2.d. - ASH PHYSICS AND CHEMISTRY SUBMODEL

Senior Investigators - Michael A. Serio, Peter R. Solomon, and Marek A. Wójtowicz
Advanced Fuel Research, Inc.
87 Church Street, East Hartford, CT 06108
(203) 528-9806

Objectives

The overall objective of this subtask was to determine and describe the ash physics and chemistry during coal conversion processes. Mineral matter in coal is a source of slagging and deposits on reactor or downstream component walls, causing corrosion of equipment. Minerals can also catalyze reactions or poison process catalysts. To accomplish the overall objective, the following specific objectives were formulated: 1) to develop an understanding of the mineral matter phase transformations during ashing and slagging in coal conversion. This information will be used for the eventual development of a predictive model of ash behavior based on the original mineral matter composition, particle size, and physical properties as well as the process conditions. It was determined based on the laboratory experiments and literature review that the completion of such a model would require more resources than were available in this study and may duplicate ongoing DOE sponsored work. Consequently, the original objective was scaled back to include only the identification of the key mineral transformation processes that need to be modeled in advanced coal conversion systems. 2) to investigate the catalytic effect of mineral matter on coal conversion processes and develop a model to include this effect on char reactivity.

Summary of Accomplishments

Under this subtask, work was performed in four areas:

- laboratory studies of mineral matter transformations
- laboratory studies of catalytic effects of minerals on char reactivity
- modeling of mineral effects on char reactivity
- literature reviews of mineral matter transformations

The modeling of mineral effects on char reactivity was integrated into the overall char reactivity model and is reported in Section II.A.10.

II.D.1. Laboratory Studies of Mineral Matter Transformations

Elemental Analysis of Coals by SEM/Dispersive Energy X-Ray

The elemental composition of the minerals in the ampoule coal samples was characterized by a Scanning Electron Microscope (SEM) with dispersive energy x-ray analysis. The samples were received in glass ampoules under an inert gas blanket and analyzed on an as received basis without further treatments. The particle size of coal samples are -100 mesh for 5 gm ampoules and -20 mesh for 10 gm ampoules. All the raw coals, except for the Wyodak samples, were received in the -100 mesh size. All the samples were reground into very fine particles using a ball-mill for 20 minutes and then pressed into a flat pellet containing about 300 mg of coal. This was done to ensure a representative sample was obtained. The samples were coated with graphite to prevent charging and then the resulting pellet was mounted in the SEM. The analysis of the elemental composition was based on the measurement of the x-ray intensities of the major elements (Fe, S, Ca, Ti, Mg, Na, Si, and Si) from 121 subsamples, where a subsample is defined as a surface portion of the sample surface (typically 20 to 200 microns square). The electron beam was scanned from one subsample to another, and the x-ray intensities for all elements of interest were recorded. The data acquisition process was completely automated and takes about 10 minutes.

In order to compare the obtained elemental analysis of coal mineral impurities with the ASTM high temperature ashing sample measurements, the elemental compositions of the coals were recalculated and converted into the oxide form (MgO , Na_2O , Al_2O_3 , SiO_2 , K_2O , CaO , TiO_2 , and Fe_2O_3). The amount of SO_3 was calculated in the ash as that portion of total sulfur could react with CaO to form $CaSO_4$. Therefore, the total number of moles of SO_3 present in the ash could not exceed the total number of moles of CaO presented in the coal. The excess amount of sulfur analyzed in raw coal was assumed to be released into the gas product stream during the coal conversion process. The iron content in the elemental composition are included only as iron in oxide form. The total iron contents were recalculated to include the iron existing in the pyrite form, based on the relative stoichiometry ratio.

The results of the mineral impurities analysis and other characteristics of raw coals are shown in Tables II.D.1-1 to II.D.1-3. Table II.D.1-1 shows the ultimate, proximate, and sulfur analyses of all raw coal samples. Most of these data were provided by Argonne, except the sulfur content and form which was analyzed at AFR. Argonne's data are also listed for comparison. The agreement is good in most cases. Table II.D.1-2 shows the results of mineral elemental composition analyses by SEM/dispersive energy x-ray analyses of nine raw coals. Table II.D.1-3 shows the results similar to those in Table II.D.1-2 but expressed in the oxide form in the ash. A comparison with the results of HTA samples analyses provided by Argonne is also presented, and the two methods show reasonable agreement.

When comparing the ash composition data obtained from AFR with Argonne's data, good agreement is found for the total ash content. For example, our data for the ash content of Upper Freeport bituminous and Wyodak subbituminous coals were 12.46 and 8.9 wt%, respectively, as compared with 13.03 and 8.83 wt% obtained from Argonne for these two coals. However, some discrepancies were observed for the sulfur and iron content. This may be due to our assumption that the CaO will react stoichiometrically to form SO_3 . In the real ashing procedure, this may not be the case.

To collect ash samples under coal conversion conditions, two sample collection probes were constructed. They were inserted into the transparent wall reactor (TWR) to allow for the collection of char with its transforming mineral matter from the flame at various stages of burnoff. Mineral matter associated with the char as well as fly ash from above the flame were also collected. Both probes result in no visual disruption of the stability, size, or ignition delay time of the flames. Sample collections were performed using these probes from Zap lignite and Montana Rosebud coal flame experiments. SEM/dispersive x-ray analysis was performed on individual ash spheres that were recovered from the preseparator and the eight stages of the cascade impactor for an "in-stack" ash collection from 200 x 325 mesh Zap lignite.

The fly ash collector (in stack) consists of an inlet nozzle, large particle preseparator, cascade impactor and adjustable air pump. The char collector (in flame) consists of a water cooled nozzle that adds cold helium to the hot particle stream. After quenching, the particle stream passes through a large particle cyclone separator, and then through the preseparator and cascade impactor. A schematic of the system, as installed in the transparent wall reactor (TWR), is shown in Fig. II.D.1-1.

The char collector nozzle inlet temperature was maintained below $300^\circ C$ by the He addition. The fly ash collector nozzle was placed in the flame exhaust stack having a typical radial temperature profile as presented in Fig. II.D.1-2.

Table II.D.1-4 and Fig. II.D.1-3 show collection and separation data for a Rosebud subbituminous coal and a Zap lignite under similar collection conditions. TGA weight loss measurements on the in-flame collected samples indicate that both cyclone fractions have a large amount of combustible material remaining (~60%). SEM photomicrographs (Figs. II.D.1-4 and II.D.1-5) show that both materials contain etched particles of the same size range as the starting materials, with some particles having discrete globules of ash stuck to the particle surface and others with a more uniform coating (possibly smaller globules) of ash as indicated by the bright (charging) areas. The Zap cyclone fraction appears to contain more particles with ash globules on particle surfaces, and more ash that has apparently been released from the char. This is also indicated in the size separation data presented in Fig. II.D.1-3. For the Zap

Table II.D.1-1. Properties of Coals to be used in Mineral Transformation Testing.

	Upper Freeport bituminous	Wyodak subbituminous	Illinois No.6 bituminous	Pittsburgh No.8 bituminous	Pocohontas No.3 bituminous	Utah Blind Canyon bituminous	Upper Knewha bituminous	North Dakota Zap lignite	Montana Rosebud subbituminous
<u>Proximate Analysis, wt%</u>									
Moisture	0.83	28.84	2.94	1.80	0.61	4.71	2.60	32.84	---
Volatile Matter	27.56	33.95	30.92	---	---	---	---	---	---
Fixed Carbon	58.56	30.84	42.72	---	---	---	---	---	---
Ash	13.05	6.37	23.42(16.2) ⁺⁺	9.27	4.87	4.68	19.81*	6.53**	---
<u>Ultimate Analysis, wt% maf.</u>									
C	87	74	77	83	91	79	81	73	72.1
H	5.5	5.1	5.7	5.8	4.7	6.0	5.5	5.3	4.9
S**	2.8	0.5	5.4	1.6	0.9	0.5	0.6	0.8	1.2
N	1.4	1.3	1.2	1.5	0.9	1.3	1.0	0.5	1.2
O	4	19	10	8	3	13	11	21	20.3
<u>Forms of S, wt%^{**}</u>									
Inorganic	0.65(1.96)	0.29(0.14)	2.58(2.72)	1.38(1.33)	0.06(0.18)	0.14(--)	0.25(--)	0.27(--)	1.60(--)
Organic	0.71(0.49)	0.45(0.42)	1.90(2.08)	0.70(0.81)	0.50(0.42)	0.24(--)	0.48(--)	0.45(--)	0.47(--)
Total:	1.36(2.46)	0.74(0.56)	4.48(5.03)	2.08(2.14)	0.56(0.60)	0.38(--)	0.73(--)	0.72(--)	2.07(--)

Notes:

** Moisture free basis

* Analyzed by SEM/dispersive energy x-ray technique of raw coals on a dry basis.

+ Values in parenthesis represent Argonne's data on a dry basis.

++ Value from a second laboratory

Table II.D.1-2. Mineral Distribution, Elemental Composition.

Metal	Upper Freeport	Wyodak	Illinois No.6	Pittsburgh No.8	Pocahontas No.3	Utah Blind Canyon	Upper Knawha	North Dakota Lignite	Montana Rosebud
Na	0.03	0.11	0.12	0.02	0.07	0.08	0.11	0.36	0.02
Mg	0.22	0.37	0.16	0.13	0.11	0.11	0.33	0.54	0.35
Al	1.67	0.73	1.35	0.94	0.57	0.3	3.57	0.49	1.08
Si	2.92	1.12	2.88	1.72	0.69	0.49	5.47	0.82	0.49
K	0.24	0.02	0.16	0.07	0.02	0.03	0.42	0.03	0.03
Ca	0.19	1.3	0.71	0.16	0.26	0.28	0.08	1.56	1.17
Ti	0.11	0.09	0.07	0.01	0.05	0.01	0.26	0.05	0.07
S(o)	0.71	0.45	1.9	0.7	0.5	0.24	0.48	0.45	0.47
S(m)	0.65	0.22	2.58	1.38	0.06	0.14	0.25	0.27	1.6
Fe	0.47	0.29	0.6	0.3	0.28	0.14	0.47	0.4	0.32
Ash	12.49	9.02	16.14	8.51	4.4	3.41	21.48	9.6	12.33

Table II.D.1-3. Mineral Distribution in Raw Coal Ash (oxide form).

Metal	Upper Freeport	Argonne's Data	Wyodak	Argonne's Data	Illinois No.6	Pittsburgh No.8	Pocohontas No.3	Utah Blind Canyon	Upper Knewha	North Dakota Lignite	Montana Rosebud
Na ₂ O	0.32	0.44	1.67	2.15	1.01	0.32	2.19	3.28	0.69	5.35	0.22
MgO	2.93	1.07	6.90	6.11	1.66	2.53	4.24	5.54	2.55	9.86	4.67
Al ₂ O ₃	25.33	23.97	15.50	17.26	15.98	20.88	25.05	17.23	31.48	10.20	16.43
SiO ₂	50.16	42.82	26.93	32.91	38.60	43.27	34.34	31.87	54.63	19.33	25.68
K ₂ O	2.71	2.46	0.32	0.33	1.41	1.16	0.66	1.29	2.76	0.47	0.34
CaO	2.13	4.60	20.44	21.81	6.22	2.63	8.46	11.91	0.52	24.04	13.18
TiO ₂	1.47	1.02	1.69	1.29	0.73	0.20	1.94	0.51	2.02	0.92	0.94
SO ₃	3.04	1.32	18.82	10.69	8.88	3.75	12.07	16.99	0.75	19.83	18.81
Fe ₂ O ₃	11.89	21.35	7.74	6.77	25.50	25.25	11.05	11.38	4.59	10.00	19.73
Total:	100.00	99.05	100.00	99.32	100.00	100.00	100.00	100.00	100.00	100.00	100.00
Ash	12.46	13.03	8.9	8.83	15.97	8.51	4.30	3.29	21.43	9.08	12.42

Table II.D.1-4. Sample Collection Data for Zap and Rosebud Flames.

Run #	Sample	% Ash	Collection Point	Collection Time Minutes	Wt. of Sample Collected (mg)	Percent Weight Loss in TGA*	
						Cyclone Fraction	Preseparator Fraction
1	200 x 325 Dry Rosebud	12.7	7 cm above Ignition Point (in flame)	2	356.0	62.24	---
4	200 x 325 Dry Zap	7.3	7 cm above Ignition Point (in flame)	3	158.8	59.42	---
2	200 x 325 Dry Rosebud	12.7	In Stack 75 cm above Injector	10	81.5	---	6.10
10	200 x 325 Dry Zap	7.3	In Stack 75 cm above Injector	20	22.1	---	3.43

* TGA analysis in air at 30K/min to 900°C

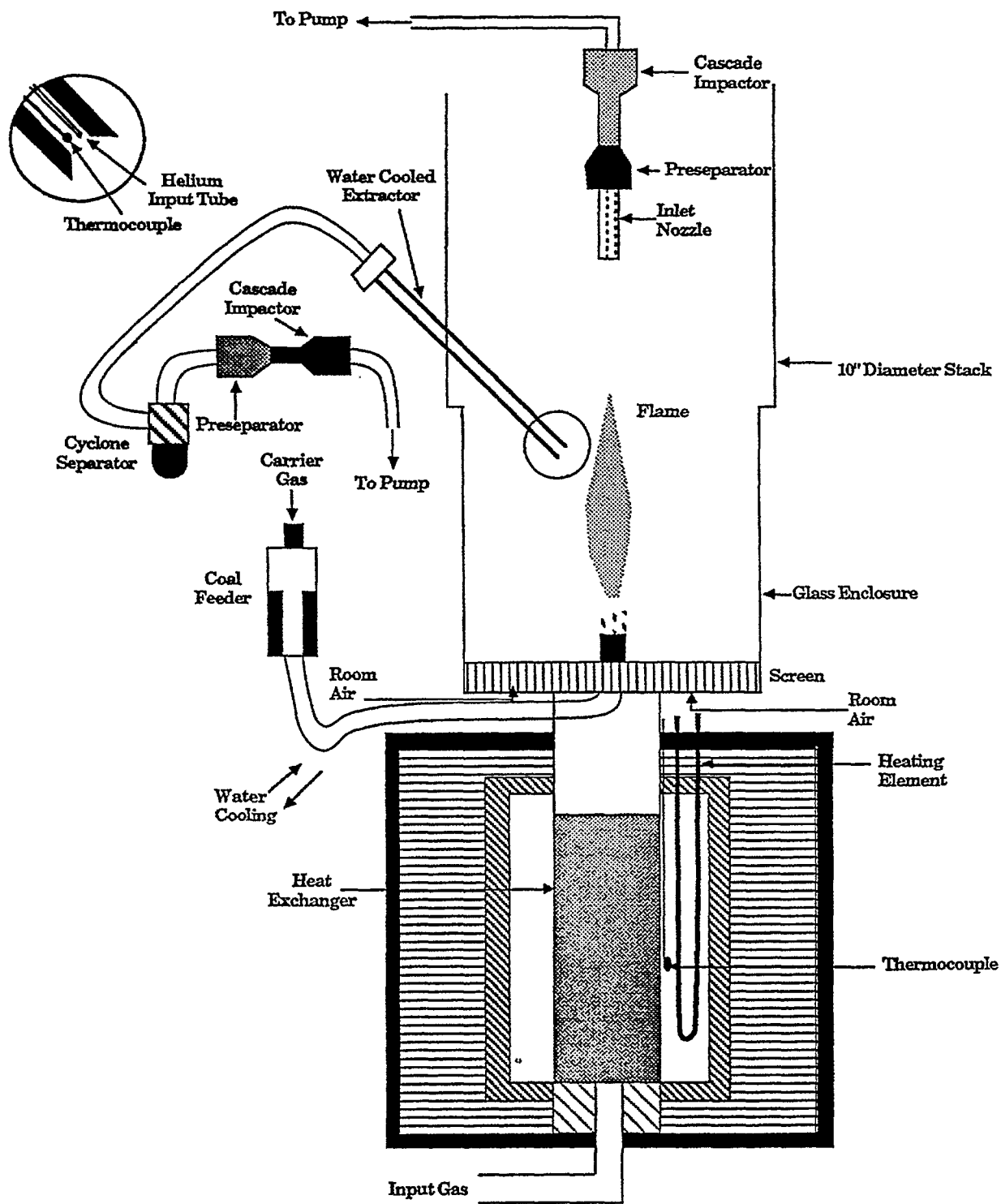


Figure II.D.1-1. Probes for Char and Ash Collection from the Transparent Wall Reactor.

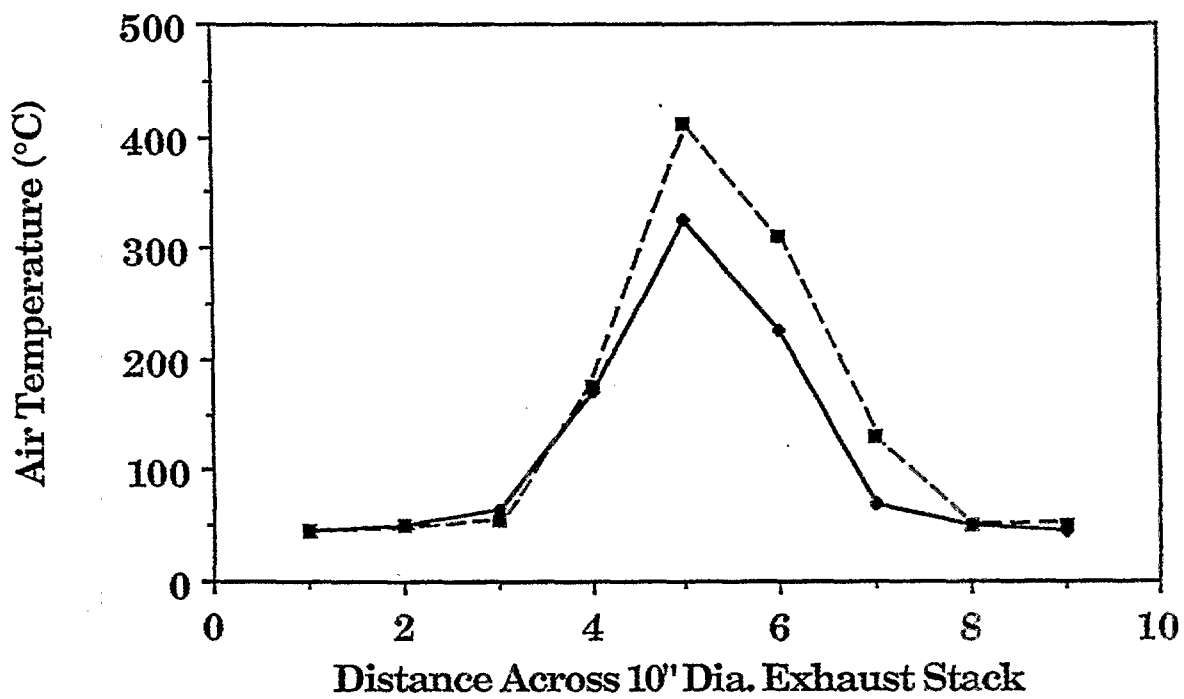


Figure II.D.1-2. Air Temperature Profile Across TWR Exhaust Stack with Rosebud (200x325) Flame On. Distance Above Injector: ■ , 70 cm; ◆ , 75 cm.

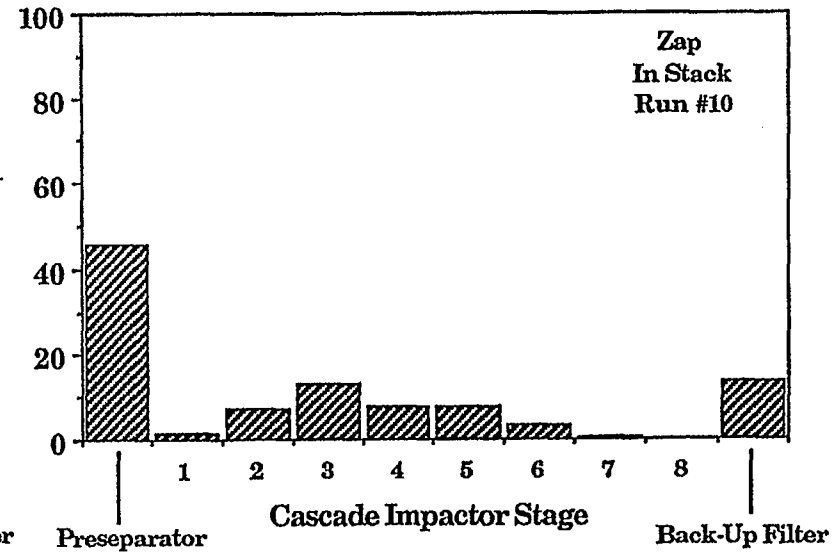
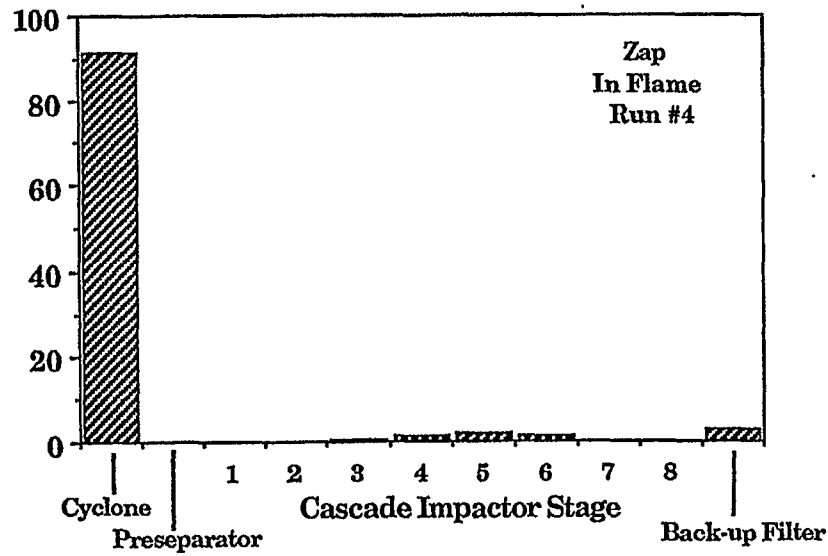
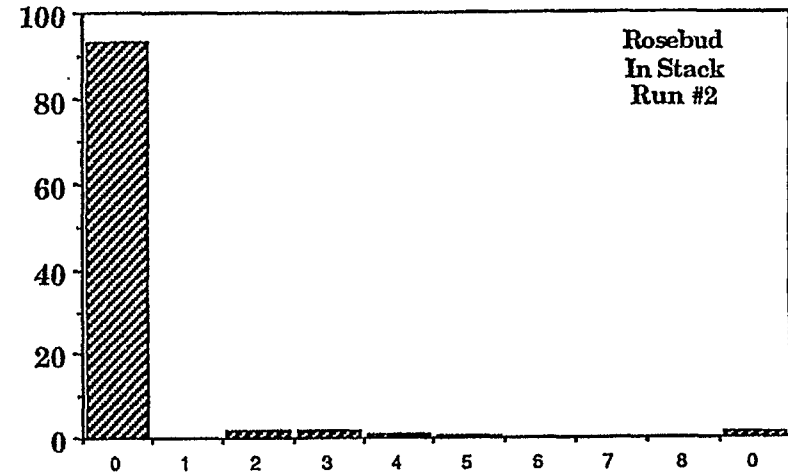
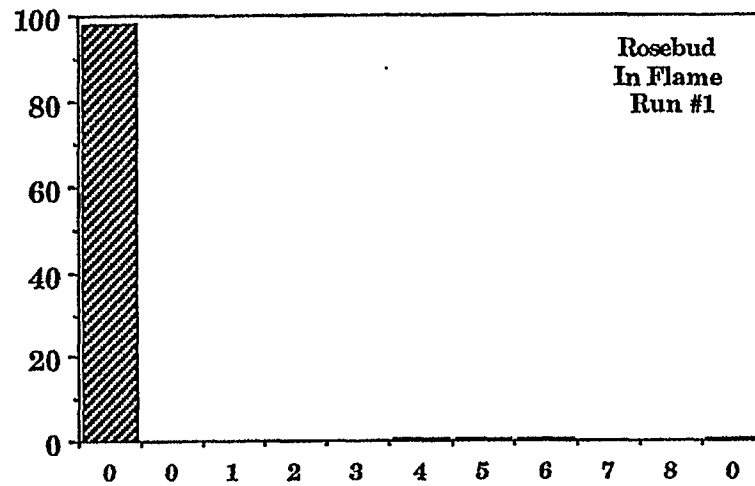


Figure II.D.1-3. Particle Separation Distributions for In Flame and In Stack Collections for Rosebud Subbituminous Coal and Zap Lignite.



Figure II.D.1-4. SEM Microphotograph of Cyclone Fraction of In Flame Collection for Rosebud Coal. Magnification: X400.



Figure II.D.1-5. SEM Microphotograph of Cyclone Fraction of In Flame Collection for Zap Lignite. Magnification: X400.

lignite sample, there is more material collected downstream of the large particle separators than for the Rosebud. Figure II.D.1-6 compares two stages of in-stack collection for the Zap, and clearly shows the individual and spheres. These photomicrographs also indicate the particle sizing ability of the cascade impactor.

To verify a difference in the ability of the starting material to "shed" ash, samples of Zap and Rosebud pyrolysis chars were quantitatively combusted in the entrained flow reactor to various levels of burnoff. The partially combusted material was collected in a cyclone separator that would clean the char of the smaller released ash and any fragmented particles. TGA weight loss analysis was then performed on the combustion char to indicate the fraction of ash present in the particles, and from this, the percent ash retained from the starting material can be calculated by

$$\text{percent ash retained} = \frac{\text{percent combustion sample} \times \text{percent ash in combustion sample}}{\text{percent ash in starting material}}$$

Table II.D.1-5 presents the percent ash retained values for several levels of combustion. The data appear to indicate two points: 1) the samples shed to a relatively constant ash level early in the combustion process, and 2) the Zap initially sheds more of its ash than the Rosebud.

To study the mineral matter to fly ash transformation, a comparison was made by SEM/dispersive x-ray analysis of the solidified ash spheres on the Zap char's surface with particles collected in the preseparator above the flame in the TWR. The ash spheres on the chars surface are rich in Ca, moderately rich in Al, and Si and have varying amounts of Fe, K and Mg. Representative qualitative analyses for these particles are presented in Table II.D.1-6. It appears that the coal's organically bound calcium accumulates in the form of molten liquids, along with the fine clay and pyrite particles.

Figure II.D.1-7a shows a photomicrograph of particles collected above the flame. Some of these particles have melted to form spheres and some have not. Qualitative analyses of the numbered particles are presented in Table II.D.1-7. In the figure, samples 1 and 2, which appear to have melted and crystallized, are almost pure iron oxide. Figure II.D.1-7b shows a close-up of the highly crystallized surface structure for these kinds of particles. Sample 3, which has not melted, is almost pure calcite. Sample 4 shows a region which has not melted and which is almost pure quartz, (like sample 5), and a part which has melted and which is a mixture of elements. Particles 1-5 appear to have been derived from individual extraneous mineral grains (pyrite, calcite, and quartz) without significant contamination by other mineral components. Small spheres (6 and 7, and those captured on the stages of the cascade impactor) as well as larger spheres (8 and 9) are mixtures of Si, Al, Ca, Fe, K, and Mg, like the particles attached to the chars surface captured in the flame.

Also of interest is that many of the pure mineral particles are of the same size (some larger) than the starting coal particles. Differences in color, magnetic attraction, and density (hollow vs solid) have also been observed.

SEM/dispersive x-ray analysis was also performed on individual ash spheres that were recovered from the eight stages of the cascade impactor for an "in-stack" ash collection from 200 x 325 mesh Zap lignite. The small spheres (< 10 μm in diameter) apparently are shed from the coal particles during the combustion process and contain inorganic components that are intrinsic to the coal.

Ash collection experiments were also performed in the entrained flow reactor (EFR), a schematic of which is shown in Fig. II.D.1-8. This system allows the use of smaller quantities of coal and provides for more complete collection of the ash. Experiments were done at different residence times to achieve a range of char burnouts. The products were collected in a cyclone/cascade impactor system for analysis by TGA for char burnout, SEM/x-ray for mineral analysis, and Quantimet for particle size distribution.

Table II.D.1-5. Percent Ash Retained in Partially Combusted Samples.

Sample	% Sample Recovered after Partial Combustion	% Ash Retained
Zap*	39.0	44.7
	27.0	37.2
	16.5	40.0
	7.6	35.0
Rosebud**	66.7	66.1
	28.0	71.0
	22.3	75.4
	21.1	67.1

* 900°C Zap Char

** 1500°C Rosebud Char

Table II.D.1-6.

**REPRESENTATIVE QUALITATIVE* X-RAY ANALYSIS FOR ASH SPHERES ON CHAR
PARTICLE SURFACES AS SHOWN IN FIG. II.D-5**

Values are in weight percent

Mineral Component	A	B	C	D	E	F
Al	4.89	0.93	0.69	1.21	1.37	1.86
Si	6.10	0.85	5.05	0.56	1.78	1.49
Fe	0.65	3.47	0.73	0	0	1.21
Mg	2.70	1.45	1.21	1.53	1.53	3.31
Ca	5.86	11.71	3.31	2.22	2.66	6.62
Ti	0.52	0.08	0.04	0.04	0	0.20
Na	-	0	0	0	0.65	0
K	0	0	0.04	0.04	0.04	0
Sulfur (O)	0.16	0.12	1.05	0.08	0.56	0.48
Sulfur (M)	0	0	0	2.14	1.53	0
x in FeS _x	0	0	0	2	2	0
Total Ash	35.86	25.73	19.06	11.87	16.44	22.45

* Not matrix-corrected for coefficient of x-ray absorption for each component.

Table II.D.1-7.

QUALITATIVE* X-RAY ANALYSIS OF ASH PARTICLES PRESENTED IN FIG. II.D-7

Values are in weight percent

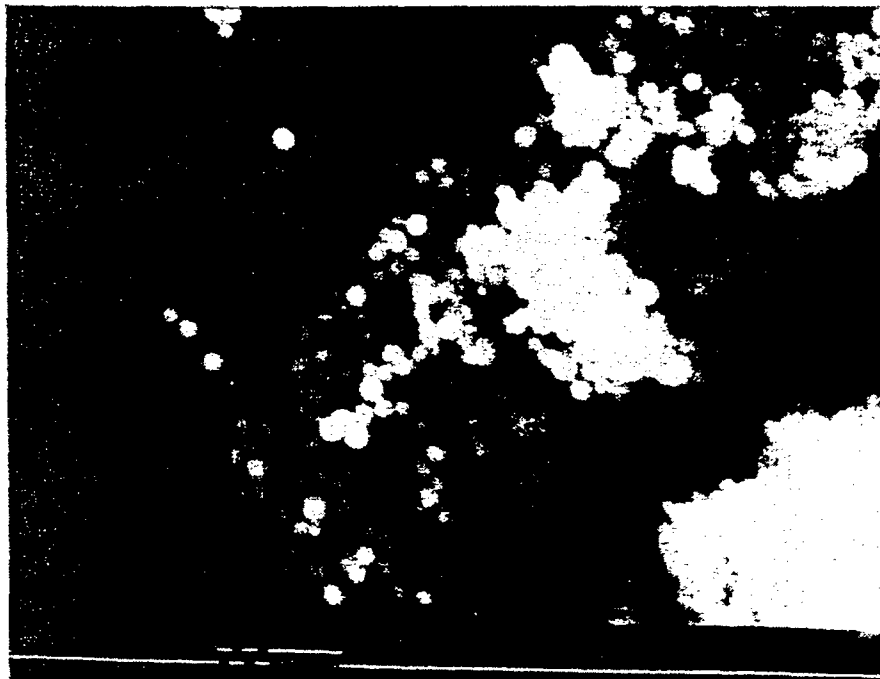
Mineral Component	1	2	3	4 (melted)	4 (not melted)	5	6	7	8	9
Al	0.23	0.19	0.36	12.18	2.52	2.20	9.78	0.84	9.13	9.55
Si	1.21	0.79	0.66	38.28	33.96	65.44	29.82	1.50	29.81	32.07
Fe	86.05	90.16	0.30	1.38	0.54	0.15	0.84	0.72	0.41	0.38
Mg	0.56	0.47	1.08	1.80	1.14	0.78	1.86	2.1	1.02	0.80
Ca	2.75	0.37	78.54	0.66	-	0.10	1.68	3.66	0.38	0.41
Ti	0	0	0.18	0.18	0.06	0	0.06	0.06	0.19	0.03
Na	0	0	0	2.04	0	0	4.14	0	1.18	2.70
K	0	0.09	0	7.14	0.90	0	0.84	0	6.81	5.15
Sulfur (O)	0	0	0	0.06	0	0.05	0.06	0	0	0
Sulfur (M)	0	0	0.60	0	0	0	0	0	0	0
x in FeS _x	0	0	2	0	0	0	0	0	0	0
Total Ash	129.69	131.41	113.46	125.22	79.98	145.48	101.10	12.36	95.55	102.60

* Not matrix-corrected for coefficient of x-ray absorption for each component.

a



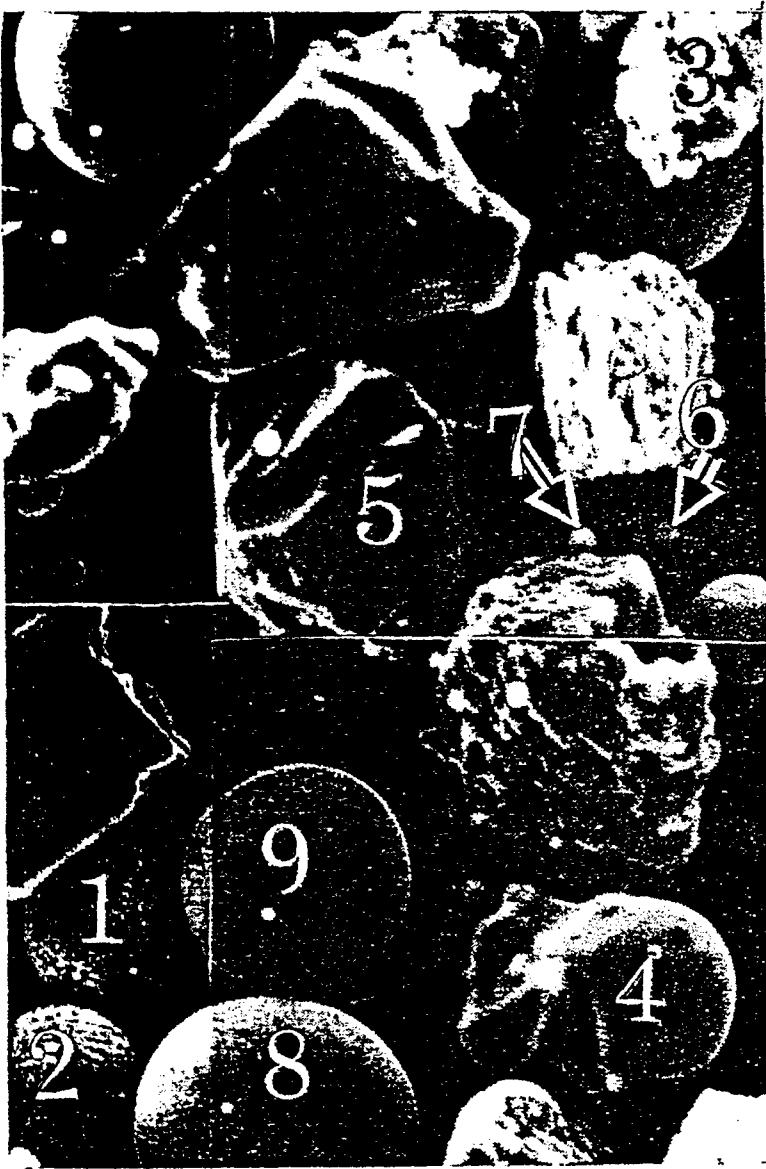
b



10 μm

Figure II.D.1-6. SEM Photomicrographs of Fly Ash Collected Above a Zap Lignite Flame. a) Stage #2 and b) Stage #4 of Cascade Impactor. Magnification: X910.

a



b

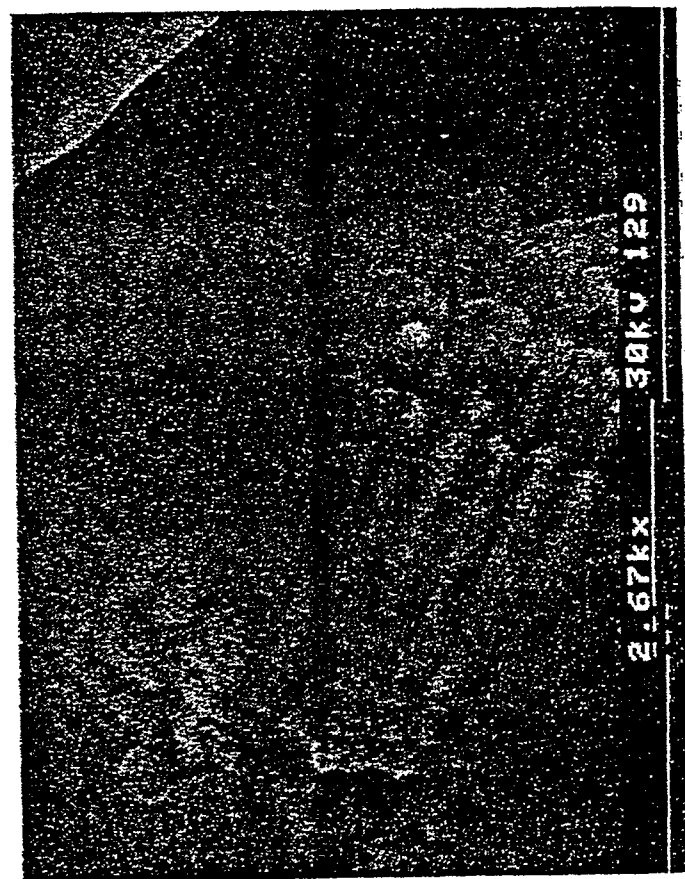


Figure II.D.1-7. SEM Micro Photograph of Fly Ash Collected Above a Zap Lignite Flame, Preseparator Fraction. a) X400 and b) Close-Up of Sample 1, X2,670.

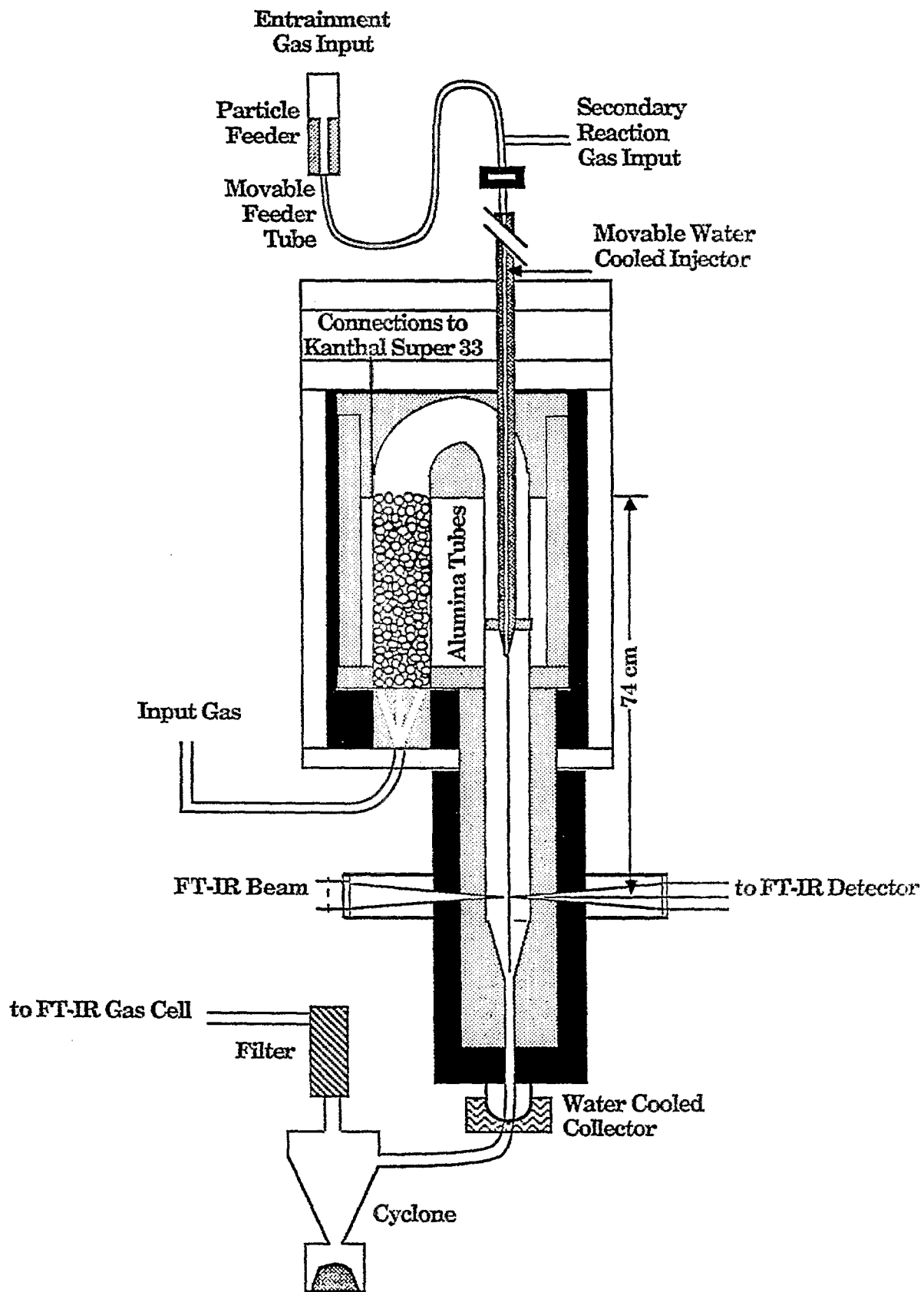


Figure II.D.1-8. Schematic of Ash Collection System Installed on the Entrained Flow Reactor.

A series of ash collection experiments was done in the entrained flow reactor. Five of the eight coals have been run over a series of burnouts ranging from 25 to 100% (see Table II.D.1-8). The results for ash collection are shown in Figs. II.D.1-9 to II.D.1-13. It is apparent that most of the ash is collected in the cyclone rather than the cascade impactor.

Elemental ash recoveries for the Upper Kanawha are shown in Figs. II.D.1-14 to II.D.1-17. These figures indicate that sodium is essentially completely lost, while magnesium is retained only until between 30% and 50% burnout. The unexpectedly high magnesium value for the 30% burnout case is consistent with the range of magnesium contents determined (up to 0.08%). Sulfur is progressively lost as burnout increases. The remaining elements appear to be well recovered (titanium is also consistent with the observed range of up to 0.44%).

In most cases, the extractor material and the cyclone collection appear to have similar compositions, with the cyclone collection possibly somewhat enriched in silicon and iron as compared to the extractor material.

In order to gain a better understanding of the mineral matter distributions, work was performed on density separations of the original feedstocks. Results for the Upper Kanawha are shown in Figs. II.D.1-18 and II.D.1-19. The results indicate that the sink fraction is enriched in silicon and iron, while the remaining elements are fairly uniformly distributed between the float and sink fractions.

II.D.2 Effects of Minerals on Char Reactivity

The reactivity of chars prepared from both raw and demineralized coals was measured. The chars were prepared by heating in N_2 at $30^\circ C/min$ until $900^\circ C$ was achieved. The char reactivity measurements were made by employing a non-isothermal technique using a TGA. With an air flow of 40 cc/min and a N_2 purge flow of 40 cc/min, the samples were heated at a rate of $30^\circ C/min$ until $900^\circ C$ was reached. The resulting critical temperatures (defined as the temperature at which the derivative of the weight loss reaches 0.11 weight fraction/min) are plotted in Fig. II.D.2-1 as a function of oxygen in the parent coal.

The trend for the raw samples is an increase in reactivity (decreasing T_{cr}) with increasing coal oxygen content, while the slope for the demineralized samples seems to flatten out at approximately $520^\circ C$. Above 10% oxygen, the mineral content of the coal dominates the char reactivity, increasing the char's reactivity (lower T_{cr}) compared to the demineralized samples. The reason for this increase appears to be the catalytic activity of the organically bound alkali metals, particularly the Ca, since Ca is naturally abundant in coals. Below 10% oxygen content, the raw coals have a lower reactivity (higher T_{cr}) than the demineralized samples. The reason for this is oxidation due to the demineralization process.

In order to ascertain why there is a systematic increase in reactivity with coal oxygen content when reactivity is thought to depend on calcium content, the calcium concentration of coals from the Exxon sample bank were plotted as a function of oxygen concentrations in Fig. II.D.2-2. Above 8% oxygen, there is a systematic increase in Ca with increasing oxygen.

Eight percent is the level at which carboxyl groups appear in coal (Blom, et al., 1957). This suggests that, above 8% oxygen content, there is a systematic increase in the amount of calcium ion-exchanged on the carboxyl groups and it is this calcium component which acts as a catalyst.

In order to further understand the roles played by the ion-exchangeable cations in char reactivity, a 200 x 325 mesh sieved fraction of Zap Indian Head, demineralized according to the standard Bishop and Ward (1958) technique, was subjected to ion-exchange with Ca, Mg, K, and Na using a modification of the procedure by Hengel and Walker (1984). The amount ion-exchanged onto the demineralized Zap lignite was controlled by using different molar solutions of the acetate salt. In the case of Ca, 1.5 M; 1.0 M; 0.5 M; 0.3 M; 0.1 M; and 0.05 M acetate salt solutions were employed. In the case of Mg, 1.5 M; and 0.05 M acetate salt solutions were employed. In the case of K, 1.5 M; 0.3 M; 0.1 M; and 0.04 M acetate

Table II.D.1-8. Actual Burnouts For Runs Completed

	<u>Burnout Desired</u>			
	<u>25%</u>	<u>50%</u>	<u>75%</u>	<u>100%</u>
Pocahontas #3 (PC)	22	(43)	(70)	(100)
Upper Freeport (UF)	22	(48)	(80)	100
Pittsburgh #8 (PT)	15	61	(75)	(100)
Upper Kanawha (UK)	30	50	87	100
Rosebud (RB)	---	---	---	100

() Without Extractor Washings

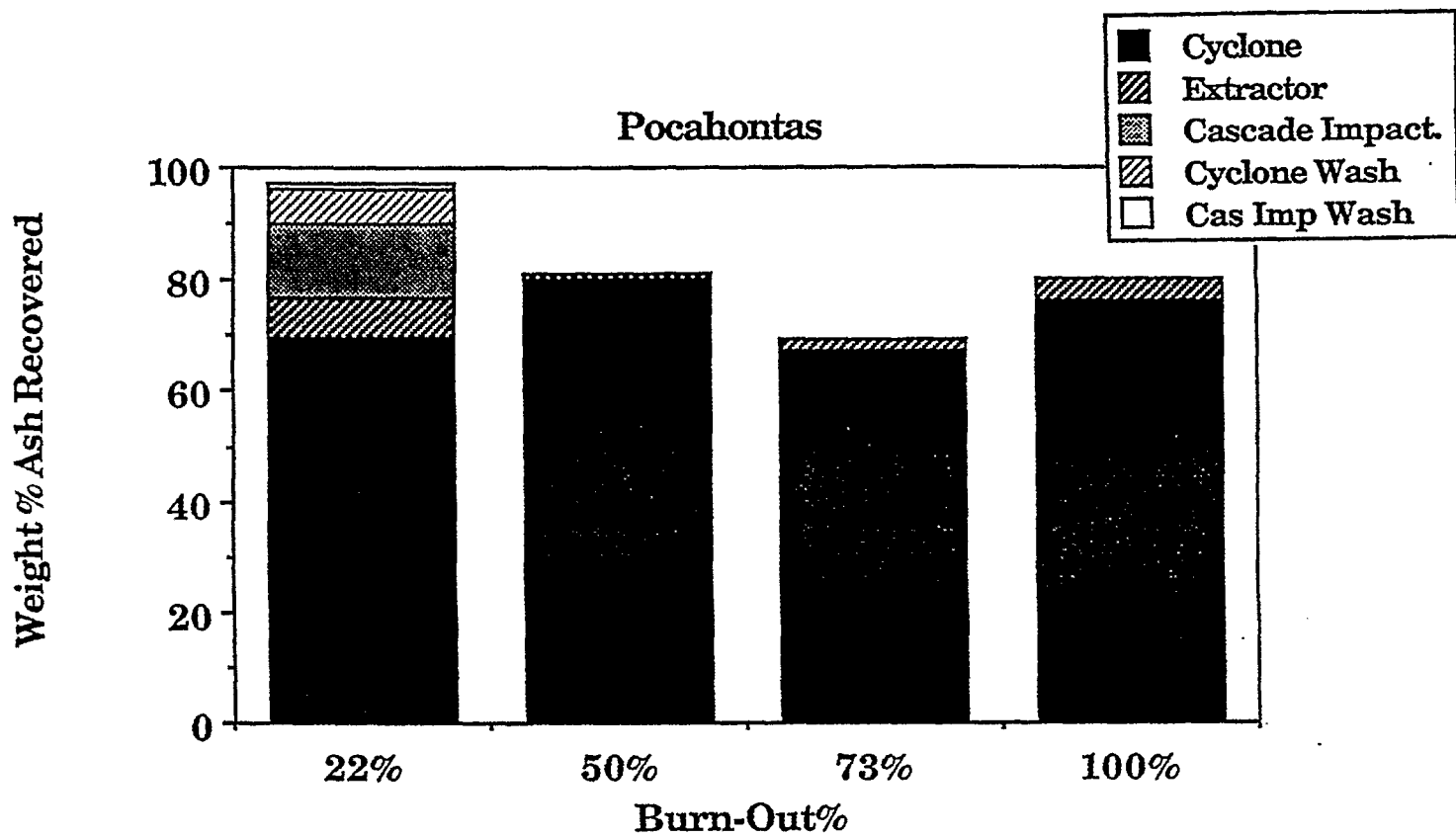


Figure II.D.1-9. Ash Recovery from Experiments over a Range of Burn-outs for Pocahontas Coal.

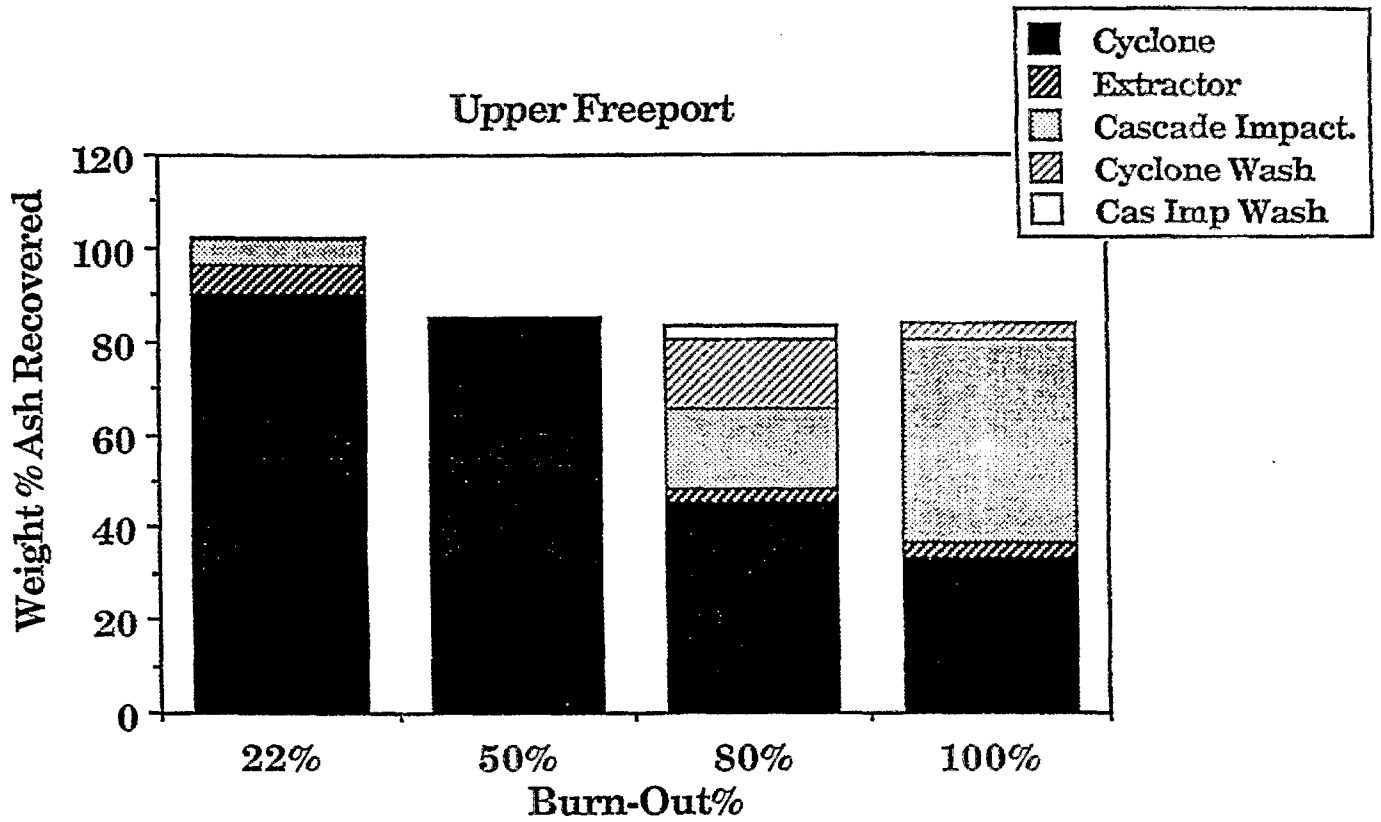


Figure II.D.1-10. Ash Collection from Experiments over a Range of Burn-outs for Upper Freeport Coal.

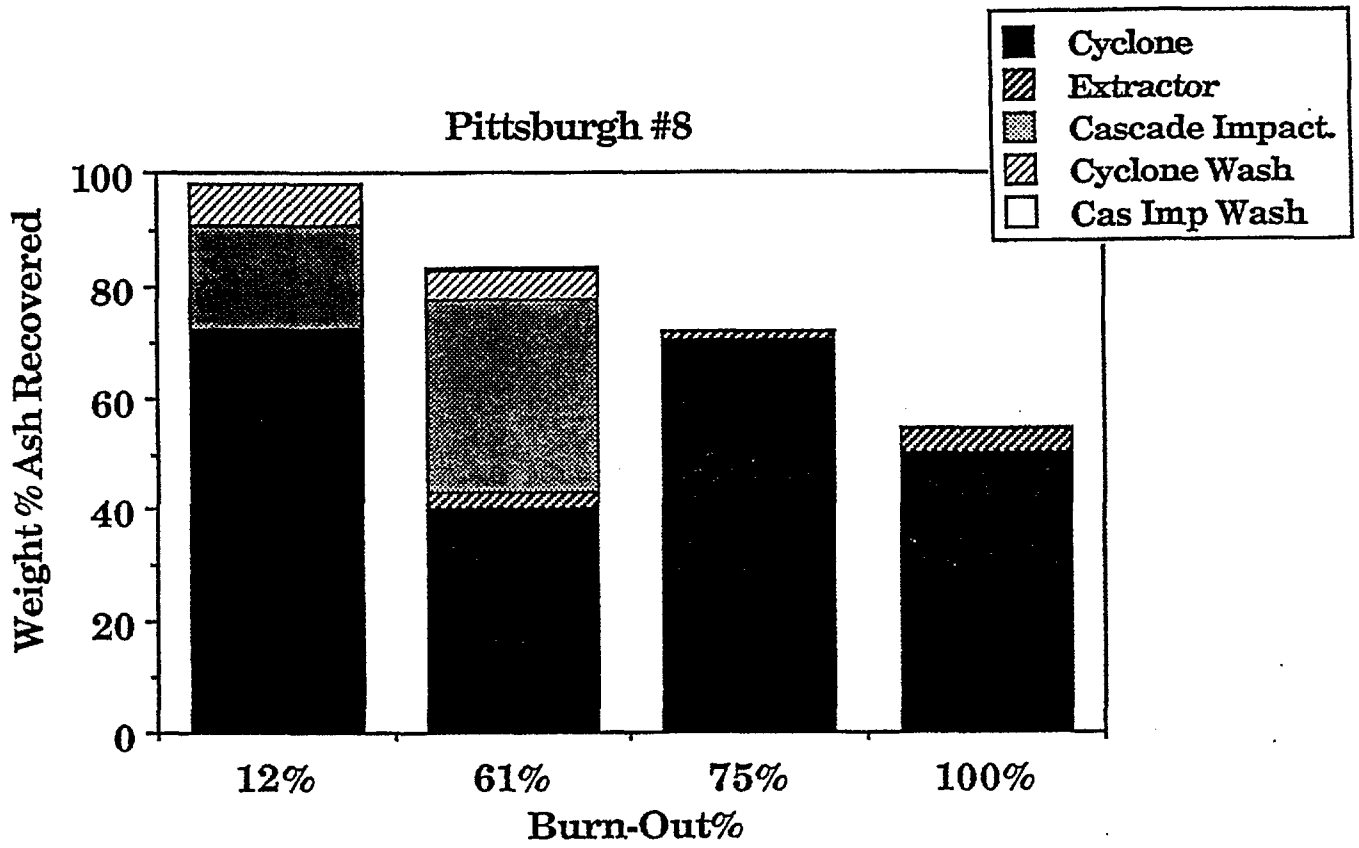


Figure II.D.1-11. Ash Collection from Experiments over a Range of Burn-outs for Pittsburgh No. 8 Coal.

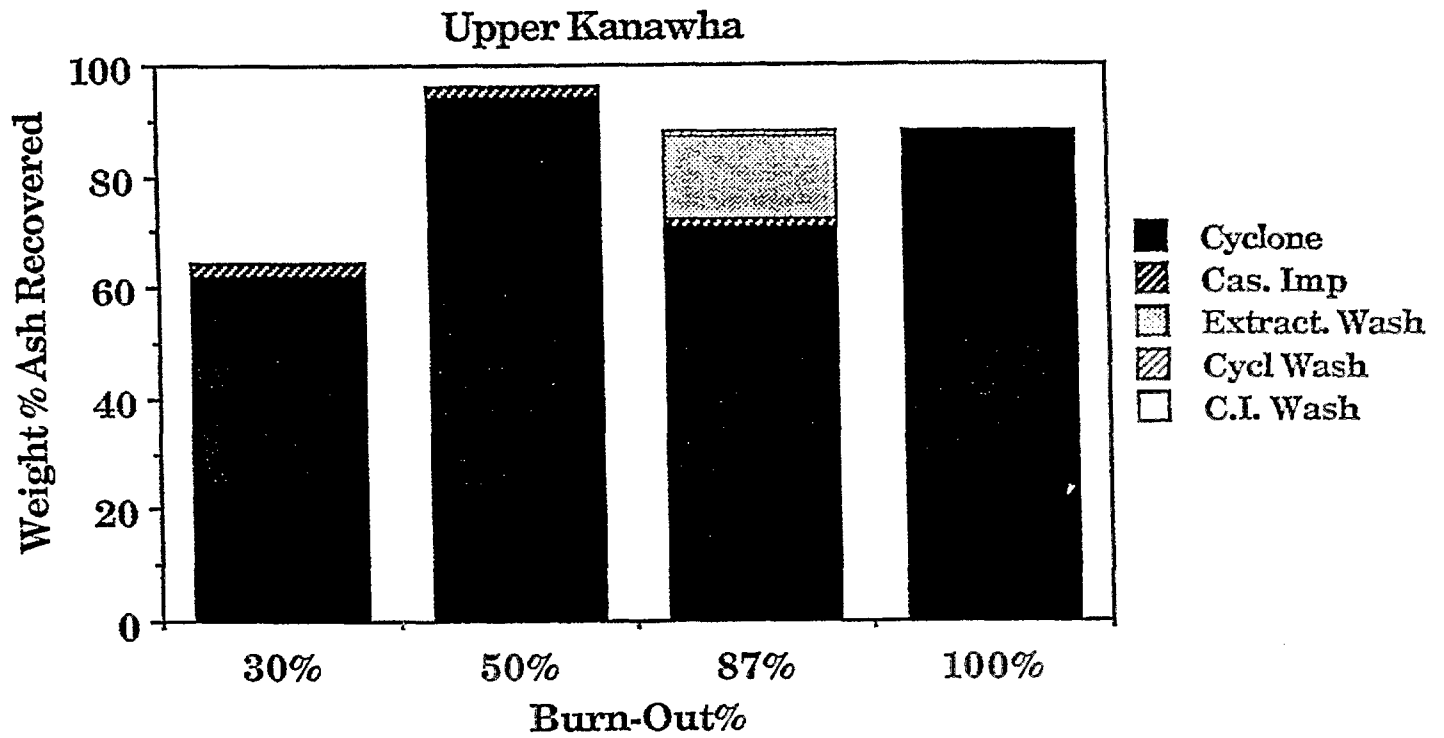


Figure I.D.1-12. Ash Collection from Experiments over a Range of Burn-outs for Upper Kanawha Coal.

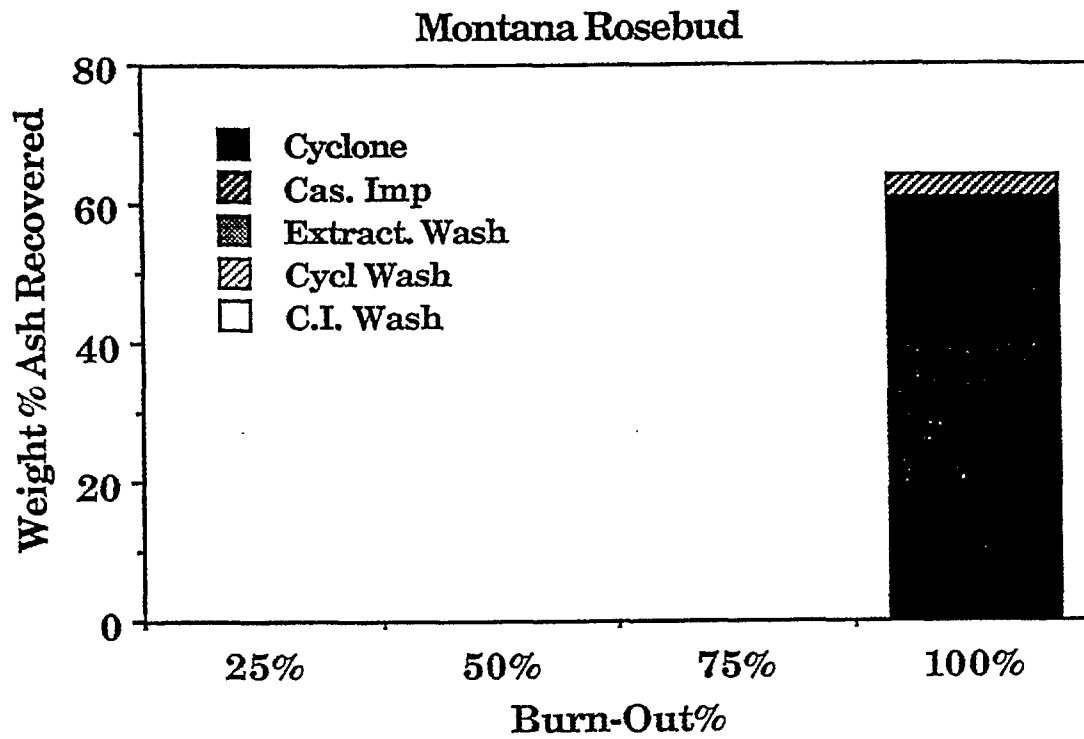


Figure II.D.1-13. Ash Collection from Experiments over a Range of Burn-outs for Montana Rosebud Coal.

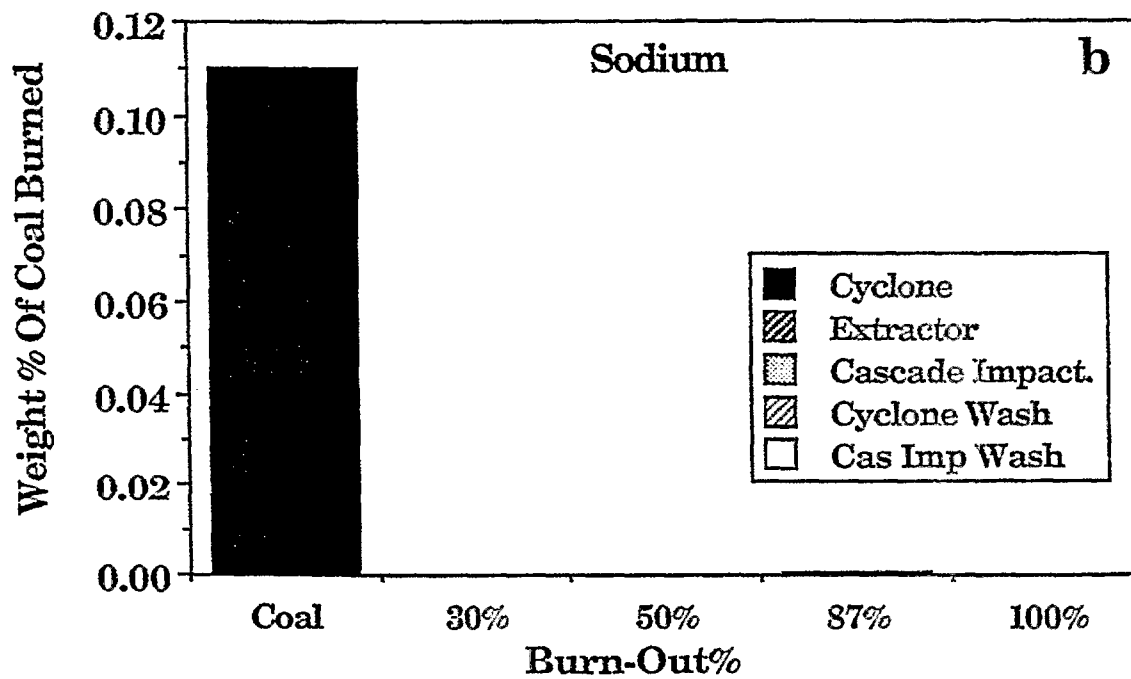
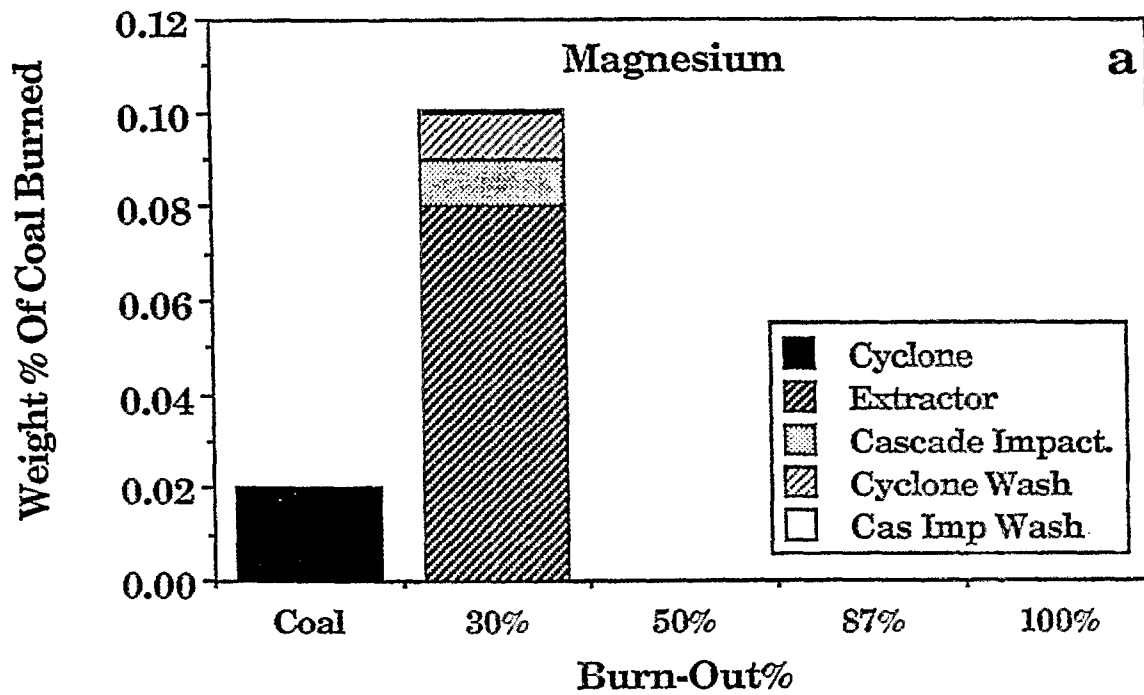


Figure II.D 1-14. Elemental Recoveries for Experiments over a Range of Burn-outs for Upper Kanawha Coal.

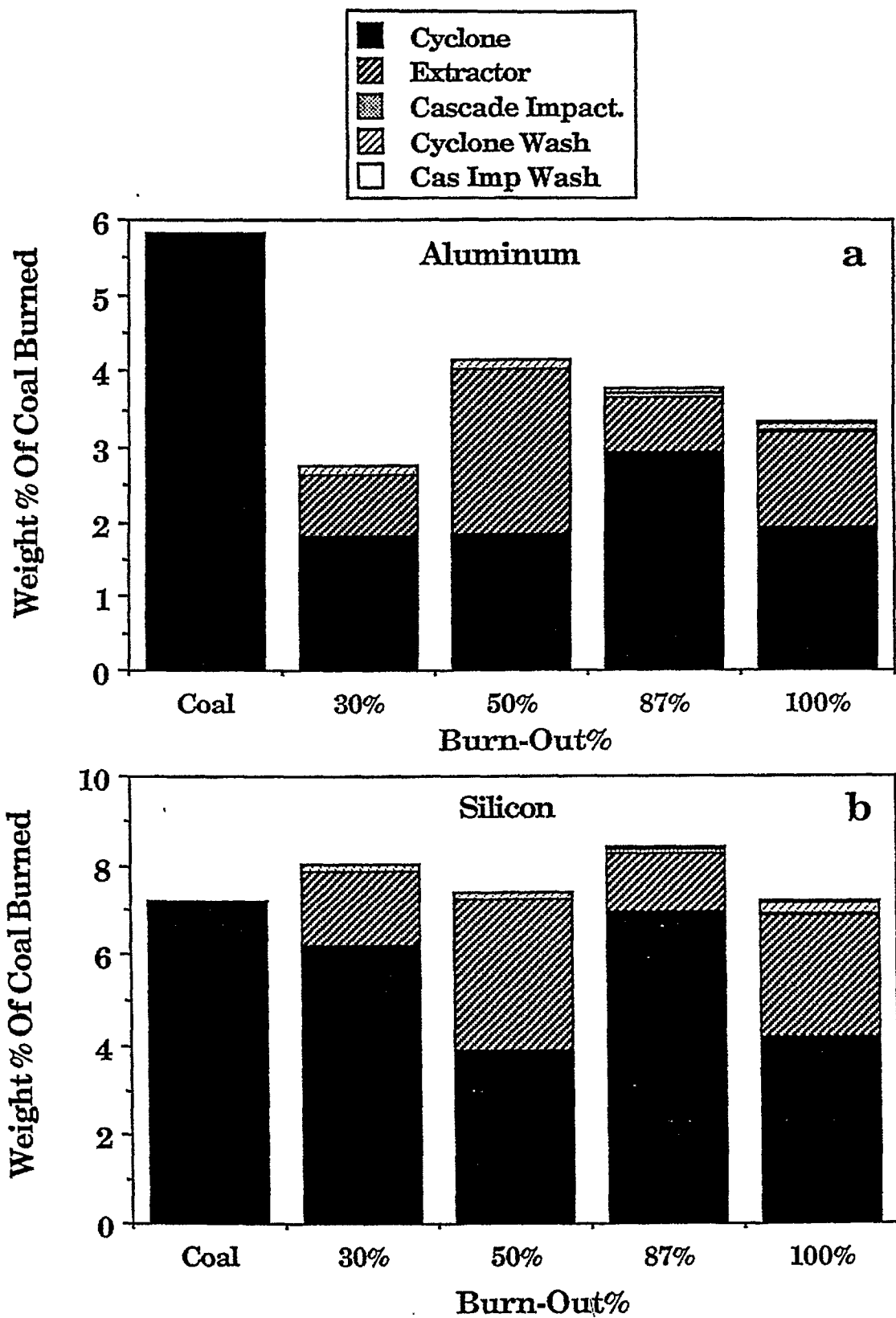


Figure II.D.1-15. Elemental Recoveries for Experiments over a Range of Burn-outs for Upper Kanawha Coal.

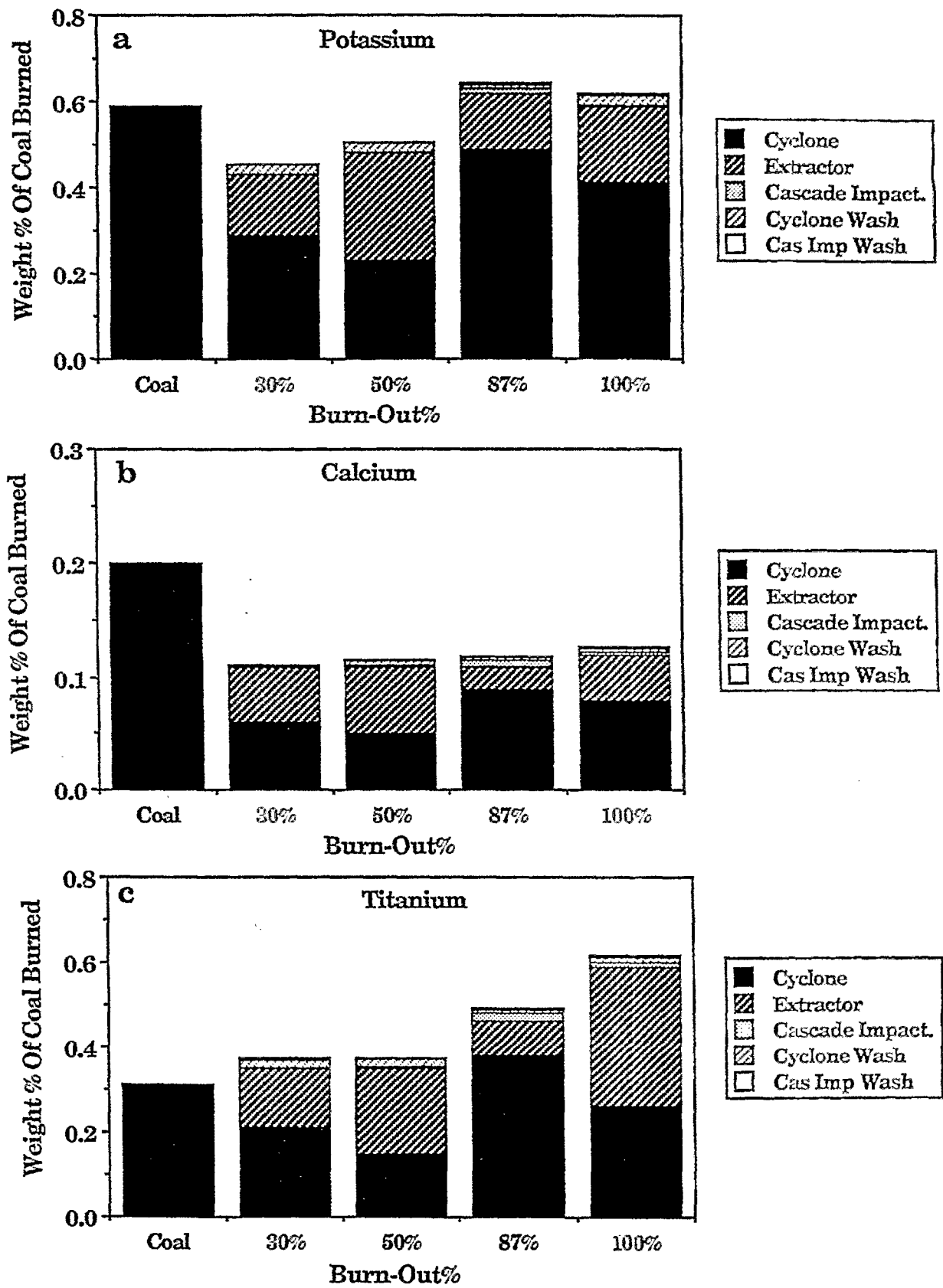


Figure II.D.1-16. Elemental Recoveries for Experiments over a Range of Burn-outs for Upper Kanawha Coal.

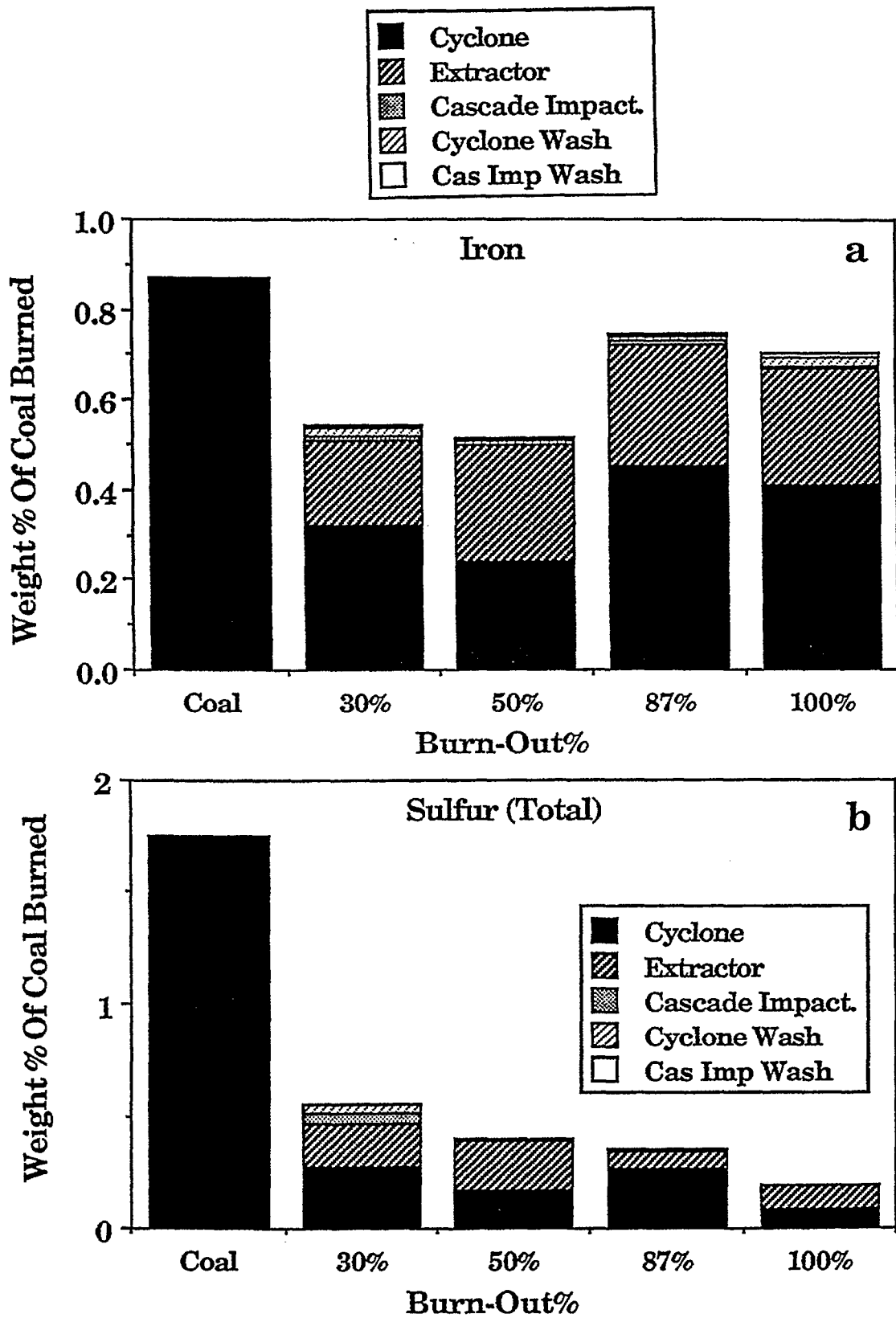


Figure II.D.1-17. Elemental Analysis of Upper Kanawha Density Separation (1.65 SG).

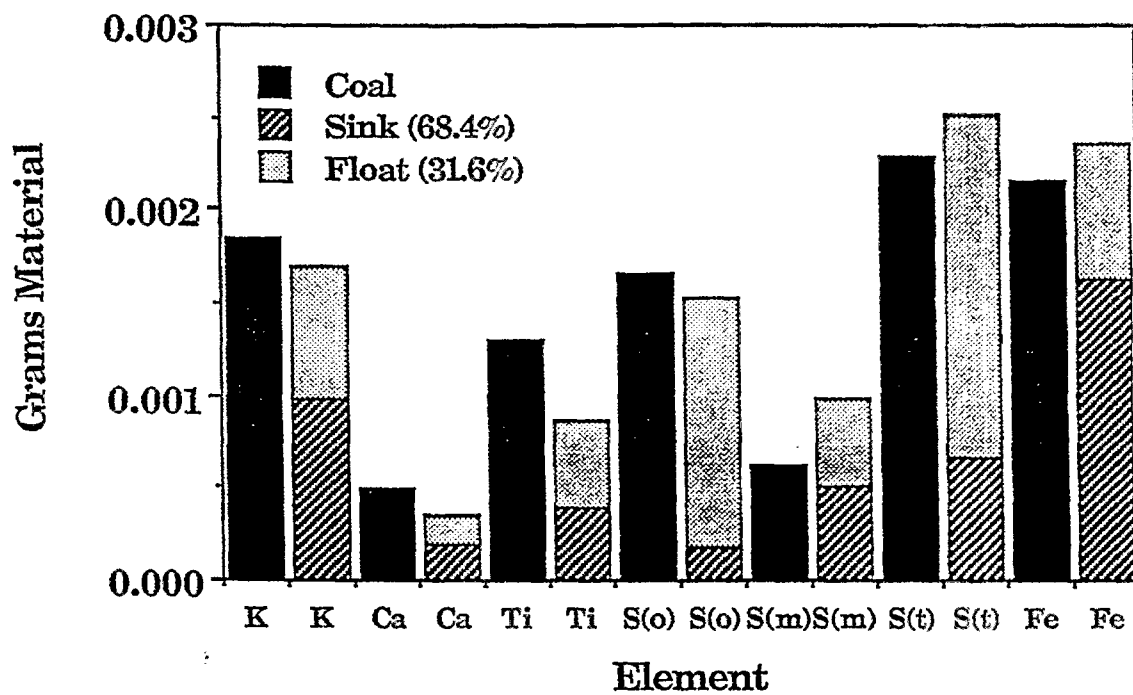


Figure II.D.1-18. Elemental Analysis of Upper Kanawha Density Separation (1.65 SG).

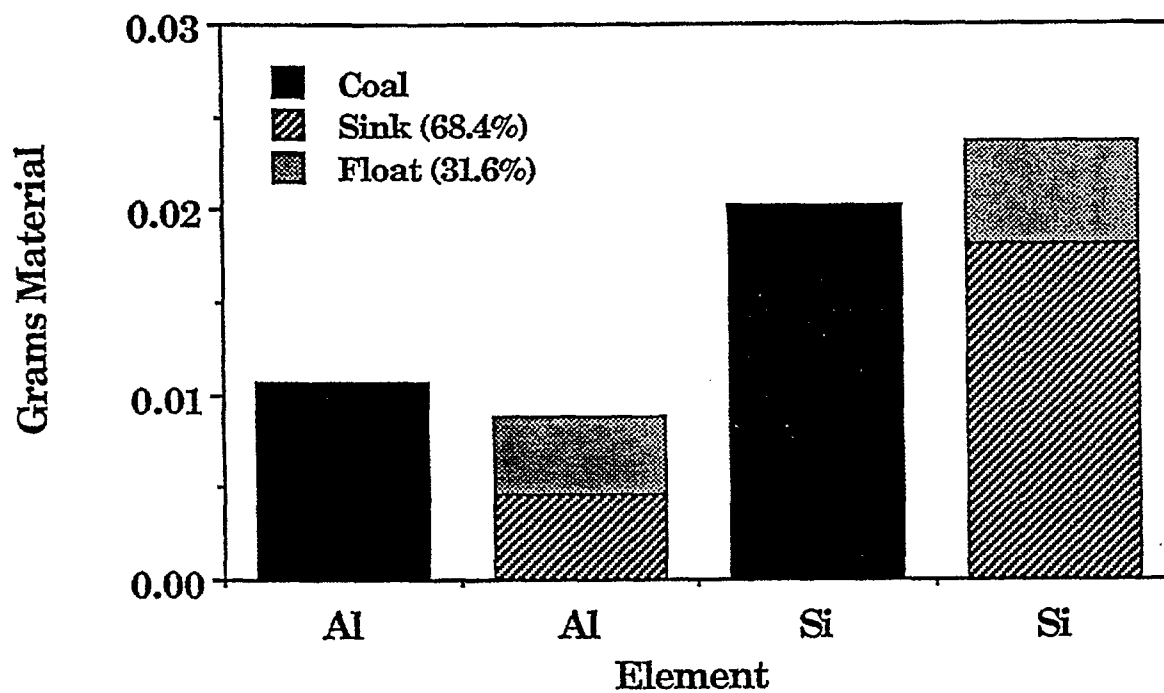


Figure II.D.1-19. Elemental Analysis of Upper Kanawha Density Separation (1.65 SG).

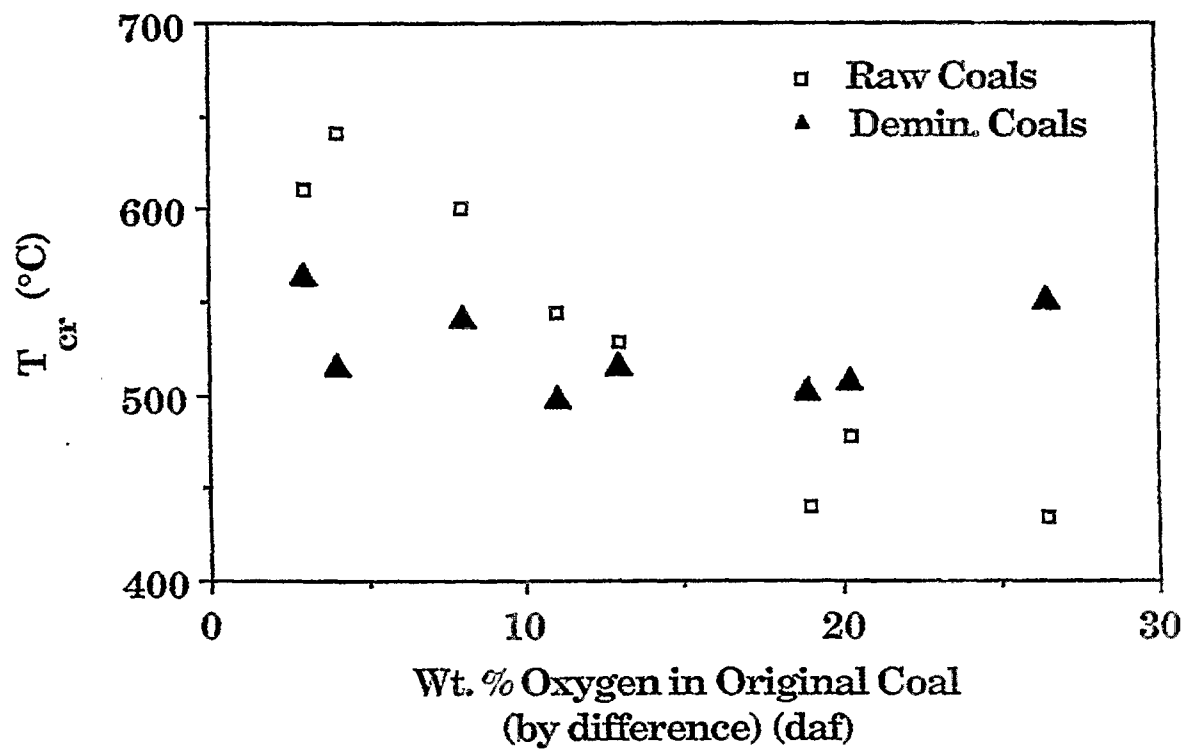


Figure II.D.2-1. Variation of Reactivity with Coal Oxygen Content for Raw and Demineralized Argonne Coals.

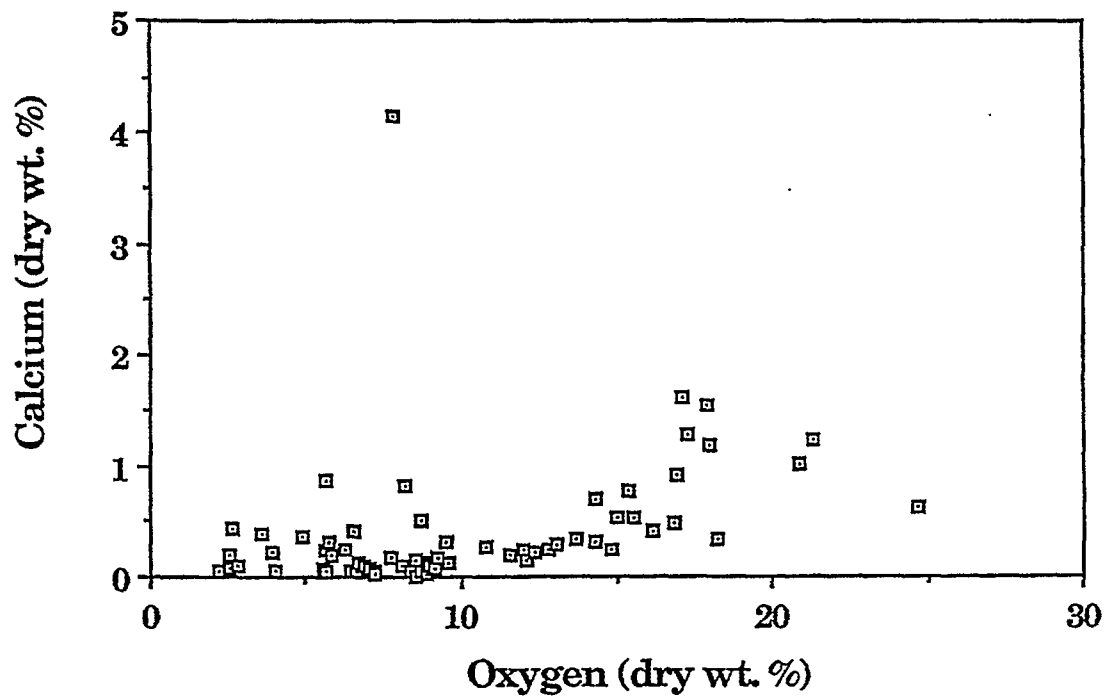


Figure II.D.2-2. Weight Percent Calcium as a Function of Oxygen in Coal.

salt solutions were employed, and in the case of Na, 1.5 M; 0.3 M; 0.1 M; and 0.05 M acetate salt solutions were used. Slurries of 5 grams of demineralized Zap and 125 ml of the desired loading solution were stirred at 57°C for 5½ hours. The solution was allowed to cool at room temperature and stirring was continued for an additional 22½ hours. The slurry was filtered, washed with deionized water and dried at 105°C in a vacuum oven for approximately two hours. The amount of cation exchanged was determined by x-ray analysis.

Chars were prepared from the cation loaded coals by heating in N₂ at 30°C/min to 900°C and these were subjected to the non-isothermal reactivity test in air. The char from demineralized Zap coal is far less reactive (higher T_{cr}) than the raw Zap char. As previously discussed, this is probably due to the removal of the organically bound alkali metals which are thought to dominate char reactivity in coals possessing more than 10% oxygen. If this is true, then cation loading should result in the resoration of char reactivity.

Plotted in Fig. II.D.2-3 is the variation of reactivity with the cation loadings. The Ca and Mg loadings effectively restored the reactivity of the demineralized Zap. In the case of Ca, the only significant change in reactivity occurs when the Ca level increase from the 0.01 wt% in the raw demineralized Zap to 1.65 wt% in the 0.05 M loading. Further increase in Ca does not cause any marked increases in reactivity. The low Na and K loadings were so effective in promoting the demineralized Zap char reactivity that the loaded samples yielded values of T_{cr} that were 45°C and 30°C, respectively, less than the T_{cr} of the raw Zap char itself. With high loadings, however, both Na and K lost their ability to increase char reactivity (lower the T_{cr}) and actually demonstrated hindering effects. The 1.5 M Na and K loadings gave values of T_{cr} which were higher by 129°C and 85°C, respectively, than the demineralized Zap sample. Surface area measurements on the raw and cation-loaded samples were done in these cases. However, significant differences were not observed between the raw and cation-loaded coals in either case. Consequently, the hindering effect must manifest itself either during the char formation process or the gasification process.

CO₂ char reactivity measurements were done on chars produced from raw, demineralized and loaded demineralized Zap samples by heating in N₂ at 30°C/min until 1000°C was achieved. The CO₂ reactivity followed similar trends as the air reactivities as shown in Fig. II.D.2-4.

A model was developed to predict the intrinsic reactivity (T_{cr}) of char based on calcium content for coals greater than 10% oxygen, while holding the extent of pyrolysis and heating rate constant. For a standard test:

$$T_{cr} = 520 + \alpha (Ca \text{ wt}\% - (\beta * \text{carbonate})) \quad (\text{II.D-1})$$

where, 520 represents the approximate T_{cr} for demineralized coals, α is the slope from the plot of T_{cr} vs Ca wt% in Fig. II.D.2-3a, β is a constant and the carbonate value is that obtained from quantitative FT-IR analysis.

Figure II.D.2-5a displays the correlation between actual T_{cr} and predicted T_{cr} with $\beta = 0$. Since it is the organically bound Ca which is thought to be catalytically active, a much better correlation is obtained when calcite corrections are included in the model (Fig. II.D.2-5b).

In order to better understand why the organically bound Ca offers catalytic activity and calcite does not, SEM Ca dot maps were done for a calcium loaded demineralized Zap coal and an Exxon sample which, from FT-IR analysis, was known to be abundant in calcite. The maps in Fig. II.D.2-6 indicate that the organically bound Ca is very well distributed throughout the Zap coal while the calcite in the Exxon coal exists in large clusters. This is consistent with the fact that the Ca in the calcite form is not nearly as effective as a catalyst when compared to the ion-exchanged Ca.

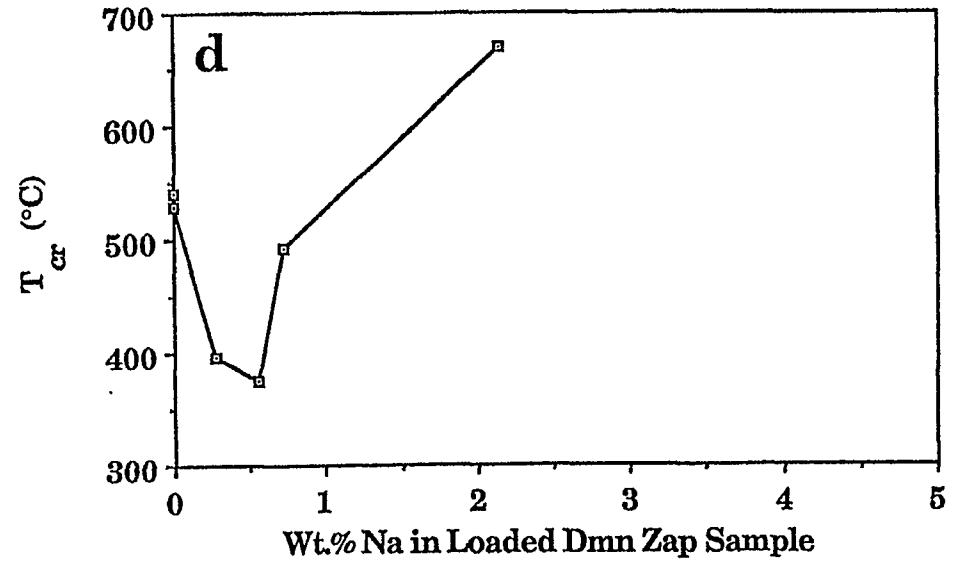
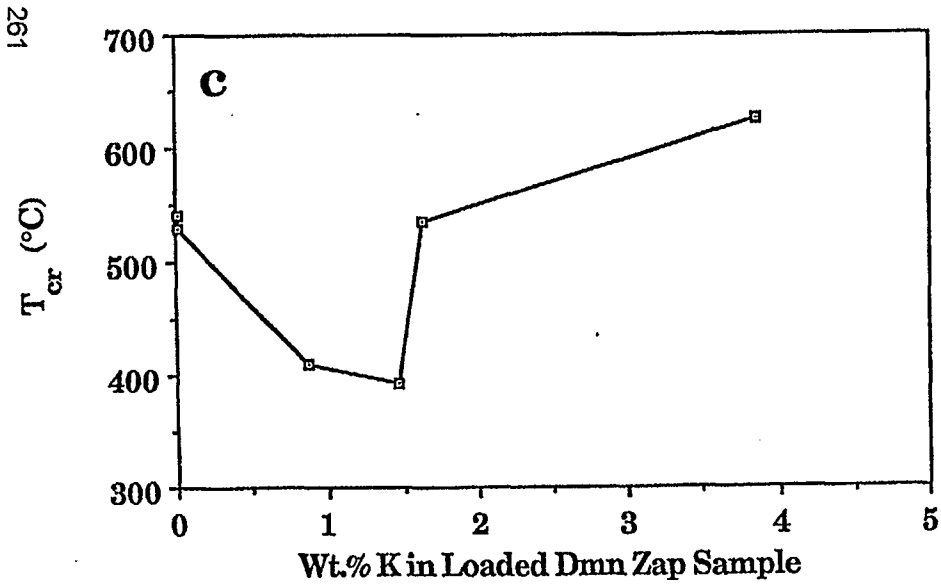
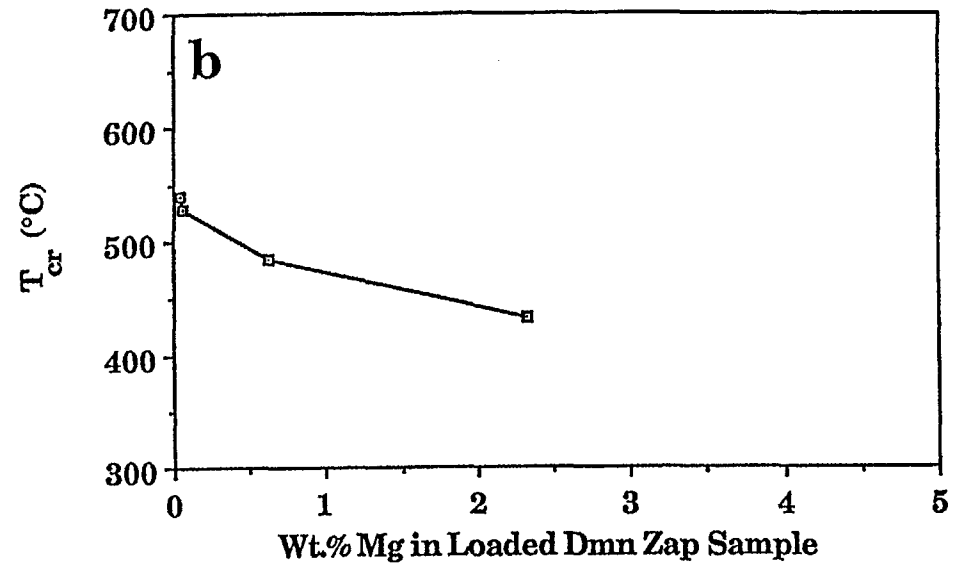
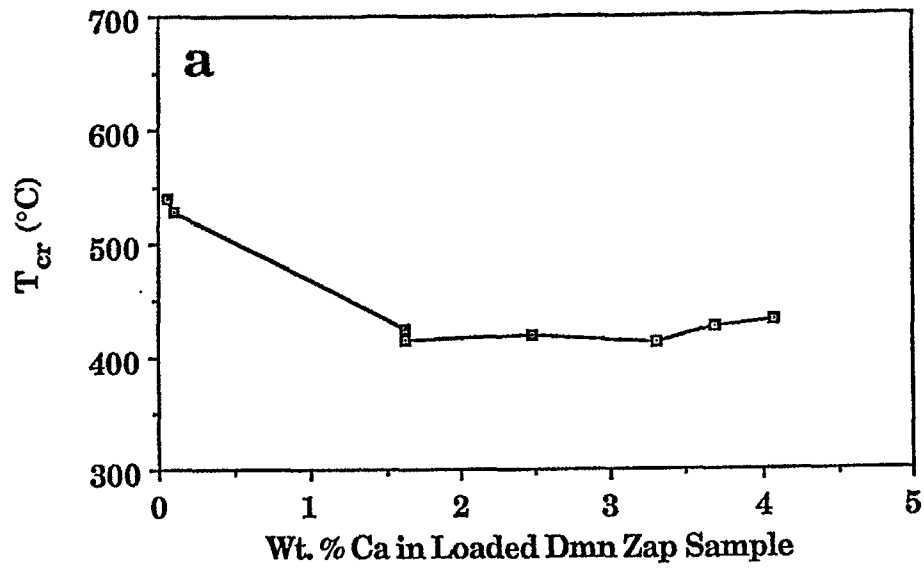


Figure II.D.2-3. Variation of Reactivity with Cation Loadings for Demineralized Zap Coal.
 a) Calcium; b) Magnesium; c) Potassium; d) Sodium.

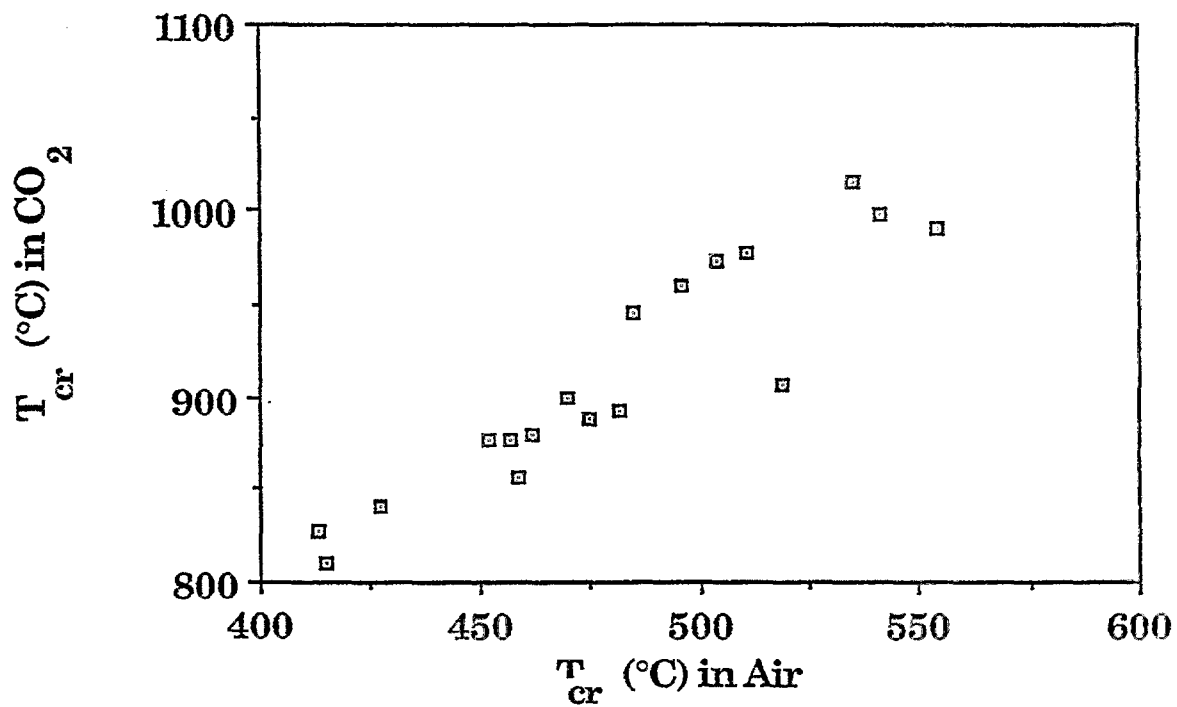


Figure II.D.2-4. Correlation Between CO_2 and Air Reactivity Parameters

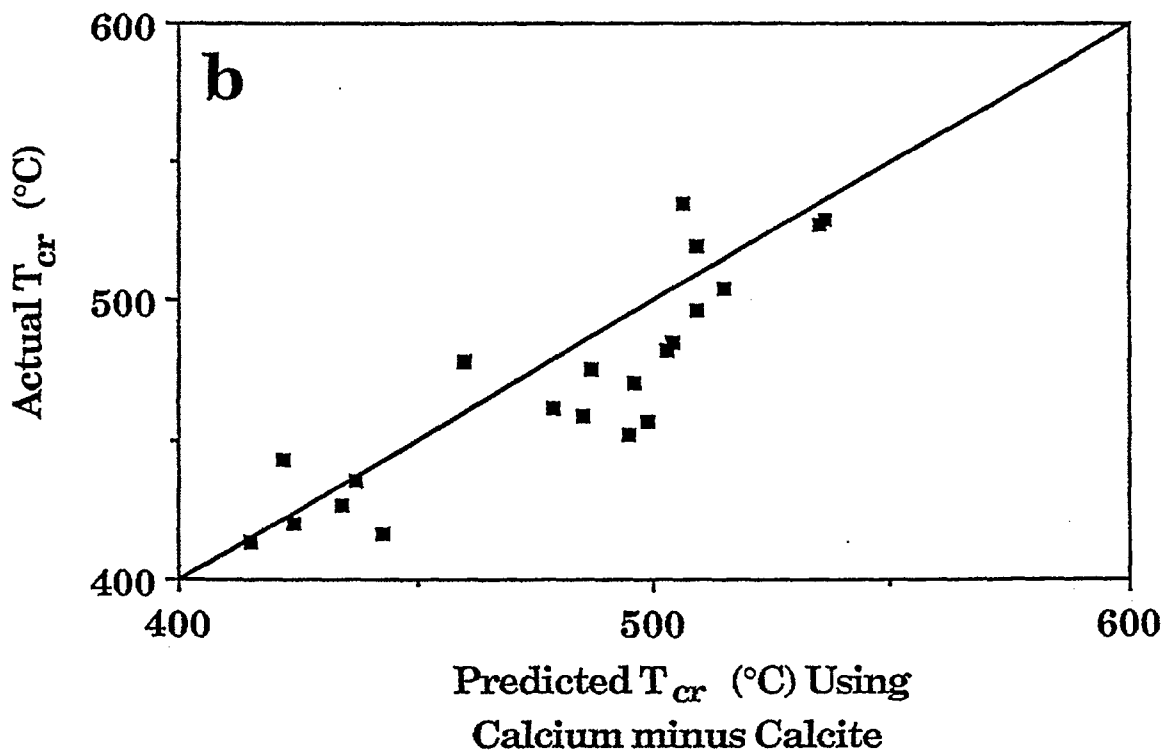
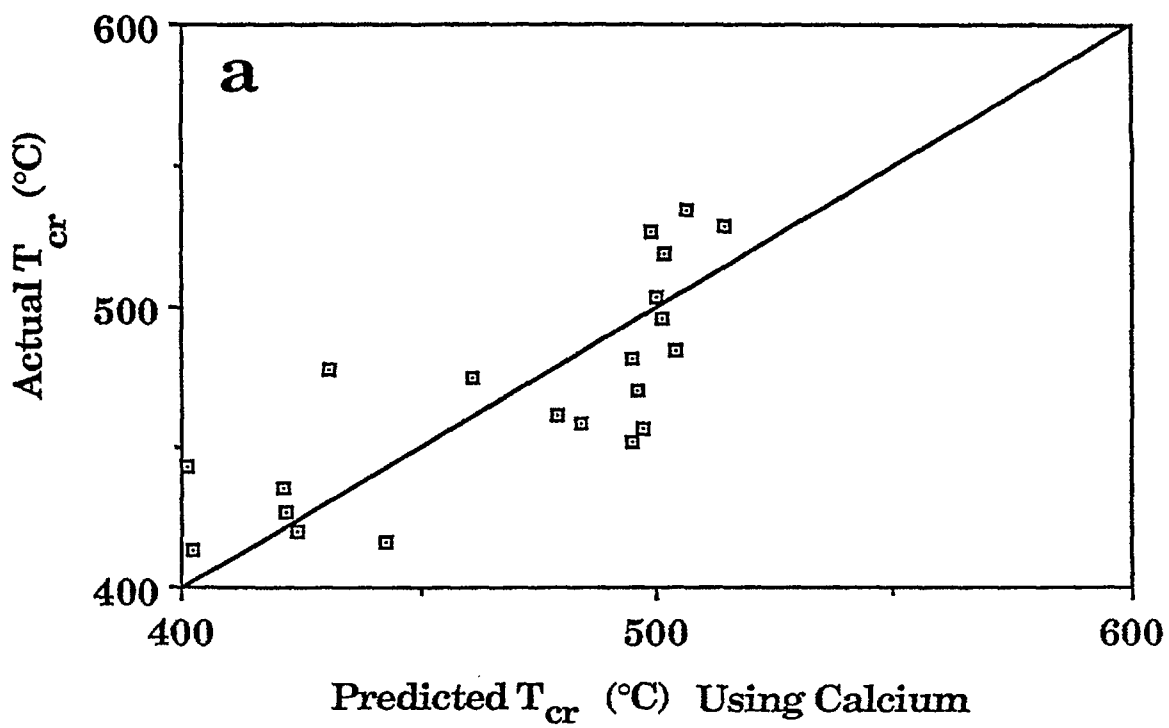
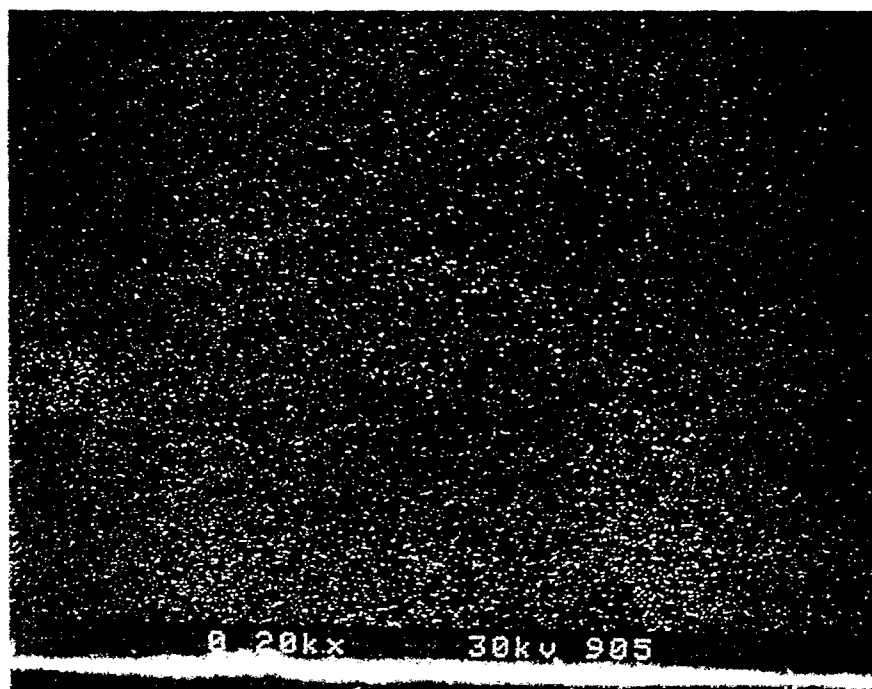


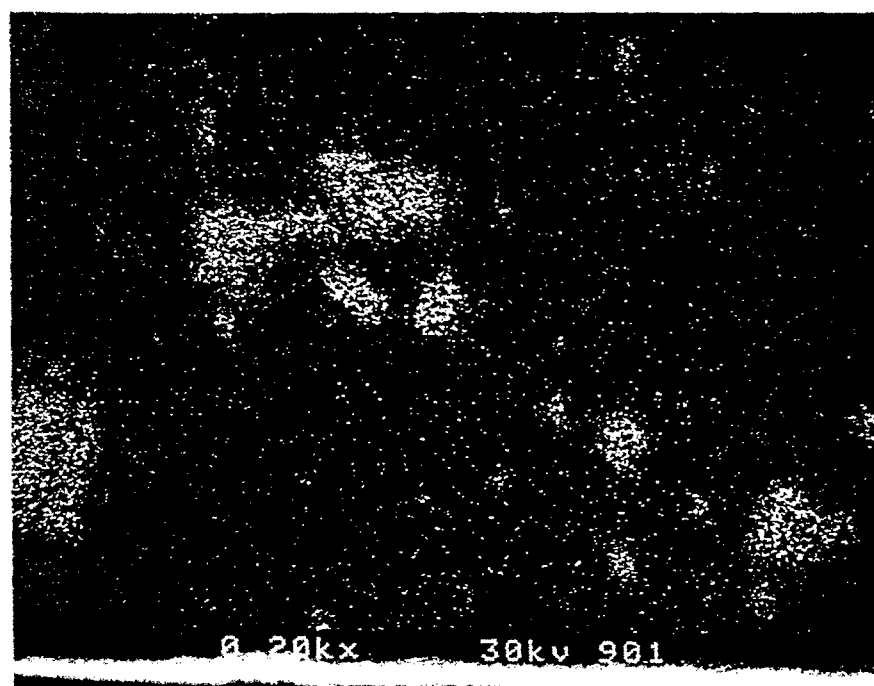
Figure II.D.2-5. Correlation Between Actual Reactivity and Predicted Reactivity Based on Ca Content. a) with Calcite; b) Without Calcite.

a



No Calcite

b



High Calcite

Figure II.D.2-6. SEM Calcium Dot Maps. a) Ca Loaded Demineralized Zap Coal, No Calcite; b) Exxon #6, High Calcite.

II.D.3. The Modeling of Mineral Matter Effects on Char Reactivity

The data from Section II.D-2 were used to develop a model for the effects of ion-exchanged alkali and alkaline earth metals on char reactivity. The model is discussed in Section II.A.10 and is described in Charpenay, et al., (1992).

II.D.4. Literature Review

To fully develop a mineral matter model for integration into PCGC-2, a number of effects must be included. The inputs will be the starting mineral concentrations and size distributions while the outputs will be the composition and size distribution of the fly ash. An outline of the proposed submodel for ash chemistry and physics is shown in Fig. II.D.4-1. Because of the complexity of this problem and the large amount of DoE and NSF supported work being done elsewhere, the eventual submodel will primarily be an integration of work done outside AFR. A brief summary of the most relevant studies appears below.

Although considerable progress has been made in understanding the underlying principles of ash formation and deposition, these processes, predictive modeling of ash behavior in the combustor still remains at the early stage of development. The ultimate objective is to provide a powerful tool for combustor design by identifying the regimes in which the fouling of heat-transfer surfaces is minimal. Three research groups have made important contributions to the study of coal-ash behavior during combustion: Energy and Environmental Research Center (EERC), University of North Dakota, Grand Forks, ND; PSI Technology Company, Andover, MA; and Massachusetts Institute of Technology (MIT), Cambridge, MA. The recent advances in characterization of mineral matter in coal as well as in the study of ash formation and deposition will be reviewed below. Unless stated otherwise, the presented material is based on references [Benson et al., 1993; Helble, 1992] and on the recent Short Course on Ash Formation and Deposition during Coal Combustion which was sponsored by EERC and the U.S. Department of Energy (St. Louis, MO, 10th May, 1993).

Review of Work Performed at EERC (and some other centers)

Precise, quantitative prediction of the fate of inorganic coal constituents during combustion is currently impossible due to an enormous complexity of the process, and due to inadequate mineral-matter characterization in the starting material. In general, the extent of ash-related problems depends upon the quantity and association of inorganic constituents in coal, the combustion conditions, and the system geometry. A detailed understanding of the critical phenomena is necessary to develop models that will accurately predict ash deposition as a function of coal characteristics and combustion conditions. The following key areas have been identified:

1. The chemical and physical characterization of inorganic matter in coal
2. The mechanisms of mineral-matter transformation into inorganic vapors, liquids and solids
3. The physical properties of the intermediate ash species as a function of temperature, atmosphere, and residence time
4. The mechanisms of ash transport to heat-transfer surfaces as a function of particle size and flow patterns in the combustor
5. The heat-transfer characteristics coupled with the reactivity and melting behavior of the deposited ash material
6. The characteristics of the liquid components in the deposit with respect to deposit growth and strength development
7. The physical characteristics of the deposit that influence its ability to be removed by conventional processes (e.g., by soot blowing).

Inorganic Constituents In Coals

Mineral matter can be present in coal in one of the three forms: (1) organically associated elements; (2) included minerals; and (3) excluded minerals. This division is illustrated in Figure II.D.4-2

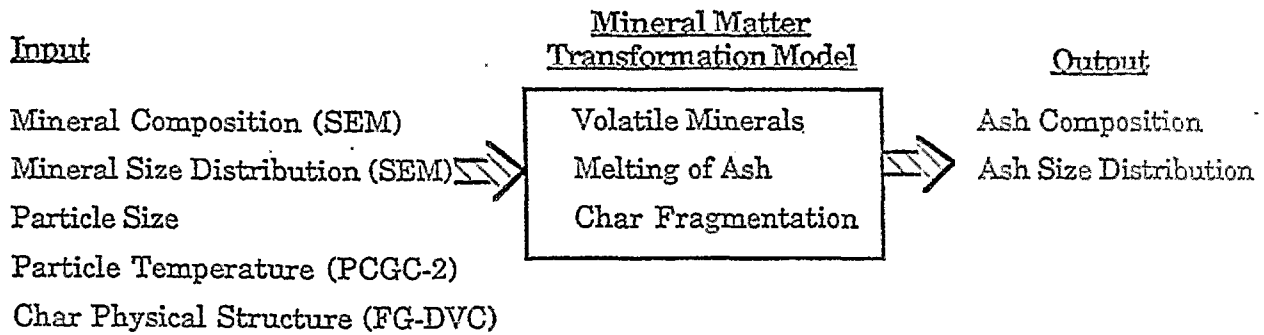


Figure II.D.4-1. Outline of Ash Physics And Chemistry Submodel.

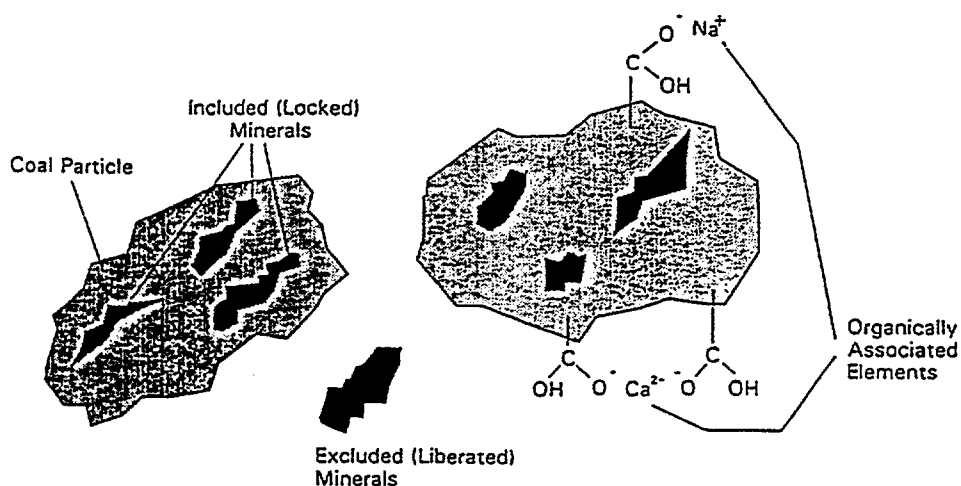


Figure II.D.4-2. Coal and associated inorganic components.

The fraction of inorganic components that are organically associated varies with coal rank. Lower-rank coals (subbituminous and lignitic) have high levels of oxygen. Approximately 25% of the oxygen is in the form of a carboxylic acid group. These groups act as bonding sites for cations such as sodium, magnesium, calcium, potassium, strontium, and barium (other minor and trace elements may also be associated in the coal in this form). In addition, some elements may be in the form of chelate coordination complexes with pairs of adjacent organic oxygen functional groups. The cations originate from the plant material from which the coal was formed and from groundwater filtering through the coal seam. In some low-rank coals, the organically associated inorganic components can comprise up to 60% of the total inorganic content of the coal (Benson and Holm, 1985). In higher-ranked coals, bituminous and anthracite, the inorganic components consist mainly of minerals.

Mineral grains are usually the most abundant inorganic component in coals. The minerals associated with coals are classified by coal geologists based on their origins as summarized by Stach *et al.* (1982). The major mineral groups found in coals include silicates and oxides, carbonates, sulfides, sulfates, and phosphates. In order to predict the behavior of the inorganic constituents during combustion, detailed information must be obtained on the abundance, size, and association of mineral grains in the coal.

The methods used to determine the association of inorganic components in coals have evolved significantly over the past 80 years. Ashing and gravity separation techniques are very common. These methods have inherent limitations and do not provide quantitative information on the association and abundance of inorganic components in coals. Recently, more advanced methods such as computer-controlled scanning electron microscopy (CCSEM) and chemical fractionation are being used to more quantitatively determine the abundance, size, and association of inorganic components in coals. Detailed information from the CCSEM and chemical fractionation allows for more effective prediction of the behavior of the inorganic components during combustion.

High-temperature ashing is a standard method that is routinely used to determine the quantity of inorganic constituents present in coal. This technique involves oxidizing the coal at 1023 K (750°C) followed by chemical analysis of the resultant ash. There are several limitations involved in this type of analysis. First, significant transformations and reactions of the inorganic components occur during the ashing process. The loss of mass due to water loss from clay minerals, carbon dioxide loss from carbonates, and sulfur loss from pyrite can significantly influence the determination of the inorganic content of coal. These species (H₂O, CO₂ and SO₂) are usually included as volatiles in the proximate analysis,

leading to erroneous results. In addition, the organically associated inorganic elements such as the alkali and alkaline earth elements absorb oxygen and SO₂ during the ashing processes, further complicating the determinations. Several investigators have developed empirical methods based on the composition of the ash and losses due to decomposition of minerals to estimate the inorganic content of coals as summarized by Given and Yarzab (1978).

Two other methods that have been used to concentrate the inorganic components in coal include gravity fractionation and low-temperature oxygen plasma ashing (LTA). Gravity separation only provides a partial separation of the minerals from the coal matrix, since some of the minerals that are small and included in the coal particles remain in the lighter fraction. In addition, the organically associated cations remain in the lighter organic-rich fraction. Therefore, gravity fractionation of the minerals is only a qualitative estimation of the minerals present in the coal. Low-temperature ashing is another technique that has been used to concentrate the inorganic species. This technique works quite well with higher-rank coal, but requires very long ashing times with lower-ranked coals containing high levels of organically associated cations.

Identification of the specific mineral species in coals (as opposed to chemical analysis) has been performed by several techniques. Jenkins and Walker (1978) provide a good summary of the techniques and applications prior to 1978. These include x-ray diffraction, infrared spectroscopy, differential thermal analysis, scanning electron microscopy, microprobe analysis, and ⁵⁷Fe Mössbauer. Unfortunately, the x-ray diffraction and infrared spectroscopy methods require low-temperature ashing prior to analysis. The technique that shows the most promise for quantitative determination of the mineral portion of the inorganic components in coal is scanning electron microscopy and microprobe (energy dispersive x-ray) analysis. Over the past ten years, this technique has been used much more rigorously to determine the mineral component in coal.

In order to determine the size, abundance, and association of mineral grains in both high- and low-rank coals, computer-controlled scanning electron microscopy (CCSEM) and automated image analysis (AIA) are the preferred techniques used to analyze polished cross sections of coal epoxy plugs (Zygarlick and Steadman, 1990). The CCSEM technique is used to determine the size, shape, quantity, and semi-quantitative composition of mineral grains in coals (Steadman et al., 1990 and Steadman et al., 1991). The key components of the CCSEM system that make it possible to image, size, and analyze inorganic particles are the backscatter electron detector, digital beam control, and the ultrathin window energy-dispersive x-ray detector. Backscatter electron imaging is used for CCSEM because the intensity of the backscattered electrons is a function of the average atomic number of the features on or near the surface. Since the mineral particles appear brighter relative to the lower atomic number background of the matrix, a distinction can be made between coal, mounting media, and mineral grains. In a typical CCSEM analysis the electron beam is programmed to scan over the field of view and locate the bright inclusions that correspond to mineral species. On finding a bright inclusion, the beam performs eight diameter measurements of the inclusion, finds the center of the inclusion, and collects an energy-dispersive spectrum (EDS) at the point for 2 seconds. Software classifies the mineral grains based on the EDS elemental composition and size. The parameters used to identify the minerals are based on published compositions of known minerals. A mineral association, such as aluminosilicate/gypsum, is a discrete particle that contains at least two adjacent or intimately associated minerals. The EDS spectra will reveal a combination of the proper elemental ratios for these associated minerals.

The differences in the chemical information provided by the ASTM versus CCSEM methods are illustrated in Figure II.D.4-3. In contrast to CCSEM, the ASTM analysis provides only a single data point which does not represent the true heterogeneity of the ash.

Quantification of the type and abundance of organically associated inorganic elements in lower-ranked subbituminous and lignitic coals is currently performed by chemical fractionation (Benson and Holm, 1985). Chemical fractionation is used to selectively extract elements from the coal based on solubility, which reflects their association in the coal. Briefly, the technique involves extracting the coal with water

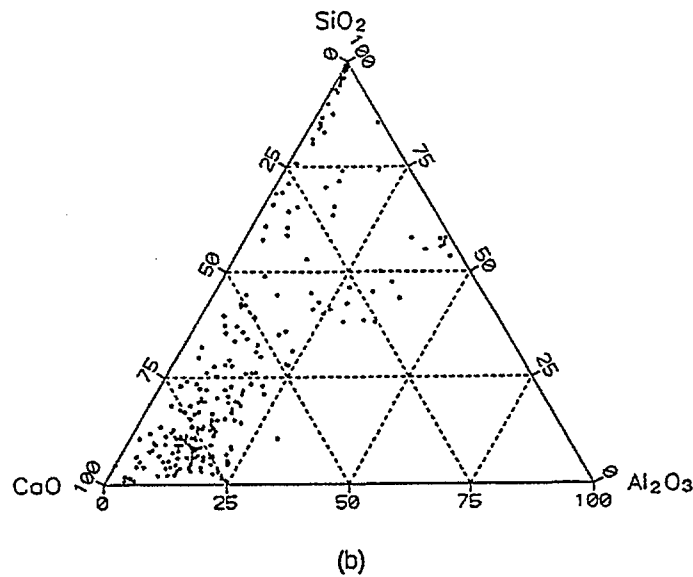
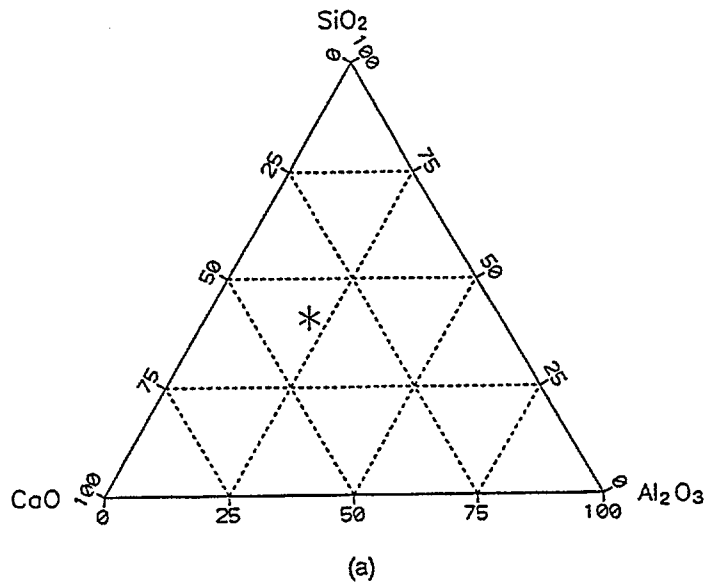


Figure II.D.4-3. Chemical information in coal ash provided by various types of chemical analysis: (a) ASTM ash analysis, and (b) CCSEM analysis of fly ash.

to remove water-soluble elements such as Na in sodium sulfate or those elements that were most likely associated with the groundwater in the coal. This is followed by extraction with 1M ammonium acetate to remove elements such as Na, Ca, and Mg that may be bound as salts of organic acids. The residue of the ammonium acetate extractions is then extracted with 1M HCl to remove acid-soluble species such as Fe and Ca which may be in the form of hydroxides, oxides, carbonates, and organically coordinated species. The components remaining in the residue after all three extractions are assumed to be associated with the insoluble mineral species such as clays, quartz, and pyrite. A number of Argonne Premium Coals have been analyzed by CCSEM and chemical fractionation, and the available data base is growing (Helbe et al., 1992 and Zygarrlicke et al., 1990).

Formation Of Ash Intermediates

The inorganic coal components undergo complex chemical and physical transformations during combustion to produce intermediate ash species (gases, liquids, and solids). The physical transformation of inorganic constituents depends on the inorganic composition of the coal and on combustion conditions. There exists a wide range of combinations of mineral-mineral, mineral-coal, mineral-cation-coal, and mineral-mineral-cation-coal associations in coal. These associations are unique to each coal sample and they include: (1) coalescence of individual mineral grains within a char particle; (2) shedding of the ash particles from the surface of the chars; (3) incomplete coalescence due to disintegration of the char; (4) convective transport of ash from the char surface during devolatilization; (5) fragmentation of the inorganic mineral particles; (6) formation of cenospheres; and (7) vaporization and subsequent condensation of the inorganic components upon gas cooling. As a result of these interactions, the fly ash usually has a bimodal size distribution, with maximum at particle sizes of $\sim 0.1 \mu\text{m}$ and $\sim 10 \mu\text{m}$. The submicron component is largely a result of the condensation of flame-volatilized inorganic components. The larger size particles have been called the residual ash by some investigators (Sarofim et al., 1977) because these ash particles resemble, to a limited degree, the original minerals in the coals.

The transformations of excluded minerals are dependent upon the physical characteristics of the mineral. Excluded minerals such as quartz (SiO_2) can be carried through the combustion system with its angular structure still intact. Excluded clay minerals can fragment during dehydration, melt, and form cenospheres. The behavior of excluded pyrite depends upon its morphology. Some of the pyrite may be present as framboids. Framboidal pyrite fragments more easily than massive pyrite particles. In addition, pyrite transforms to pyrrhotite and oxidizes to FeO , Fe_3O_4 , and Fe_2O_3 during combustion. The transformations of pyrite have been examined and modeled in detail by Srinivasachar et al. (1990). The carbonate minerals will fragment during the loss of carbon dioxide. According to Raask (1985), some of the carbonate minerals fragment and produce submicron-sized particles.

There are two extreme kinds of behavior that the inorganic constituents may exhibit during combustion (Field et al., 1967): (1) Each mineral grain forms a single ash particle; (2) One ash particle is formed per coal particle. Some of the differences in the fly ash size distribution exhibited for different coals are probably due to the burning char characteristics of the chars. For example, some coal particles swell and become hollow and porous during combustion. The degree of swelling depends on coal composition or maceral distribution and the combustion conditions.

Depending upon the distribution of minerals and other inorganic components, coalescence may occur to a larger or smaller extent. If the ash particles are similar in size to the original minerals in the coal, coalescence is insignificant and one ash particle per mineral grain is formed. In contrast, coalescence of minerals into a large particle occurs when the receding carbon surface brings the ash particles together. Thus, shrinking sphere represents the limiting case where one fly ash particle is produced per coal particle. In most cases, the actual fly ash size falls between the fine limit of one ash particle per mineral grain and the coarse limit of one ash particle per coal particle. In cases where mineral fragmentation occurs, the fine limit on size may be exceeded. In addition, shedding or convective transport of small ash particles originating from organic associations or submicron mineral grains can contribute to fine particle formation.

Vaporization and condensation of inorganic elements also contribute to the formation of fine particulate when the vapors condense homogeneously. In lower-rank coals, organically associated inorganic elements such as sodium, calcium, magnesium, and potassium have the potential to vaporize during combustion. The evidence for vaporization and condensation of sodium and potassium is abundant. The reactions of calcium and magnesium are less clear.

The chemical composition of the intermediate ash particles will influence their melting behavior in combustion systems. Figure II.D.4-4 illustrates the composition evolution of Upper Freeport fly ash. The figure shows that the major minerals such as pyrite, aluminosilicates, and K-aluminosilicates are transformed during the combustion process. The result is the formation of iron oxides, iron aluminosilicates, and other complex glass phases. These fly ash particles vary widely in size and chemical composition.

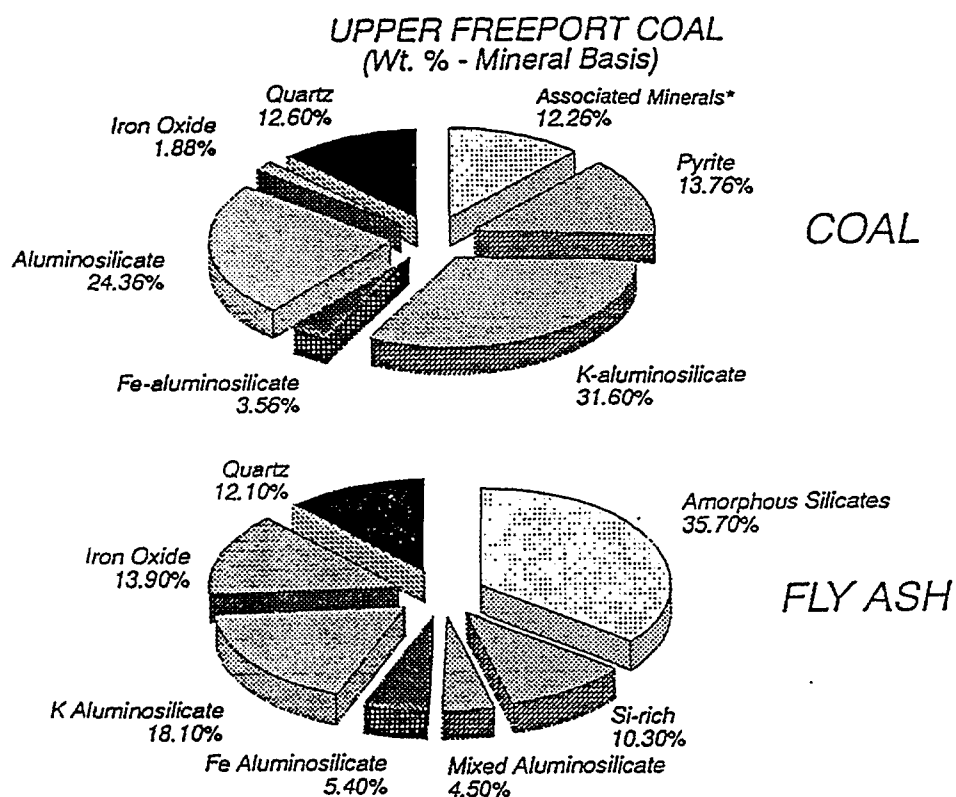


Figure II.D.4-4. Composition evaluation of Upper Freeport Bituminous coal ash during combustion (wt % mineral basis): (a) coal composition, (b) fly ash composition. * Mixed minerals such as quartz and pyrite.

In general, fly ash produced during pulverized coal combustion is approximately 90 to 95% amorphous and consists mainly of silicate glass. The conditions for glass formation have been discussed by Kingery et al. (1976). Glass-forming oxides, sometimes referred to as network formers, have the ability to build and form three-dimensional, random networks. The oxides that are good network formers include SiO_2 , B_2O_3 , GeO_2 , P_2O_5 , and AsO_4 . These network formers form highly covalent bonds with the oxygen atoms. In contrast, a network-modifying oxide is incapable of building a continuous network. The addition of such a modifying oxide to a network causes weakening of the network. Good examples of network modifiers are oxides of sodium, magnesium, calcium, and potassium.

An element that can act as either a network modifier or an intermediate oxide is iron. In coal ash systems, the effect of iron on the silicate glasses is extremely important. The oxidation state of the iron dictates whether iron will exist as a network modifier or an intermediate. Iron present as FeO (Fe^{2+}) will act as a network modifier, resulting in the formation of nonbridging oxygens and weakening the network. Iron present as Fe_2O_3 (Fe^{3+}) will act as an intermediate oxide and may take part in the glass network.

Liquid sulfate phases also contribute to the formation of depositions in combustion systems. These phases have very little tendency to form chains, rings, and network structures typical of silicates. The sulfate phases form as a result of the reaction of sulfur oxides with alkali and alkaline earth oxides such as sodium and calcium, respectively. The sulfur oxides form from the oxidation of sulfides and organic sulfur during combustion. These oxides can then react with ash in the combustor. It has been shown that the maximum amount of reaction between sulfur oxides and ash occurs at approximately 830 K and is dependent upon the quantity of alkali and alkaline earth oxides in the ash (Reid, 1981). The exact manner in which sulfates form is not well understood.

The behavior of alkali species such as sodium is extremely important with respect to the formation of convective pass fouling deposits. The mechanisms by which sodium forms deposits have been investigated by a number of researchers (Jones and Benson, 1987 and Sondreal et al., 1977). Sodium present as salts of organic acid groups in the coal will readily volatilize in a pulverized coal flame. According to Raask (1985), volatile sodium can easily dissolve in the surfaces of silicate particles or become sulfated. Sodium silicate ($\text{Na}_2\text{Si}_2\text{O}_5$) was found to be thermodynamically more stable than sulfates at temperatures from 1470 - 1870 K, while sodium sulfate was stable below approximately 1370 K. In fact, the formation of Na_2SO_4 at temperatures less than approximately 1300 K inhibited the formation of sodium silicate (Wibberley and Wall 1982). Therefore, the distribution of volatile sodium between silicate components of the ash and sulfate is influenced by temperature, as well as the residence time, of the particle in the flame.

Deposit Initiation

The transport of intermediate ash species is a function of the state and size of the species and system conditions such as gas flow patterns, gas velocity, and temperature. Several processes are involved as described by Raask (1985) and Rosner et al. (1992).

The primary transport mechanisms are illustrated in Fig. II.D.4-5. The small particles ($<1 \mu\text{m}$) and vapor phase species are transported by vapor phase and small particle diffusion. These particles are characteristically rich in flame-volatilized species that condense upon cooling in the bulk gas or in the gas boundary layer next to the tube.

An additional transport mechanism which is important for the intermediate size range of particles is that of thermophoresis, as illustrated in Fig. II.D.4-5. This transport mechanism is important for particles $<10 \mu\text{m}$. Electrophoresis is another transport mechanism that may be important with respect to the formation of deposits (Raask, 1985).

Larger particles, greater than $10 \mu\text{m}$ in diameter, may impact a heat transfer surface due to their inertia which prevents them from following the gas streamlines (e.g. around a tube). Inertial impaction accounts for the bulk of the deposit growth.

The factors that influence the adhesion of an ash deposit to a heat-transfer surface include:

1. Temperature of the steel surface.
2. Thermal compatibility between the deposited material and the heat transfer surface.
3. Chemical compatibility between the initiating particles and the heat transfer surface.
4. Surface tension of the initiating ash droplet.

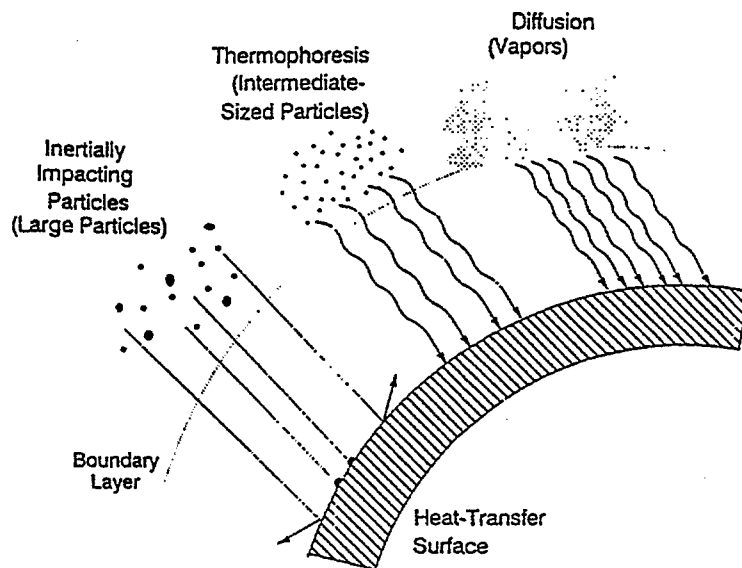


Figure II.D.4-5. Ash transport mechanisms to heat-transfer surfaces.

In the high-temperature radiant section of a utility boiler, molten ash particles may impact on the waterwalls resulting in the formation of a deposit. The initiating layers next to the heat-transfer surface may contain condensed, flame-volatilized species, in the form of small particles, that are rich in alkali and alkaline earth sulfates. These particles are held in place by van der Waals and electrostatic forces (Raask, 1985). Particles impacting this layer may incorporate some alkali and alkaline earth elements. The alkali and alkaline elements will cause the formation of lower melting point phases that can contribute to increased bonding to the surface.

If the thermal characteristics (i.e., thermal expansion coefficients) of the heat-transfer surface and the depositing material are similar, the deposit will not shed easily when the unit is cycled. On the other hand, if the thermal expansion coefficients of the ash and the surface are different, the deposits will shed much more easily during cycling.

Detailed fundamental studies of factors that influence the sticking of coal ash slags to heat-transfer surfaces were conducted by Austin et al. (1981 and Abbot and Austin, 1985). They developed a simplified apparatus to produce molten droplets of slag and allow them to fall and stick to a boiler steel coupon that was held at a controlled temperature. The information generated with this apparatus led to an improved understanding of the factors that influence the sticking behavior of slag droplets on boiler steel surfaces. The factors include slag droplet composition, droplet temperature, nature of the steel surface, steel temperature, and the contact angle of the droplet.

Deposit Characteristics And Growth

The characteristics of a deposit depend upon the chemical and physical characteristics of the intermediate ash species, geometry of the system (gas flow patterns), gas temperature, gas composition, and gas velocity. Figure II.D.4-6 illustrates ash deposition phenomena in utility boilers. Deposits that form in the radiant section are called slag deposits. Deposits that form in the convective pass on steam tubes are called fouling deposits. Slag deposits are exposed to radiation from the flame, and are usually associated with a high level of liquid phase components. Silicate liquid phases are typically the most

prevalent, although the deposit may also contain moderate to high levels of reduced iron phases. Initial layers of slag deposits may consist of very fine particulate which can be highly reflective. Fouling deposits form in the convective passes of utility boilers and, in most cases, do not contain the high levels of liquid phases that are usually associated with slagging type deposits. Rather, fouling deposits contain low levels of liquid phases (e.g. a combination of silicates and sulfates) that bind the particles together. The formation of these deposits on heat-transfer surfaces can significantly reduce heat transfer. The heat transfer through a deposit is related to the temperature, thermal history, and physical and chemical properties of the deposited material. Properties which have a significant effect on heat transfer include the thermal conductivity, emissivity, and absorptivity.

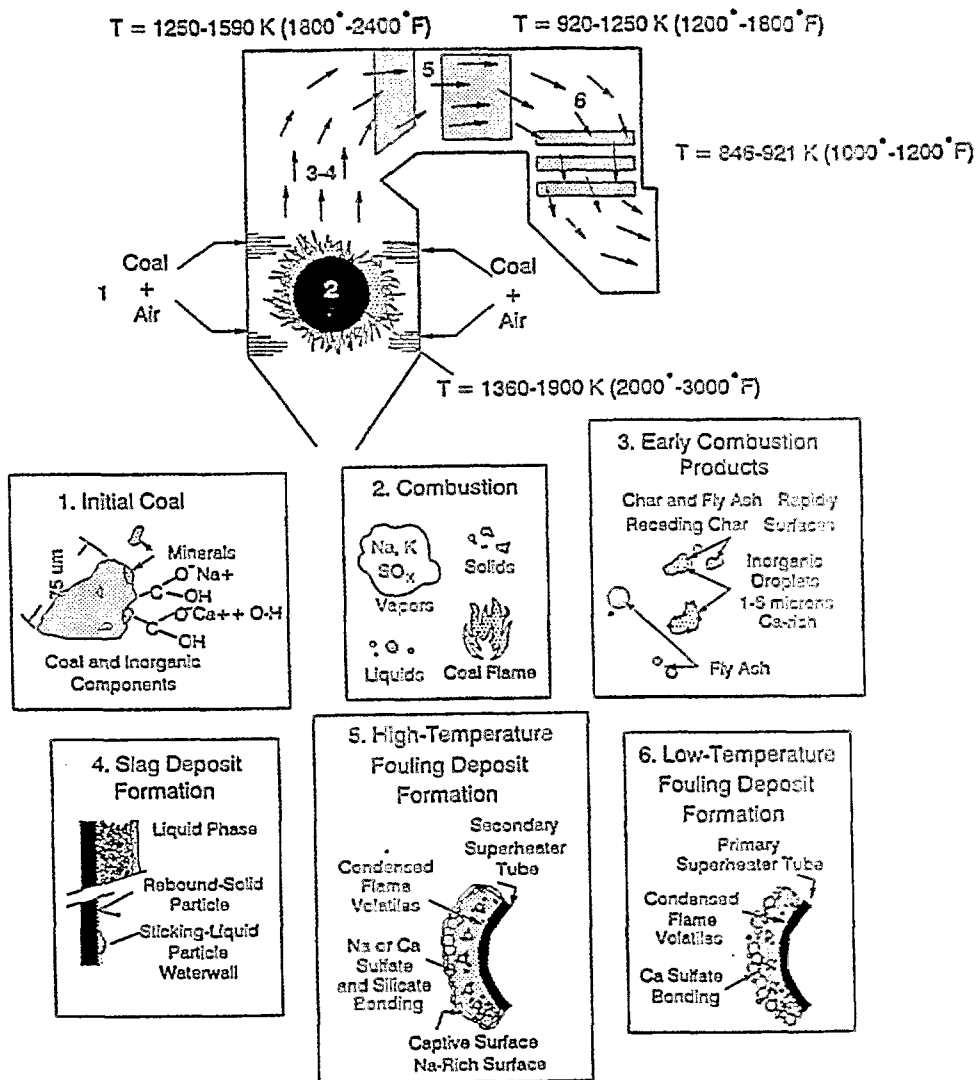


Figure II.D.4-6. Ash deposition phenomena in utility boilers.

The factors that contribute to the formation of slag deposits include (1) gas flow patterns resulting in impacting and sticking of the particles, (2) low-excess air conditions (3) the formation of a molten captive deposit that becomes an efficient collector of impacting particles, and (4) an increase in gas temperature

caused by less efficient heat transfer. Hatt et al. (1990) have classified slag deposits from utility boilers into four principal types which include (1) metallic slags that have a metallic luster and are usually associated with the combustion of pyrite-rich coals (reducing conditions cause the separation of the metallic portion from the other slag components), (2) amorphous, glassy slag that is relatively homogeneous with a high degree of assimilated ash particles, (3) vesicular slags that consist of amorphous slag that contain trapped bubbles and have a sponge-like appearance, and (4) sintered slag deposits that are only partially fused.

Fouling problems in utility boilers have been classified into two principal types: high temperature fouling and low temperature fouling (Hurley et al., 1991). This distinction is needed since the bonding mechanism of the deposits differ. In high-temperature fouling, the bonding of particles is due to silicate liquid phases, whereas in low-temperature fouling, the bonding is a result of the formation of sulfates. Condensed sulfur species, principally in the form of CaSO_4 , are stable and form the matrix or bonding material in the low-temperature deposits.

In combustors burning coals that contain high levels of alkali and alkaline earth elements, high-temperature fouling can be a significant problem. In most cases, the innermost layers consist primarily of small particles, rich in flame-volatilized species such as sodium and sulfur, which are transported to the surface by vapor phase diffusion and thermophoresis.

Properties Of Deposits

The development of deposit strength is due primarily to sintering or densification of the deposit. Sintering may occur by several mechanisms, as discussed in Kingery et al. (1976). Liquid phase or viscous flow sintering appears to be the dominant mechanism but other mechanisms, such as solid state sintering, may also be involved.

The driving force for densification is derived from capillary pressure of the liquid phase between particles. When two particles that are coated with a liquid phase are in contact with each other, the interparticle space becomes a capillary in which substantial capillary pressure can develop. For example, in silicate systems containing capillary diameters between 0.1 and 1 μm can range from 1.2-12.1 MPa (Kingery et al., 1976).

The capillary pressure increases densification by:

1. Rearranging the particles to increase packing effectiveness
2. Increasing the number of contact points between particles
3. Promoting the dissolution of smaller particles to produce large particles (Ostwald ripening)
4. Transferring material away from particle contact points to bring particle centers closer together.

The reactivity and liquid forming propensity of the deposited ash particles can be approximated from the base-to-acid ratio distribution of the particles. Basic components include network modifiers such as calcium or sodium. Acidic components include species such as silica which are network formers. A mixture of acidic and basic components tend to react to form low melting point species. Therefore, deposit which contains both acidic and basic particles has a high potential for liquid phase formation. In contrast, a deposit consisting of particles which are either all basic or all acidic has less potential for liquid phase formation. Crystallization is another factor which may affect the densification process. In general, crystallization tends to slow the densification process and weaken the deposit. Relationships are currently being developed between the chemical composition and physical properties of coal ash slags (Nowak and Benson, 1992).

The properties of the deposit that influence the heat transfer in a utility boiler are the emissivity and the thermal conductivity. Wall et al. (1979) reviewed the effect of deposit properties on the emissivity and thermal conductivity of the deposit. The emissivity was affected by the physical structure, shape, and

chemical composition (color) of the deposit. Emissivity of coal ashes decreased with temperature at lower temperatures, and then increased sharply at higher temperatures as sintering and fusion occurred. Particle size was the most dominant variable which affected the emissivity of unsintered samples.

The thermal conductivity of the deposit is also related to the physical structure and chemical composition of the deposit. A deposit that is highly porous and composed of insulating materials will have a low thermal conductivity, while low-porosity materials containing iron will have higher thermal conductivities. Figure II.D.4-7 shows thermal conductivities for deposits as measured by Wall et al. (1979) and Benson et al. (1990).

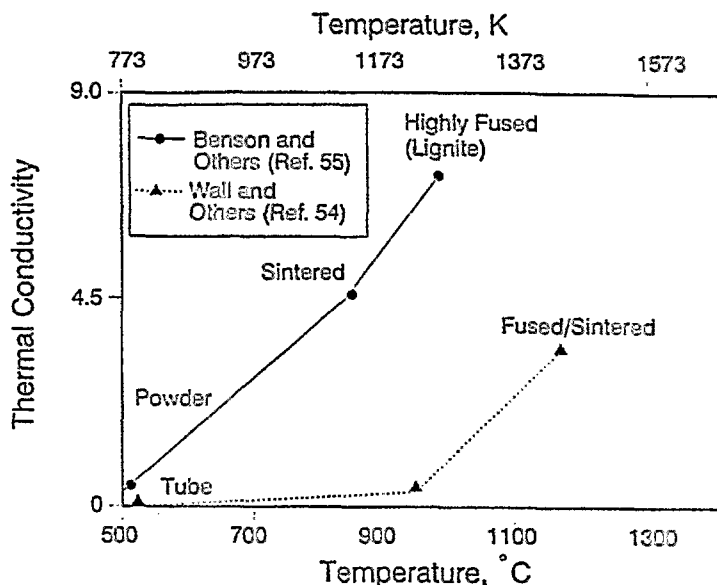


Figure II.D.4-7. Thermal conductivity of deposits having different characteristics.

Model Development

Modeling of ash formation and deposition has a goal of producing the following information as an end-product:

1. Deposition rate, which will provide information as to the frequency of soot blowing or load shedding required to operate the unit
2. Heat-transfer recovery after cleaning by soot blower or load-drop methods
3. Potential for catastrophic deposition.

This information will provide users with the ability to ascertain the limits on system performance due to ash deposit formation. Utility operators want to determine when the deposition rate is less than or equal to the heat-transfer recovery due to soot blowing (Case 1 in Fig. II.D.4-8). Under Case 1, the unit can operate continuously at the current conditions. If the deposition rate becomes greater than the heat-transfer recovery due to soot blowing, as illustrated for Case 2, load must be dropped in order to shed deposits.

The approach required to develop a model that can predict the deposition index illustrated in Fig. II.D.4-8 is shown in Fig. II.D.4-9. This is an overview diagram representing a phenomenological approach. The diagram does not illustrate the effects of boiler design and localized deposition in the radiative and convective passes of a utility boiler. A model is needed to predict the deposition index shown in Fig. II.D.4-8 as a function of the operating conditions, coal composition, and boiler geometry.

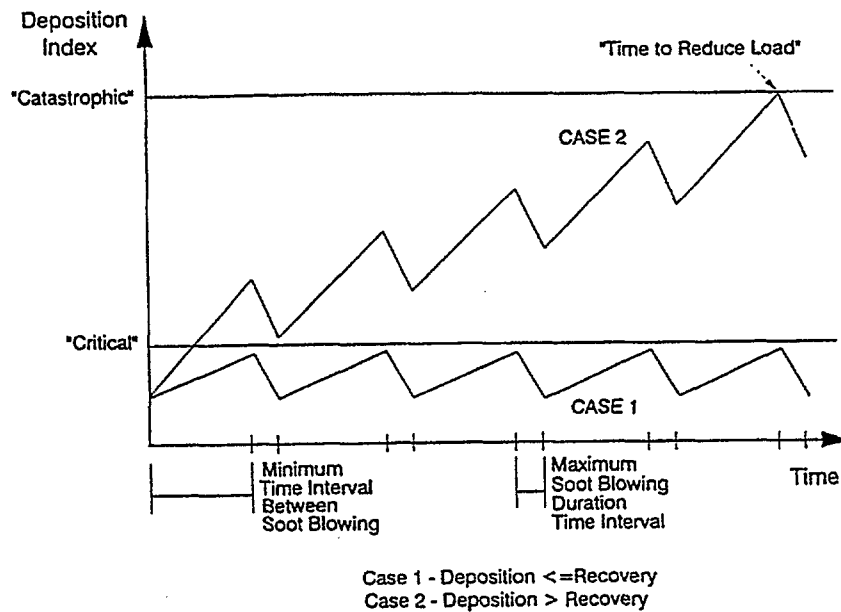


Figure II.D.4-8. Deposition index versus time for ash growth in utility boilers (Pavlish et al., 1991).

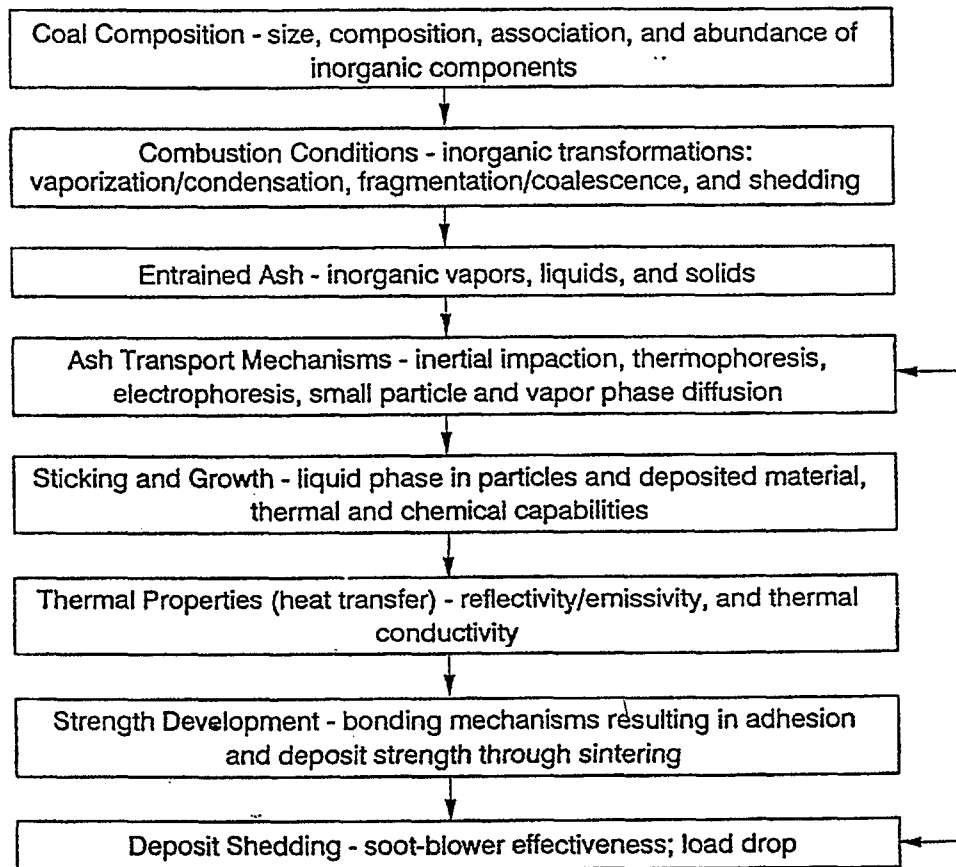


Figure II.D.4-9. Description of Coal Inorganic Components.

Modeling the behavior of inorganic constituents during combustion is limited, to a large extent, by the description of the coal inorganic components that is provided as input to the model. Model input parameters should include: (1) chemical information on both the coal and coal minerals, (2) the particle-size distribution of the coal and minerals, (3) information on the association between the coal and mineral phases, and (4) the abundance of organically associated inorganic components. Chemical information may be obtained from standard ASTM procedures, CCSEM and chemical fractionation, as discussed before.

One method of describing ash transformations is to follow the mineral behavior during combustion of a single coal particle. In order to do this, it is necessary to know the mineral composition of the coal on a particle-by-particle basis. In other words, a knowledge of the particular minerals associated with a given coal particle is required. CCSEM typically gives the size and composition of only the mineral particles that are greater than 1 μm , but does not associate particular mineral particles with coal particles. Therefore, it is necessary to randomly redistribute the minerals (as measured by CCSEM) back into the coal in order to approximate the particle-by-particle mineral composition of the coal.

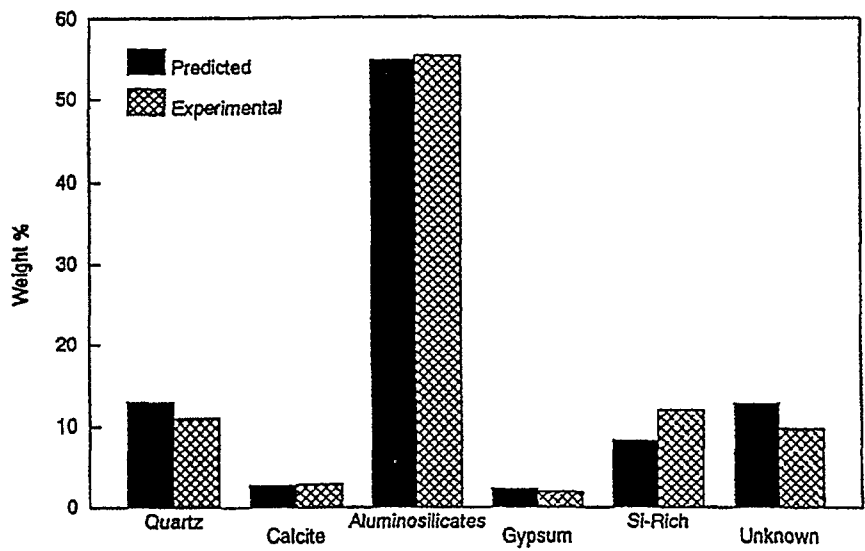
Methods for mineral redistribution have been discussed by Wilemski et al. (1992) and Beer et al. (1992). Redistribution techniques usually involve a Monte Carlo simulation and/or the use of Poisson distribution functions to represent the distribution of mineral particles in coal.

Modeling of Ash Formation

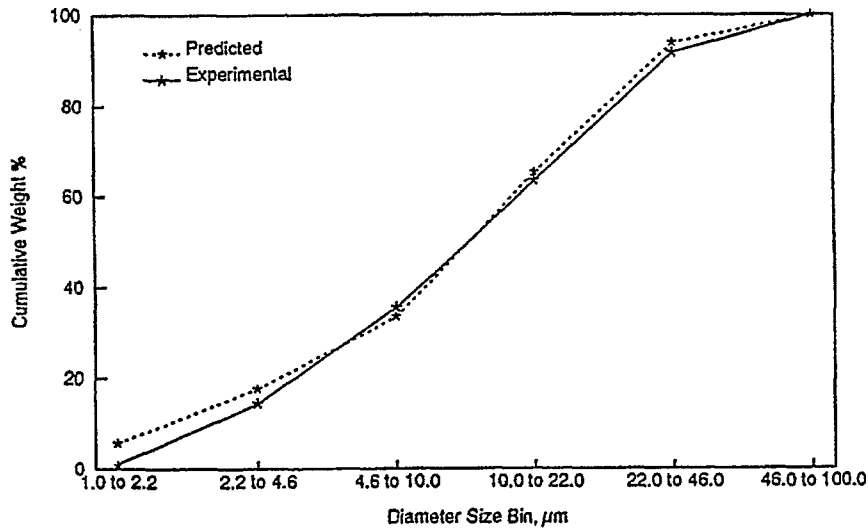
Two previously mentioned limiting cases have been extensively studied. The first of these is the coarse limit or full coalescence limit that assumes all of the ash in the char coalesces to form a single ash particle. The second limiting case is the fine limit in which no coalescence occurs and each mineral inclusion forms one ash particle. The actual fly ash distribution probably lies between these two extremes. These two limiting cases were recently used to predict the size and composition of fly ash from three bituminous and one lignitic coal (Wilemski et al., 1992). Predictions with the full coalescence model compared well with experimentally measured size and composition. In contrast, predictions with the no-coalescence assumption did not compare well with either the size or composition for the coals examined. Less satisfactory agreement between the full-coalescence model and experimental data was observed by Loehden et al. (1989), who found that the no-coalescence model gave a better estimate of the fly ash size distribution. Other studies have shown that the fly ash particle-size distribution approaches that of the mineral inclusions (i.e., no coalescence) for high-rank coals (Beer et al., 1990). However, even when the no-coalescence model approximates the fly ash particle-size distribution, the predicted composition distribution may be very inaccurate as discussed by Beer et al. (1992). The above results indicate that the simple "limiting case" models lack the sophistication necessary to describe inorganic transformation for a variety of coals and operating conditions. This is why partial coalescence models have been developed.

There are two basic types of partial coalescence models found in the literature. The first type makes the transition from coal inorganic components to fly ash by modeling char combustion explicitly and tracking the inorganic transformations as the char burns. The second type uses random combinations of the coal minerals to form the fly ash without explicitly considering char combustion. Both types of models require the detailed chemical data available from CCSEM.

Sample results from the latter procedure are shown in Fig. II.D.4-10. This method has the distinct advantage of eliminating the need to redistribute the mineral grains back into the coal matrix; the fly-ash distribution is generated directly from the CCSEM data. Excluded minerals are known to behave differently from included minerals which are intimately associated with the char combustion process. Srinivasachar and Boni (1989) recently developed a mathematical model to describe the transformations of excluded pyrite, a mineral form that is important in the slagging of boilers burning eastern coals. They found that, for the simulated conditions, approximately 80% of the total time required to oxidize pyrite to solid magnetite was spent in the molten phase. Clearly, the presence of the molten phase is significant with



(a)



(b)

Figure II.D.4-10. Particle-size and composition distribution predictions using the EERC model for Kentucky #9 on an iron-free basis: (a) predicted and experimental phase distribution, and (b) predicted and experiment size distribution (Zygarlicke et al., 1992).

respect to deposit formation. Other excluded minerals of interest include illite, which melts under typical combustion conditions (Srinivasachar et al., 1990), and silica which reacts with vaporized alkali or alkaline earth metals.

Simulation of the behavior of vaporizable species should consider the following areas:

1. Release of the species into the vapor phase
2. Chemistry of the species in the vapor phase
3. Transport of vapor species to locations where reaction or condensation may take place
4. Reaction or condensation of the vapor species

Equilibrium calculations have been used by a variety of investigators to determine the behavior of inorganic elements in the vapor phase (Wilson and Redifer 1973, Wibberley and Wall 1982, and Benson 1987). These calculations appear to adequately represent the species present in the vapor phase, with the exception of species like sodium sulfate that are thermodynamically stable, but are not readily formed due to kinetic constraints (Srinivasachar et al., 1990 and Steinberg and Kchofield, 1990).

Transport Processes

A single cylinder in cross-flow most closely represents a leading heat-exchanger tube in the convective pass. Quantitative impaction rates have been determined for particles transported by both inertial impaction and thermophoresis. The most frequently cited correlation of inertial impaction rates is perhaps that of Israel and Rosner (1983) who correlated the impaction efficiency in terms of a generalized Stokes number for a clean tube (free of deposit). Thermophoresis may also significantly impact the transport rates of small particles ($<10 \mu\text{m}$) as discussed before. Both Eulerian (Rosner, 1986) and Lagrangian (Wessel and Righi, 1988 and Jacobsen and Brock, 1965) approaches have been used to simulate thermophoretic transport for a cylinder in cross-flow.

There are locations in a boiler or combustor where the gas flow is predominantly parallel to the surface, as opposed to the perpendicular or impinging flow of the cylinder in cross-flow. In such cases, eddy impaction due to turbulence may play an important role in particle transport. Methods for calculations of particle deposition from turbulent flows were reviewed with regard to assumptions, accuracy, and range of application by Papavergos and Hedley (1984). These authors identified two basic types of models: (1) models based on theories of classical turbulence, and (2) stochastic models. Models based on the classical concepts of turbulence possessed the following characteristic: (1) incorporation of the "stopping distance" concept, (2) use of the multilayer fluid model adjacent to the wall (laminar sublayer, buffer layer, and turbulent core), (3) a particle diffusivity which is equal or proportional to the eddy diffusivity of momentum, (4) use of the r.m.s. radial fluid velocity to approximate the free flight velocity of the particle. It was concluded that theories based on the classical concepts of turbulence were "of limited application and accuracy, but easy to use in design calculations" (Papavergos and Hedley, 1984). Stochastic models are generally more accurate, but also more complex. A recent example of the stochastic approach is the study of Kallio and Reeks (1989), who used a Lagrangian random-walk approach to model particle deposition in turbulent ducts.

Particle Capture and Deposit Growth

Several different factors influence the sticking probability of a given particle, including the particle velocity, viscosity, surface tension, temperature, size, and impact angle, as well as the condition of the substrate upon which the particle impacts. In theory, it should be possible to describe quantitatively all of the above factors and simulate deposit growth on a particle-by-particle basis. However, the excessive amount of computer time that would be required and the inherent complexity of the deposition process itself preclude the use of such simulations for practical systems. Consequently, models of particle capture and deposit growth have focused on the factors considered most important to the particular system of interest. A significant amount of work remains to be done before it will be possible to quantitatively predict

particle capture and deposit growth. In order for this to be successful, theoretical work must be coupled with experiments at every stage of development.

Thermal Properties of Deposits

Two key physical properties are the emissivity and the thermal conductivity, both of which vary with the particle size, chemical composition, temperature, and thermal history of the deposit.

Wall et al. (1979) reviewed the influence of ash deposits on wall emissivities. Methods for laboratory measurement of emissivity were discussed and problems identified. Problems included the fact that boiler deposits are not flat, and that rough deposits have effective emissivities that are well above laboratory values. The chemistry of the deposits also has an effect on emissivity. The authors recommend in-situ measurement of this important physical property.

Ash deposits are often characterized by an effective thermal conductivity (k_{eff}) which is a single value used to represent the entire thickness of the deposit. Measurements of effective thermal conductivities have been made for both particulate and fused deposits. They clearly show that the magnitude of the effective conductivity varies significantly with the type of deposit formed. Caution should be exercised when using k_{eff} values measured in the laboratory since these measurements are typically made by grinding a sample of ash into a powder and pressing it into a pellet for the measurements. Consolidation and sintering invariably occur to one degree or another in boiler deposits, leading to an effective conductivity which is greater than values generally derived from laboratory measurements (Wall et al., 1979). In the absence of other information, a reasonable value for the effective thermal conductivity of deposits which are not highly fused is 0.5 W/m K (Creek, 1985 and Anderson et al., 1987).

Review of Work Performed at PSI

Between 1986 and 1992 PSI Technology Company (PSIT) conducted a mineral and ash study for DoE/PETC. The goal of the study "was the development of a comprehensive model to predict the size and chemical composition distributions of ash produced during pulverized coal combustion". The results of the study are reported in Phase I and Phase II Final Reports (Boni, et al., 1990; and Helble, et al., 1992).

The study developed techniques for characterizing the size and composition of both minerals included in coal particles as well as fly ash. The most important characterization technique was (CCSEM) in which sample of each coal fly ash was analyzed by Computer Controlled Scanning Electron Microscopy to determine the type, composition, and size of the coal mineral matter. This technique was eventually employed as the primary input for the engineering model.

The engineering model is illustrated in Fig. II.D.4-11. The model starts with the evaluation of the mineral inclusion compositions and sizes. This analysis is performed once for any coal and a mineral redistribution model is used to determine how the minerals are distributed among particles for any coal grind. This statistically calculated mix of particles with their included and excluded minerals is used to predict the ash particle distribution. To do this requires answers to specific questions on the chemical and physical transformation of the minerals such as:

- Do mineral grains coalesce?
- What happens to the organically bound alkali metals?
- What happen to the pyrite?

To answer these questions, the PSI Technology study included a wide range of experiments. For the purpose of the engineering model, the most important findings were as follows:

**PSI
Engineering
Model**

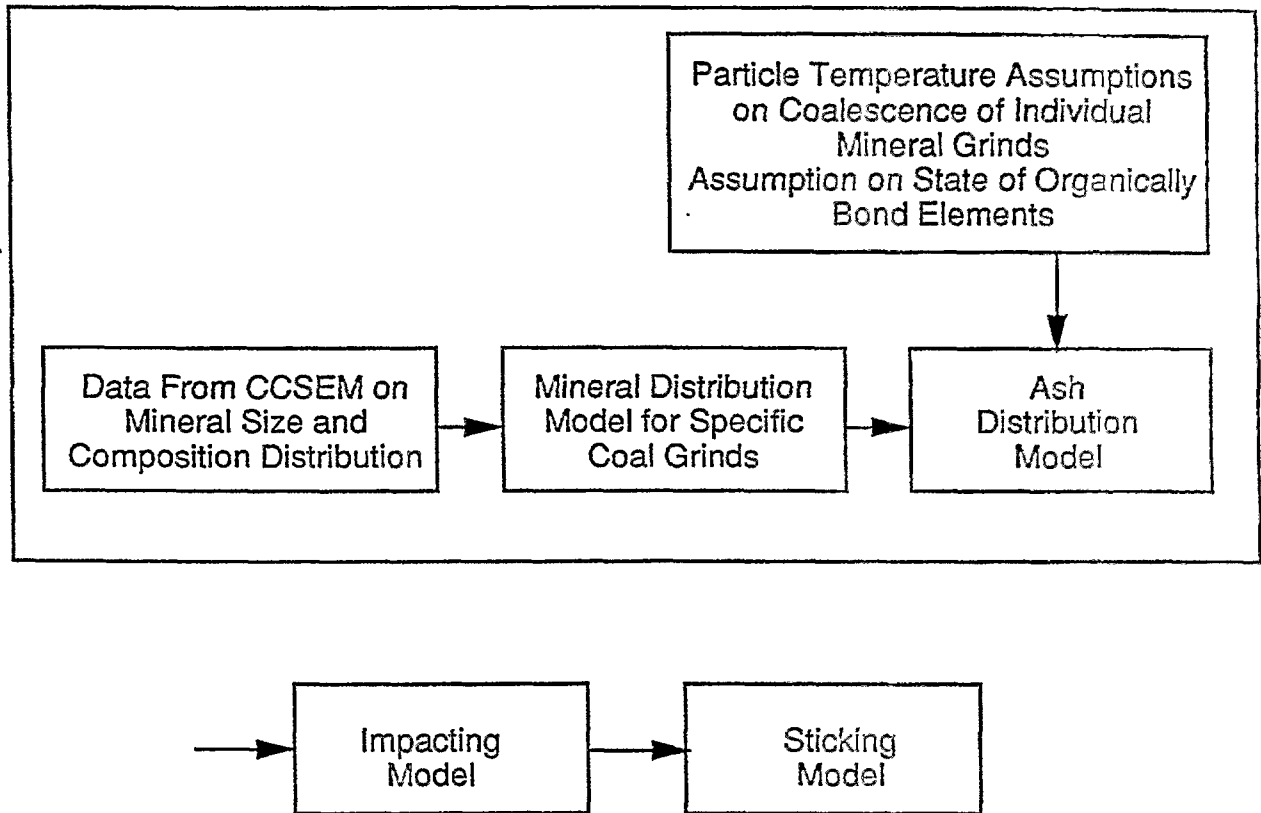


Figure II.D.4-11. PSI Technology Engineering Model for Ash Particle Size and Composition.

- "The full coalescence model gives generally acceptable predictions of ash composition and size distributions. On the other hand, the no coalescence model fails to identify several ash composition categories and consistently predicts too fine an ash size distribution in the smaller size range".
- "Calcium aluminosilicate ash results mainly from the interaction of organically-bound calcium with aluminosilicate minerals. Calcium, present as calcite, does not interact with other minerals, unless it is present as very fine inclusions. The compositions and concentrations of calcium-containing ash particles are sensitive to the amount of organically-bound calcium in the coal".
- "Char fragmentation, was found to have little influence on the ash distributions for all but the lowest ash (< 5%) coals".
- "Alkali vaporization (mainly sodium) was found to be affected by the presence of aluminosilicate minerals, with the formation of alkali aluminosilicates retarding alkali vaporization".
- "Calcium-rich aluminosilicates were found to lead to significant particle deposition under a wide range of conditions".
- "Pyrite-derived ash particles were also found to deposit over a wide range of conditions, provided that a molten phase was present".
- "Coalescence of ash particles during char combustion is enhanced by the presence of alkali and alkaline earth metals in the coal".
- "Coal mineralogy and combustion temperature (not combustion scale) are the most important parameters determining the composition distribution of combustion-derived fly ash particles".
- "Traditional indices for slagging and fouling based on mean ASTM ash compositions are inadequate because they fail to account for the wide variability in compositions and sizes of ash particles".

General Modeling Issues and Concluding Remarks

Previous sections have discussed several aspects of mineral matter behavior, all of which are relevant to the development of a complete model of inorganic transformations and ash deposition. The quantitative description of each of these aspects alone requires a relatively complex mathematical model. In fact, it is still not possible to accurately predict some of the key aspects (e.g., deposition rate). Clearly, then, the combination of all the different aspects of mineral behavior into a single submodel represents a formidable task.

As this task is approached, it is important to realize that different fuel and boiler combinations require different aspects of mineral behavior in order to predict ash formation and deposition. Therefore, the sophistication of the mineral matter submodel should be reduced to the key aspects needed to solve the problem set of interest. In addition, the type of information needed by the user will determine the level of simulation which must be performed. With this in mind, there is a need for at least two principal levels of modeling, namely, (1) simple simulations to determine the relative behavior of different fuels, and (2) comprehensive simulations with localized resolution in the boiler. The simple model (1) should be designed to run efficiently on a low-level platform, such as a personal computer. The second level of modeling is a mineral matter submodel incorporated into a comprehensive combustion code. The development of a first-generation submodel is currently in progress.

During the past several years, significant advances have been made in our understanding of the fundamental mechanisms of ash formation, transport, growth, and strength development. Many of these advances are related to the development of analytical techniques, such as CCSEM, which enable determination of the size, composition, abundance, and association of mineral grains in coal. This detailed analytical information has been an important factor in the identification of the key mechanisms which govern ash behavior, and has led to the development of mechanistic models to describe ash transformations and depositions. These models provide the basis for predictive tools which can be applied to practical systems.

Although considerable progress has been made, there is still much work to be done. For example, there is a need to develop quantitative relationships between the characteristics of the entrained ash (e.g. fly-ash chemistry and morphology) and the physical properties of ash deposits that influence deposit growth, strength development, and cleanability. Also, data from bench-scale, pilot-scale, and full-scale units are needed for verification of mechanistic models. Once verification is complete, the predictive models will be available for simulation of practical systems in order to determine operating conditions which will minimize deposition problems, maximize efficiency, and reduce emissions.

References for Subtask 2.d.

- Abbott, M.F., Moza, A.K., and Austin, Studies on Slag Deposit Formation in Pulverized Coal Combustors: 2. Results on the Wetting and Adhesion of Synthetic Ash Drops on Different Steel Substrates, Fuel, Vol. 60, pp. 1065-1072 (1981).
- Abbott, M.F., and Austin, L.G., Studies on Slag Deposit Formation in Pulverized-Coal Combustors: 4. Comparison of Sticking Behavior of Minerals and Low-Temperature and ASTM High-Temperature Coal Ash on Medium Carbon Steel Substrates, Fuel, Vol. 61, pp. 765-770 (1982).
- Abbott, M.F., Conn, R.E., and Austin, L.G., Studies on Slag Deposit Formation in Pulverized Coal Combustors: 5. Effect of Flame Temperature, Thermal Cycling of The Steel Substrate, and Time on the Adhesion of Slag Drops to Oxidized Boiler Steels, Fuel, Vol. 64, pp. 827-831 (1985).
- Abbott, M.F., and Austin, L.G., Studies on Slag Deposit Formation in Pulverized-Coal Combustors: 6. Stricking Behavior of Slag Drops form Three Pennsylvania Steam Coals, Fuel, Vol. 64, No. 6, pp. 832-838 (1985).
- Anderson, D.W., Viskanta, R., and Incropera, F.P., Effective Thermal Conductivity of Coal Ash Deposits at Moderate to High Temperature, Trans. ASME, J.Eng., Gas Turbine Power, Vol. 109, p. 215 (1987).
- Beer, J.M., Sarofim, A.F., Barta, L.E., From Coal Mineral Properties to Fly Ash Deposition Tendencies: A Modeling Route, in S.A. Benson (Editor), Inorganic Transformations and Ash Deposition During Combustion, Engineering Foundation Press, ASME, New York, NY (1992).
- Benson, S.A., Jones, M.L. and Harb, J.N., Ash Formation and Deposition, in Fundamentals of Coal Combustion for Clean and Efficient Use, (L. D. Smoot, Ed.), Elsevier, Amsterdam, pp. 299-373 (1993).
- Benson, S.A., and Holm, P.L., Comparison of Inorganic Constituents in three Low-Rank Coals, Ind. Eng. Chem. Prod. Res. Dev., Vol. 24, p. 137 (1985).
- Benson, S.A., Laboratory Studies of Ash Deposit Formation During the Combustion of Western U.S. Coals, PhD. Thesis, The Pennsylvania State University, University Park, PA , p. 266 (1987).
- Bishop, M. and Ward, D.L., Fuel, 37. 191 (1958).
- Blom, L., Edelhausen, L., and van Krevelen, D.W., Fuel, 36 (1957).
- Boni, A.A., Beér, J.M., Bryers, R.W., Flagan, R.C., Helble, J.J., Huffman, G.P., Huggins, F.E., Peterson, T.W., Sarofim, A.F., Srinivasachar, S., and Wendt, J.O.L., Transformations of Inorganic Coal Constituents in Combustion Systems, Phase I Final Report for U.S. DOE Contract No. DE-AC22-86PC90751 (1990).
- Charpenay, S., Serio, M.A., and Solomon, 24th Symposium (Int) on Combustion, The Combustion Institute, Pittsburgh, PA, 1189-1197 (1992).
- Creek, R.C., Thermal Properties of Boiler Ash Deposits, State Electricity Commission of Victoria, Research and Development Dept., Brown Coal Research Division, Rep. No. ND/85/014, (May 1985).
- Field, M.A., Gill, D.W., Morgan, B.B., and Hawksley, P.G.W., Combustion of Pulverized Coal, BCURA, Leatherhead, p 186 (1967).

- Given, P.H., and Yarzab, R.F., Analysis of the Organic Substance of Coals: Problems Posed by the Presence of Mineral Matter, in C.J. Karr (Editor), *Analytical Methods for Coal and Coal Products*, 2nd ed., Academic Press, New York, NY, Chapter 20, pp 3-41 (1978).
- Hatt, R.M., Fireside Deposits in Coal-Fired Utility Boilers, *Prog. Energy Combust. Sci.*, Vol. 16, pp. 235-241 (1990).
- Helble, J.J. (Ed.), Transformations of Inorganic Coal Constituents in Combustion Systems, Final Report (Contract No. DE-AC22-86PC90751), PSI, MIT, University of Arizona and University of Kentucky, Vol. I—III (Nov. 1992).
- Helble, J.J., Srinivasachar, S., Wilemski, G., Boni, A.A., Kang, S-G., Sarofim, A.F., Graham, K.A., Beér, J.M., Peterson, T.W., Wendt, J.O.L., Gallagher, N.B., Bool, L., Huggins, F.E., Huffman, G.P., Shah, N., and Shah, A., Transformations of Inorganic Coal Constituents in Combustion Systems, Phase II Final Report for U.S. DoE Contract No. DE-AC22-86PC90751, (Vols. I, II, and III) (1992).
- Hengel, T.D. and Walker, P.L., Jr., *Fuel*, 63, 1214 (1984).
- Hurley, J.P., Erickson, T.A., Benson, S.A., and Brobjorg, J.N., Ash Deposition at Low Temperatures in Boilers Firing Western U.A. Coals, International Joint Power Generation Conference, San Diego, CA (1991).
- Israel, R., and Rosner, D.E., Use of a Generalized Stokes Number to Determine the Aerodynamic Capture Efficiency of Non-Stokesian Particles from a Compressible Gas Flame, *Aerosol Sci. and Tech.*, Vol. 2, pp. 45-51 (1983).
- Jacobsen, S., and Brock, J.R., The Thermal Force on Spherical Sodium Chloride Aerosols, *J. Colloid Sci.*, Vol. 20, pp. 544-554 (1965).
- Jenkins, R.G., and Walker, P.L., Analysis of Mineral Matter in Coal, in C. Karr Jr. (Editor), *Analytical Methods for Coal and Coal Products*, 2nd ed., Academic Press, New York, NY, Chapter 26, pp. 265-292 (1978).
- Jones, M.L., and Benson, S.A., An Overview of Fouling/Slagging with Western Coals, Presented at the EPRI-Sponsored Conference on Effects of Coal Quality on Power Plants, Atlanta, GA, p.22, October 13-15 (1987).
- Kallio, G.A., and Reeks, M.W., A Numerical Simulation of Particle Deposition in Turbulent Boundary Layer, *J. Multiphase Flow*, Vol. 15, pp. 433-446 (1989).
- Kingery, W.D., Bowen, H.K., Uhlmann, D.R., *Introduction to Ceramics*, 2nd ed., John Wiley & Sons, New York, NY, p. 1032 (1976).
- Loehden, D., Walsh, P.M., Sayre, A.N., Beer, J.M., and Sarofim, A.F., Generation and Deposition of Fly Ash in the Combustion of Pulverized Coal, *J. Inst. Energy*, pp. 119-127 (June 1989).
- Moza, A.K. and Austin, L.G., Studies on Slag Deposit Formation in Pulverized Coal Combustors: 1. Results on the Wetting and Adherence of Synthetic Coal Ash Drops on Steel, *Fuel*, Vol. 60, pp. 1057-1064 (1981).
- Moza, A.K., and Austin, L.G., Studies on Slag Deposit Formation in Pulverized-Coal Combustors: 3. Preliminary Hypothesis for the Sticking Behavior of Slag Drops on Steels, *Fuel*, Vol. 61, pp. 161-165 (1982) .

- Nowok, J.W., and Benson, S.W., Correlation of Interfacial Surface Tension/Viscosity Ratio with Base/Acid Ratio, Nonbridging Oxygen Factor, and Compressive Strength Development in Coal Ashes, in S.A. Benson (Editor), *Inorganic Transformation and Ash Deposition During Combustion*, Engineering Foundation Conference, ASME, New York, NY (1992).
- Papavergos, P.G., and Hedley, A.B., Particle Deposition Behavior from Turbulent Flows, *Chem. Eng. Res. Dev.*, Vol. 62, p.275 (1984).
- Raask, E., *Mineral Impurities in Coal Combustion*, Hemisphere Publishing Company, Washington, (1985).
- Reid, W.T., Coal Ash--Its Effect on Combustion Systems, in M.A. Elliot (Editor), *Chemistry of Coal Utilization*, 2nd ed., John Wiley & Sons, New York, NY, pp. 1389-1445 (1981).
- Rosner, D.E., Konstandopoulos, A.G., Tassopoulos, M., and Mackowski, D.W., Deposition Dynamics of Combustion-Generated Particles: Summary of Recent Studies of Particle Transport Mechanisms, Capture Rates, and Resulting Deposit Microstructure/Properties, in S.A. Benson (Editor), *Inorganic Transformations and Ash Deposition During Combustion*, Engineering Foundation, ASME, New York (1992).
- Rosner, D.E., *Transport Processes in Chemically Reacting Flow Systems*, Butterworth, Stoneham, MA, (1986), p. 539.
- Sarofim, A.F., Howard, J.B., and Padia, A.S., The Physical Transformation of the Mineral Matter in Pulverized Coal Under Simulated Combustion Conditions, *Combust. Sci. Technol.*, Vol. 16, pp. 187-204 (1977).
- Sondreal, E.A., Tufte, P.H., and Beckering, W., Ash Fouling in the Combustion of Low-Rank Western U.S. Coals, *Combustion Science and Technology*, Vol. 16, p. 95 (1977).
- Srinivasachar, S., Helble, J.J., and Boni, A.A., Mineral Behavior During Coal Combustion: 1. Pyrite Transformations, *Prog. Energy Combust. Sci.*, Vol. 16, pp 281-292 (1990).
- Srinivasachar, S., and Boni, A.A., A Kinetic Model for Pyrite Transformations in a Combustion Environment, *Fuel*, Vol. 68, p. 829 (1989).
- Srinivasachar, S., Helble, J.J., Boni, A.A., Shah, N., Huffman, G.P., and Huggins, F.E., Mineral Behavior During Coal Combustion: 2. Illite Transformations, *Prog. Energy Combust. Sci.*, Vol. 16, p. 293 (1990).
- Srinivasachar, S., Helble, J.J., Ham, D.O., and Domazetis, G., A Kinetic Description of Vapor Phase Alkali Transformations in Combustion Systems, *Prog. Energy Combust. Sci.*, Vol. 16, p. 303 (1990).
- Stach, E., Mackowski, M., Teichmuller, M., Taylor, G.H., Chandra, D., and Teichmuller, R., *Coal Petrography*, 3rd Edition, Gebruder Borntraeger, Berlin, (1982).
- Steadman, E.N., Zygarlicke, C.J., Benson, S.A., and Jones, M.L., A Microanalytical Approach to the Characterization of Coal, Ash, and Deposits, in Seminar on Fireside Fouling Problems, ASME Research Comm. on Corrosion & Deposits from Combustion Gases, Washington, DC (1990).
- Steadman, E.N., Benson, S.A., and Zygarlicke, C.J., Digital Scanning Electron Microscopy Techniques for the Characterization of Coal Minerals and Coal Ash, Presented at the Low-Rank Fuels Symposium, Billings, MT, p.16, May 20-23 (1991).

- Steinberg, M., and Schofield, K., The Chemistry of Sodium with Sulfur in Flames, Prog. Energy Combust. Sci., Vol. 16, p 311 (1990).
- Wall, T.F., Lowe, A., Wibberley, L.J., and Stewart, I., Mineral Matter Redistribution and Ash Formation in Pulverized Coal Combustion, in S.A. Benson (Editor), *Inorganic Transformations and Ash Deposition During Combustion*, Engineering Foundation Press, ASME, New York, NY (1992).
- Wessel, R.A., and Righi, J., Generalized Correlations for Inertial Impaction of Particles on a Circular Cylinder, Aerosol Sci. Tech., Vol. 9 (1988) pp. 29-60.
- Wilson, J.S., and Redifer, M.W., Equilibrium Composition of Simulated Coal Combustion Products: Relationship to Fireside Corrosion and Ash Fouling, Paper No. 73-WA/CD-6, ASME, (1973).
- Wibberley, L.J., and Wall, T.F., Alkali-Ash Reactions and Deposit Formation in Pulverized Coal-Fired Boilers: Thermodynamic Aspects Involving Silica, Sodium, Sulphur and Chlorine, Fuel, Vol. 61 (1982) p. 87.
- Wibberley, L.J., and Wall, T.F., Alkali-Ash Reactions and Deposit Formation in Pulverized Coal-Fired Boilers: Experimental Aspects of Sodium Silicate Formation and the Formation of Deposits, Fuel, Vol. 61, p. 93 (1982).
- Zygarlicke, C.J., and Steadman, E.N., Advanced SEM Techniques to Characterize Coal Minerals, Scanning Electron Microsc., Vol. 4, No. 3, pp. 579-590 (1990).
- Zygarlicke, C.J., Jones, M.L., Steadman, E.N., and Benson, S.A., Characterization of Mineral Matter in ACERC Coals, Prepared for the Advanced Combustion Engineering Research Center, Brigham Young University, Provo, UT (1990).
- Zygarlicke, C.J., Ramanathan, M., and Erickson, T.A., Fly Ash Distribution and Composition: Experimental and Phenomenological Approach, in S.A. Benson (Editor), *Inorganic Transformations and Ash Deposition During Combustion*, Engineering Foundation Press, ASME, New York, NY (1992).

SATISFACTION GUARANTEED

NTIS strives to provide quality products, reliable service, and fast delivery. Please contact us for a replacement within 30 days if the item you receive is defective or if we have made an error in filling your order.

- ▶ **E-mail: info@ntis.gov**
- ▶ **Phone: 1-888-584-8332 or (703)605-6050**

Reproduced by NTIS

National Technical Information Service
Springfield, VA 22161

This report was printed specifically for your order from nearly 3 million titles available in our collection.

For economy and efficiency, NTIS does not maintain stock of its vast collection of technical reports. Rather, most documents are custom reproduced for each order. Documents that are not in electronic format are reproduced from master archival copies and are the best possible reproductions available.

Occasionally, older master materials may reproduce portions of documents that are not fully legible. If you have questions concerning this document or any order you have placed with NTIS, please call our Customer Service Department at (703) 605-6050.

About NTIS

NTIS collects scientific, technical, engineering, and related business information – then organizes, maintains, and disseminates that information in a variety of formats – including electronic download, online access, CD-ROM, magnetic tape, diskette, multimedia, microfiche and paper.

The NTIS collection of nearly 3 million titles includes reports describing research conducted or sponsored by federal agencies and their contractors; statistical and business information; U.S. military publications; multimedia training products; computer software and electronic databases developed by federal agencies; and technical reports prepared by research organizations worldwide.

For more information about NTIS, visit our Web site at <http://www.ntis.gov>.

NTIS

**Ensuring Permanent, Easy Access to
U.S. Government Information Assets**



U.S. DEPARTMENT OF COMMERCE
Technology Administration
National Technical Information Service
Springfield, VA 22161 (703) 605-6000
